LOW-COST MODAL IDENTIFICATION SENSORS FOR BRIDGE FIELD TESTING

Principal Investigators:

Daniel G. Linzell, Ph.D., PE, F. ASCE, F. SEI

Saeed Eftekhar Azam, Ph.D.

Postdoctoral Research Associate: Samira Ardani, Ph.D.

Graduate Research Assistant: Ahmed Rageh, Ph.D.

University of Nebraska – Lincoln

Department of Civil and Environmental Engineering

900 N 16th St

Lincoln, NE 68588

FINAL REPORT

Sponsored By:

The Nebraska Department of Transportation

March 2021

NEBRASKA
Good Life. Great Journey.
DEPARTMENT OF TRANSPORTATION

UNIVERSITY OF Nebraska Lincoln

TECHNICAL REPORT DOCUMENTATION PAGE

1. Report No. M105	**2. Government Accession No.**	**3. Recipient's Catalog No.**
4. Title and Subtitle M105: Low-Cost Modal Identification Sensors for Bridge Field Testing		**5. Report Date** March 2021 **6. Performing Organization Code**
7. Author(s) Daniel G. Linzell, Saeed Eftekhar Azam, Samira Ardani, Ahmed Rageh		**8. Performing Organization Report No.** 26-1107-01800-01
9. Performing Organization Name and Address The University of Nebraska-Lincoln 1400 R Street Lincoln, NE 68588		**10. Work Unit No.** **11. Contract** SPR-P1(20) M105
12. Sponsoring Agency Name and Address Nebraska Department of Transportation Research Section 1400 Hwy 2 Lincoln, NE 68502		**13. Type of Report and Period Covered** Final Report July 2019 – March 2021 **14. Sponsoring Agency Code**
15. Supplementary Notes		

16. Abstract

This report provides a framework for experimental load rating of bridges via inclusion of low-cost dynamic sensors and dynamic tests. Currently 25% of the bridges in Nebraska are posted for live load. According to the National Bridge Inventory (NBI) in 2012, 93% of all postings in the US were based analytical load ratings, 7% were posted using field evaluation and engineering judgement, and 1% were posted using experimental load rating methods.

Instrumentation costs and traffic interruptions can be problematic when load testing is necessary to accurately assess in-situ bridge live load capacity. Recent advances in (i) sensing technology and (ii) numerical methods used to process test data permit more cost-effective data-enabled decision making. According to the AASHTO *Manual for Bridge Evaluation* (MBE), dynamic tests can be used for calibration of bridge numerical models which could enhance the value of a diagnostic load test. This project helps engineers select and use inexpensive, off the shelf dynamic sensors for dynamic testing and load rating of bridges in Nebraska and elsewhere.

To help identify low-cost dynamic sensors suitable for Operational Modal Analysis (OMA), a set of bridges featuring various construction materials, span lengths, and structural systems were selected for vibration tests. Via tests conducted on the bridges, two low-cost sensors were downselected from five initial candidates. To ensure applicability of vibration tests to perform experimental load ratings, bridges were chosen as test beds for conducting vibration-based load ratings under operational conditions with results compared to data produced from strain measurements from controlled live load testing using. It was shown that vibration tests conducted using low-cost sensors and OMA can help engineers accurately complete bridge load ratings.

17. Key Words Bridges, Low-cost sensors, Smartphones, Dynamic load rating, Static load rating, Vibration testing, Finite element modeling, Model calibration.	**18. Distribution Statement** No restrictions. This document is available through the National Technical Information Service. 5285 Port Royal Road Springfield, VA 22161

19. Security Classification (of this report) Unclassified	**20. Security Classification (of this page)** Unclassified	**21. No. of Pages** 133	**22. Price**

Form DOT F 1700.7 (8-72) Reproduction of completed page authorized

DISCLAIMER

The contents of this report reflect the views of the authors, who are responsible for the facts and the accuracy of the information presented herein. The contents do not necessarily reflect the official views or policies neither of the Nebraska Department of Transportations nor the University of Nebraska-Lincoln. This report does not constitute a standard, specification, or regulation. Trade or manufacturers' names, which may appear in this report, are cited only because they are considered essential to the objectives of the report.

The United States (U.S.) government and the State of Nebraska do not endorse products or manufacturers. This material is based upon work supported by the Federal Highway Administration under SPR-P1(20) M105. Any opinions, findings and conclusions or recommendations expressed in this publication are those of the author(s) and do not necessarily reflect the views of the Federal Highway Administration."

TABLE OF CONTENTS

LIST OF FIGURES

LIST OF TABLES

ABSTRACT

This report provides a framework for experimental load rating of bridges via inclusion of low-cost dynamic sensors and dynamic tests. Currently 25% of the bridges in Nebraska are posted for live load. According to the National Bridge Inventory (NBI) in 2012, 93% of all postings in the US were based analytical load ratings, 7% were posted using field evaluation and engineering judgement, and 1% were posted using experimental load rating methods.

Instrumentation costs and traffic interruptions can be problematic when load testing is necessary to accurately assess in-situ bridge live load capacity. Recent advances in (i) sensing technology and (ii) numerical methods used to process test data permit more cost-effective data-enabled decision making. According to the AASHTO *Manual for Bridge Evaluation* (MBE), dynamic tests can be used for calibration of bridge numerical models which could enhance the value of a diagnostic load test. This project helps engineers select and use inexpensive, off the shelf dynamic sensors for dynamic testing and load rating of bridges in Nebraska and elsewhere.

To help identify low-cost dynamic sensors suitable for Operational Modal Analysis (OMA), a set of bridges featuring various construction materials, span lengths, and structural systems were selected for vibration tests. Via tests conducted on the bridges, two low-cost sensors were downselected from five initial candidates. To ensure applicability of vibration tests to perform experimental load ratings, bridges were chosen as test beds for conducting vibration-based load ratings under operational conditions with results compared to data produced from strain measurements from controlled live load testing using. It was shown that vibration tests conducted using low-cost sensors and OMA can help engineers accurately complete bridge load ratings.

1 INTRODUCTION

This report contributes to the state of the art related to experimentally load rating bridges using low-cost dynamic sensors. Two sensors of varying price and precision were downselected from an initial group of five sensors for field evaluation and used for dynamic testing. Measured data was processed using multiple operational modal analysis (OMA) methods in the time and frequency domains to determine suitable instruments and software for obtaining dynamic characteristics. These features were used to calibrate numerical models and develop a process to complete load ratings based on vibration data. Subsequently, dynamic load ratings were compared to ratings calculated using strain measurements from live load bridge tests to assess proposed framework effectiveness.

1.1 Background

This project seeks to provide a framework for experimental load rating of bridges via use of low-cost dynamic sensors for dynamic testing. Currently 25% of bridges in Nebraska are posted for live load. According to National Bridge Inventory in 2012 [1], of all posted bridges in the US, 93% were posted using analytical load ratings, 7% were posted using field evaluation and engineering judgement, and only 1% were posted using experimental load rating methods.

Instrumentation costs and traffic interruptions can be problematic when load testing is necessary to accurately assess in-situ bridge live load capacity. Recent advances in (i) sensing technology and (ii) numerical methods used to process load test data permit more cost-effective data-enabled decision making. According to the AASHTO Manual for Bridge Evaluation (MBE), vibration tests can be used for calibration of bridge numerical models and would enhance the value of a diagnostic test [2]. This study aims to develop a procedure for selection and use of inexpensive, off the shelf dynamic sensors for dynamic testing of typical bridges in Nebraska.

1.2 Research Objectives

This project has one overarching objective: to provide a framework for experimental load rating of bridges via use of low-cost dynamic sensors. More specifically, this project aims to:

- Examine and select cost-effective dynamic sensors for use during field tests.
- Develop cost effective procedures for bridge modal identification that will make experimental load rating viable for owners.
- Develop protocols for performing bridge tests and load ratings that will limit traffic disruption.

As mentioned earlier, currently 25% of bridges in Nebraska are posted for live load. About 99% of US bridges were posted using engineering judgement and/or simplified numerical analyses. Given that field tests can be costly, the primary benefit of this project is reducing experimental load rating cost without sacrificing accuracy. This, in turn, facilitates data-enabled decision making for many bridge owners and improves bridge management and resource allocation. Development of the proposed framework also has the potential to be directly integrated into existing or new bridge health monitoring systems.

1.3 Research Scope

The scope of this research includes two main parts. In first part, two low-cost sensors, those found in cellphones (iPhone) and a sensor manufactured by PCB Piezotronics (model no. 393B04), were downselected from a larger group of sensors and their performance evaluated. Modal parameters from selected bridges were determined using both devices and compared against one another. Seven bridges of different type and size were tested. In the second part, three bridges were selected and load rated experimentally and analytically to assess the efficacy using low-cost, dynamic sensors for load rating and develop testing framework.

1.4 Report Organization

Chapter 2 of this report contains a brief literature survey. Chapter 3 presents: the research methodology, summarizes initial sensor selection and subsequent downselection processes; OMA software, applications and algorithms selected for the study; bridge selection rationale; and the procedure used for dynamic load rating using vibration testing in conjunction with finite element modeling. Analysis results are presented in Chapter 4 and Chapter 5 presents recommendations for low-cost sensor selection, software selection, and the developed dynamic load rating procedure. Appendices A and B provide additional information needed to consider before using the dynamic low-cost sensors for field testing.

2 LITERATURE REVIEW

The use of wireless sensor nets for structural health monitoring, bridge load rating, and other field tests has been widely studied as wireless sensors reduce testing time, travel restrictions and cost. Even though wireless structural health monitoring applications have significantly improved over time, associated costs are still significant, and their implementation requires trained personnel.

An alternative to wireless sensor nets could be the use of strategically placed, independently acquired and self-contained wireless sensor systems. Applicable, independent systems commonly measure structural dynamics and can range between (1) extremely precise units costing thousands of dollars to (2) simple accelerometers available as independent data acquisition and processing units to (3) smartphones that use inexpensive, third-party applications for data collection and processing. The sections that follow summarize several recent studies that explored using low-cost sensors for bridge tests.

2.1 Laboratory Tests

Morgenthal and Hopfner [3] examined the use of smartphones to monitor displacement, vibration frequency and rotation with the selected device mounted to a structure. The study involved the use of a smartphone's accelerometer, speaker, and microphone. Evaluations of each internal device's accuracy and limitations were completed. The study indicated that smartphones could be used for structural health monitoring; however, accuracy limitations existed. It is important to note that the study involved application of proposed measurement methods to a small-scale laboratory test without exploring field applications.

Feng et al. [4] investigated use of smartphones acceleration measurements to experimentally estimate modal parameters. Included experiments involved small and large shake tables to examine a smartphone effectiveness when mounted to a dynamically excited masonry column and a full-

scale bridge. Comparisons made between smartphone and reference sensor measurements showed close agreement. The study indicated that: (i) observed error between the smartphone and high accuracy reference sensor was less than 5%; (ii) smartphone acceleration measurements allowed for highly accurate estimation of modal parameters under a variety of dynamic loads; and (iii) smartphones can be easily installed and data collected when compared with traditional sensors.

Kong [5] examined the use of smartphones to monitor building response as a part the MyShake project. The study performed a full-scale dynamic test of the Millikan Library in Pasadena, California using a total of 25 smartphones and the MyShake application. Measurements were compared against data from traditional accelerometers. The 25 smartphones were placed on the roof at the northwest corner of the building. Comparisons made between acceleration measurements from a single smartphone, a set of seven smartphones, and a reference sensor showed good agreement with translational and torsional frequencies detected from a single smartphone. The study concluded that displacement time-histories derived from smartphone accelerations matched well with reference sensor measurements.

Oraczewski et al. [6] proposed a damage detection framework that involved sensors and an Android smartphone. The smartphone was used to collect and analyze data and to present damage detection results. The developed framework was validated experimentally via studying fatigue crack growth in an aluminum plate and the crack was detected.

Yu et al. [7] further investigated smartphone use for measuring structural response via development and implementation of the Mobile-SHM application. A smartphone using the developed app with either internal or external sensors connected to the phone was shown to effectively monitor structural response. The developed application was validated against multiple structures whose dynamic response was measured using wired and wireless acquisition systems.

Tested structures included a three degree-of-freedom laboratory scale steel frame, a reduced-scale bridge cable and a full-scale cable-stayed bridge. It was observed that good agreement existed between responses measured using traditional, expensive sensors and those measured using smartphones internal or external sensors.

Structural health monitoring model updating using smartphone acceleration measurements was studied analytically and experimentally by Dey et al. [8]. Healthy and damaged, simply supported, reinforced concrete beams were dynamically tested using excitations from an instrumented hammer. Acceleration recordings were collected using three smartphones located at mid-span and near the ends using the keuwlsoft application [9]. Frequency responses for healthy and cracked beams were estimated from the acceleration measurements and used to update finite element models. It was observed that a clear shift in frequencies took place after damage and the maximum difference between experimental estimated and updated model frequencies was 5%.

2.2 Field Tests

Estimating modal parameters for in-service, concrete bridges using smartphones was investigated by Ndong et al. [10]. Studied bridges were instrumented using traditional accelerometers and smartphones. The study involved testing simply-supported T-beam and slab bridges having spans of 42 ft. 6 in. and 32 ft., respectively. Acceleration measurements were recorded under excitations from passing traffic as well as an impact hammer. It was concluded that the first three natural frequencies of the studied [11] bridges were accurately captured using smartphone measurements.

Ndong et al. [10] proposed computing load carrying capacity of a reinforced concrete T-beam bridge using modal parameters from ambient vibrations and finite element models. The studied bridge was simply supported with a 42 ft. 6 in. span and 29 ft. width. The study used a hybrid, optimization algorithm that incorporated a genetic algorithm and gradient-based optimization to

minimize the objective function and included differences between field-estimated and model predicted frequencies. Selected model updating parameters included modulus of elasticity, reinforcing bar cross-sectional areas and end support restraint. The study concluded that in-service bridge load rating based on ambient vibrations and finite element model updating is cost-effective.

Ozer [11] proposed the use of smartphones measuring pedestrian induced accelerations for bridge monitoring. The study used pedestrian smartphones to measure accelerations and estimate applied loads from people walking across bridge while stationary pedestrians measured accelerations for modal identification. The proposed framework was validated on a pedestrian bridge. The study concluded that bridge modal properties could be estimated using from walking pedestrian smartphones.

Ozer and Feng [12] developed a framework featuring smartphone accelerometers, and crowdsourcing for continuous health monitoring. The study developed an iOS application that measured and recorded smartphone accelerations and uploaded recorded signals to a server. A web-based application automatically processed uploaded data and extracted modal parameters. The proposed framework was validated using a simply supported steel arch bridge between two buildings with a span of 36 ft. The research found that close agreement existed between smartphone modal parameters and those estimated using high accuracy reference accelerometers.

Studies that utilize dynamic measurements to perform bridge load ratings have occurred. Chen et al [13] performed ambient dynamic-based load ratings of small, county bridges. They assumed that the bridges behaved like elastic springs with the spring stiffness is determined by knowing bridge mass and frequency. Islam et al [14] used load-displacement relationships obtained from dynamic measurements to determine bridge stiffness and capacity. Harris et al. [15] conducted operational load ratings by performing dynamic tests of Virginia Department of Transportation

(VDOT) bridges via installing accelerometers and measuring ambient vibrations. Two approaches were used to measure bridge response: BDI accelerometers measuring response to normal traffic; and forced vibration response with forcing functions provide from an electro-dynamic shaker. Findings confirmed the promise of using dynamic-based FE model updating for lowering costs associated with experimental bridge load rating. It was also concluded that further research is needed prior to implementing this approach for experimental load rating.

2.3 Research Gaps

In the previous sections studies that implemented dynamic sensors for measuring bridge dynamics and completing load ratings were summarized. It was found that the existing literature does not address the following questions:

1- Is it feasible to use low-cost sensors for experimental load rating of a wide range of bridge systems?
2- What reliable, low-cost dynamic sensors are suitable for bridge load rating are readily available?
3- Do load rating results obtained from dynamic tests under operational conditions favorably comparable against those obtained from ratings performed using data from conventional strain gages and known loads?

In the next section the methodology for addressing these research gaps is presented.

3 RESEARCH METHODOLOGY

3.1 Overview

To address project objectives, a variety of dynamic sensors, ranging from educational sensors, embedded smartphone sensors, to more sophisticated, low-cost industry grade accelerometers were investigated. Downselected sensors were then used for operational dynamic measurements on select, testbed bridges. Dynamic data from each sensor was processed using Operational Modal Analysis (OMA) for identification of fundamental frequencies and results from the downselected sensors were compared against each other and against results from calibrated finite element models. Sensitivities of fundamental dynamic frequencies from the FE models to variations in model parameters via comparisons to measured frequencies were also examined. In addition to helping calibrate the models, the field testing helped identify sensors that could be reliably, easily and cost effectively used for modal identification of bridges of varying dimensions and types. A single bridge was then selected for study and validation of a proposed dynamic-based, load rating technique using selected low-cost sensors. Results were compared against load ratings obtained from strains measured during controlled live load tests. Load ratings were carried out using Load Factor Rating (LFR) and Load and Resistance Factor Rating (LRFR) approaches outlined in the *AASHTO Manual for Bridge Evaluation* (MBE) [2]. Figure 1 contains a schematic summarizing the research methodology and steps.

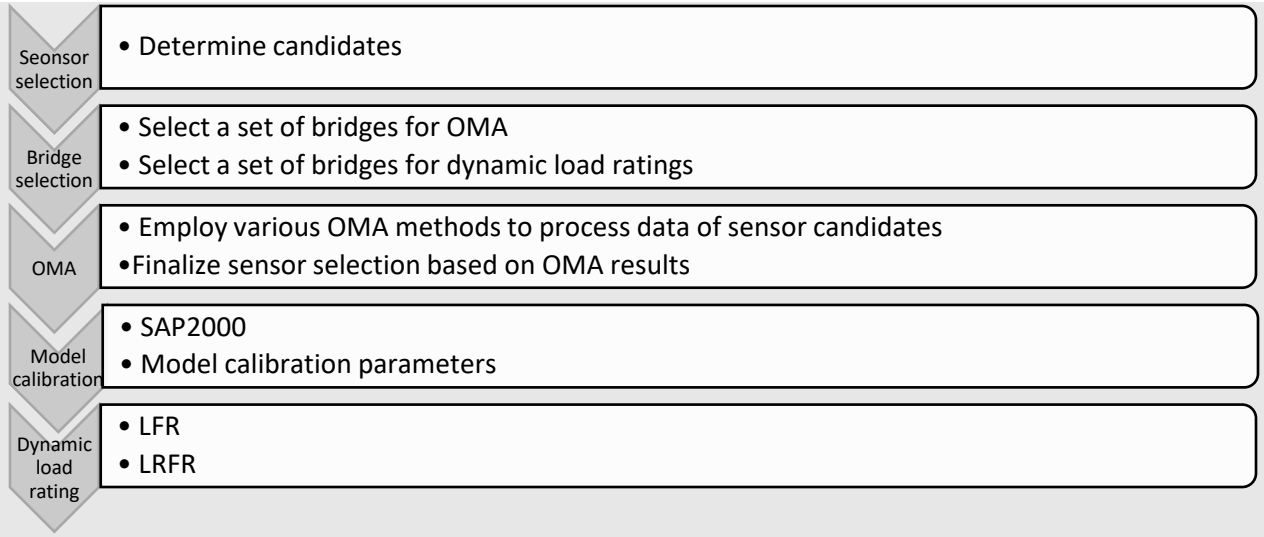

Figure 1: Research methodology.

3.2 Sensor Selection

An extensive search helped identify low-cost sensors that could potentially be used for bridge dynamic testing and dynamic load rating. In Table 1selected sensors and required data acquisition equipment, prices at the time of search (September 2019), and nominal resolutions are provided. The following sections detail each sensor's technical specifications and, in certain cases, discuss preliminary evaluation tests that were completed. Measurements provided by both sensors were repeatedly subjected to instabilities, even though their resolution was comparable to the resolution of iPhone 7+ accelerometer. A Monnit system was purchased and tested in the lab to ensure measured sensor data could be accessed at high sampling rates. However, the system's low IoT network bandwidth permitted sampling, recording, and transferring data at 1 Hz. This sampling frequency is not suitable for bridge modal analysis and the Monnit system was returned to the manufacturer.

Table 1: Studied Sensors

Sensor	Price	Resolution ($^{m}/_{s^2}$)
Pasco (PS-3216)	$85~$95	0.005
Vernier (GDX-ACC)	$99	0.005
iPhone 7+	$400~$500	0.005
Monnit (MNS2-9-W2-AC-ADV)	$567	0.001
PCB (393B04)	$1,100	0.00003

3.2.1 Pasco (PS-3216)

Pasco dynamic sensors are manufactured for educational purposes. They are somewhat inexpensive and have the capability of forming a wireless network including up to three triaxial sensors. These properties made Pasco sensors a suitable candidate for dynamic testing. Sensor data can be acquired using a dedicated SPARK LX Data Logger or the SPARKvue app that can be installed on a smartphone or a tablet. See Figure 2.

Figure 2: Pasco PS-3216.

3.2.2 Vernier (GDX-ACC)

Like Pasco, Vernier also manufactures dynamic measurement devices for educational purposes. They are also relatively inexpensive and can form a wireless network of up to three sensors. However, sensor resolution was not documented by the manufacturer. To address this gap, an experiment was performed to determine the resolution. The measured resolution and attributes also made Vernier sensors potential candidates. See Figure 3.

Figure 3: Vernier GDX-ACC.

3.2.3 Monnit Accelerometer (MNS2-9-W2-AC-ADV) and Data Acquisition Gateway

Monnit's dynamic measurement equipment is comprised of a sensor unit, an onboard data acquisition (DAQ) unit, and a wireless data access gateway. Its user manual indicates that the sensor features a sampling rate of over 200 Hz, and a sensitivity of 0.001 $^{m}/_{s^2}$, which combined with its relatively low cost made it a suitable candidate. See Figure 4.

Figure 4: Monnit (MNS2-9-W2-AC-ADV).

3.2.4 iPhone 7+

Smartphone accelerometers were also examined as low-cost, dynamic sensors. Built-in smartphone sensors can measure, record, and wirelessly transfer structural response data relatively easily. In this study an iPhone 7+ and the VibSensor application (Figure 5) were selected. The VibSensor app was selected based on its cost and because it allows for real-time recording of acceleration at a sampling rate of 100 Hz, which is appropriate for bridge dynamic testing. Data is stored in .csv (comma separated values) and .mat (MATLAB) file formats and can be readily postprocessed by the user. Another appealing app feature is that recorded data files can be directly emailed to the user. To guarantee the accuracy of the results, the iPhone should be placed in a secure position on a smooth surface. It is also recommended that the user calibrates the iPhone sensor against other industry grade dynamic sensors before initiating field testing.

3.2.5 PCB Accelerometer (393B04) and Signal Conditioner (485B39)

A PCB accelerometer and ICP signal conditioner were also examined. The ICP signal conditioner acts as a DAQ and permits direct access to sensor data via a tablet, smartphone, or computer. The signal conditioner is a cost-effective replacement for expensive DAQs. The sensor and signal conditioner are shown in Figure 6. A coaxial cable connects the sensor to the conditioner, which can acquire two channels. One use for the second channel could be acquiring instrumented hammer data to facilitate Experimental Modal Analysis (EMA). For this project, the PCB sensor and ICP conditioner were connected to a laptop with a USB cable. SpectraPLUS-SC software (Figure 7), which permitted viewing real-time, recorded, and post-processed data, was used for data viewing and processing.

Figure 5: iPhone 7+ and VibSensor app.

Figure 6: PCB 393B04 and ICP 485B39

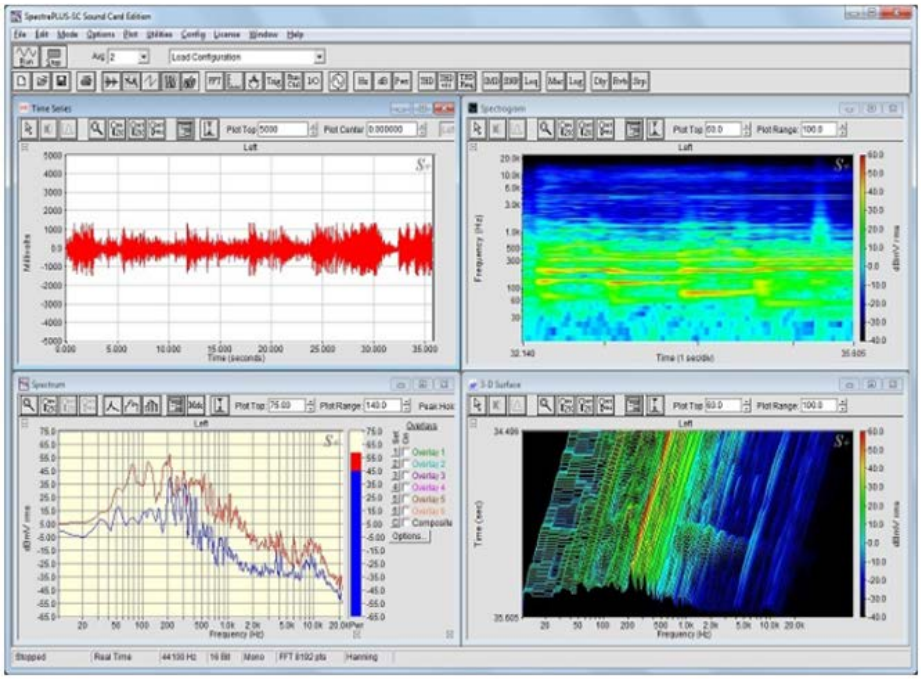

Figure 7: SpectraPLUS-SC

3.3 Bridge Selection

As shown in Table 2, bridges of differing geometry, type, and age were selected for cross-comparison of downselected sensor performance using Operational Modal Analysis (OMA). Three bridges (Table 3) were selected to further investigate the feasibility of using dynamic tests for bridge load rating by cross-comparing results obtained using dynamic-based load ratings against those obtained using strain-based load ratings.

Table 2: Bridge sensor performance testbeds.

Structure Number	County	Location	Precise Lat	Precise Lon	Span No.	Year Built	Design Type
S01502037	Jefferson	568TH AVENUE	40.294980	-97.179810	3	1958	Stringer/Multi-beam or Girder
C005502010	Lancaster	W Bluff Rd.	40545760	96460840	1	1983	Stringer/Multi-beam or Girder
C005510535	Lancaster	NW 112 St.	40491920	96522280	1	1968	Stringer/Multi-beam or Girder
U142503815L	Lancaster	LINCOLN SHERIDAN @ 33RD	40.465030	96.402557	1	2016	Stringer/Multi-beam or Girder
U142503455	Lancaster	O ST OVER ANTELOPE CREEK	40.484877	96.412441	3	2009	Slab
U142503410P	Lancaster	J ST @ S 24TH ST	40.482903	96.411232	3	2008	Slab
U142503610	Lancaster	A ST @ NORMAL BLVD	40.475400	96.403600	1	1956	Culvert
U142503113	Lancaster	S 70TH ST @ HOLMES PRK RD	40463614	96373025	3	1986	Slab
N/A	Lancaster	Holmes Lake footbridge	N/A	N/A	1	N/A	Truss and Concrete slab

Table 3: Bridge dynamic-based load rating testbeds.

Structure Number	County	Location	Precise Lat	Precise Lon	No. of Spans	Year Built	Design Type
S01502037	Jefferson	568th Avenue	40.294980	-97.179810	3	1958	Stringer/Multi-beam or Girder
C005512015	Lancaster	W Bluff Rd.	40545760	96460840	1	1983	Stringer/Multi-beam or Girder
C005510535	Lancaster	NW 112 St.	40491920	96522280	1	1968	Stringer/Multi-beam or Girder

3.4 Operational Modal Analysis (OMA)

OMA is the process of extracting dynamic characteristics of a structural system from its response to unknown loads, as opposed to EMA which focuses on extracting dynamic characteristics of structures subjected to known loads. OMA is particularly suitable for experimental load rating as it does not necessitate traffic disruptions. Several OMA algorithms were developed in the past ten years and can be classified as time or frequency domain methods. OMA is an intricate process in general as it deals with systems with unknown input. When dealing with low-cost sensors and for bridges under operational conditions subjected to various sources of excitation, OMA can become even more challenging, as theoretical assumptions can be violated, leading to suboptimal estimates of modal properties. To mitigate those issues, it is a common practice to use more than one OMA method to extract bridge modal properties. This approach was adopted throughout the project. In this section methods used in this report are briefly summarized to provide a general understanding of the fundamental theoretical assumptions used to interpret results presented in Chapter 4.

3.4.1 Time Domain OMA

3.4.1.1 Stochastic Subspace Identification (SSI) via Unweighted Principal Components (UPC)

SSI is currently the standard for time domain OMA [16]. This method directly fits a parametric model to raw structural response time histories and extracts dynamic properties of the structure from the fitted model. In doing so, the parametric model can often be a state-space model, which in discrete time is a recursive equation that explicitly links states of the system at a present time instant to the previous time instant. When fitting the parametric model to raw data, its order (i.e., complexity) needs to be determined, which will establish the number of parameters needed for the state space model. In practice, SSI is performed over a wide range of model orders and dynamic characteristics are extracted for each order. If a mode consistently presents for various model orders it is called a stable mode. Stable modes are commonly identified graphically using a

stabilization diagram. The original SSI algorithm calculated dynamic frequencies, damping ratios, and modes without any information regarding uncertainty. In this simplest implementation, SSI utilizes UPC for realization of the state space model by giving equal weight to any source of data. This approach is referred to as SSI-UPC [17].

3.4.1.2 SSI via Principal Components (PC)

PC is the most common method for calculating the weighting matrix used in the SSI algorithm for realization of the state space model underlying the data. PCs of the block Toeplitz matrix are used for weighting within SSI. The block Toeplitz is calculated using the covariance matrix of past and future data and contains blocks of measured response in discrete time that are repeated down the matrix diagonals. The main advantage of SSI-PC over SSI-UPC is its computational efficiency and its robustness to noise [17].

3.4.1.3 SSI via Extended Unweighted Principal Components (UPCX)

When dealing with identification of bridge modal characteristics under operational conditions, the unknown nature of the applied loads, measurement noise (especially for low-cost sensors), and the finite duration of measurements leads to uncertain estimates of modal parameters. When using OMA it is highly desirable to calculate these associated uncertainties. Döhler et al. recently developed a method for rigorous calculation of modal property uncertainties for linear dynamic systems by extending SSI-UPC [18]. The developed algorithm is referred to as SSI-UPCX [18].

3.4.2 Frequency domain OMA [19]

Frequency Domain Decomposition (FDD) and its extensions are some of the most widely used OMA frequency domain methods. The fundamental assumption behind OMA FDD methods is whiteness associated with system input, which means it has the same power spectra over all

frequency ranges. This assumption makes the input power spectral density (PSD) constant, which facilitates calculation of frequency response function directly from the system output PSD [19].

3.4.2.1 FDD

FDD is a simple and robust frequency domain OMA method [19]. The first step is calculating the PSD matrix for the output. Singular Value Decomposition (SVD) is then applied to find singular values of the PSD at discrete frequencies. Singular Value (SV) PSD peaks provide dynamic frequencies and Singular Vectors corresponding to the SV peaks represent corresponding dynamic modes [19].

3.4.2.2 Enhanced Frequency Domain Decomposition (EFDD)

A major drawback of FDD is that it does not calculate damping ratios. Brinker et al. extended FDD to determine the damping ratios [20]. The procedure, referred to as EFDD, is based on decomposition of the PSD matrix to obtain a set of Single Degree of Freedom (SDOF) auto spectral density functions that are then transformed into the time domain to calculate decay in amplitudes because of damping [20].

3.4.2.3 Curve-Fit Enhanced Frequency Domain Decomposition (CFDD)

One of the challenges of OMA when using FDD and EFDD is related to the existence of harmonic signals in the system input that are reflected in measured the structural response. Existence of harmonics violates the assumption of system input whiteness. To address this issue, Jacobsen et al. developed an algorithm using kurtosis checking, which provides a measure of tailedness of a probability distribution, and efficiently identified harmonics even in cases where the harmonic was close to system natural frequencies. They also developed efficient curve fitting for accurate estimation of dynamic frequencies and damping ratios [21].

3.4.3 OMA Software

ARTeMIS Modal Pro v.6.1 from Structural Vibration Solutions was selected for OMA. ARTeMIS Modal Pro allows for each of the OMA methods summarized in the previous sections to be used to estimate natural frequencies, damping ratios, dynamic modes, and their corresponding uncertainties. ARTeMIS Modal Pro time domain methods include SSI and its extensions to estimate structural system parameters including frequencies, damping levels and mode shapes using different system orders, and subsequently constructs stabilization diagrams to distinguish physical from spurious modes. Distinction between noise and structural modes complicates SSI based OMA. Frequency domain methods, however, provide a simple and intuitive “first look” at the data to determine if it is suitable for OMA. The software provides a unique opportunity to take advantage of strengths associated with previously summarized time and frequency domain methods to ensure OMA accuracy. Figure 8 depicts ARTeMIS Modal Pro 6.1’s graphical user interface (GUI).

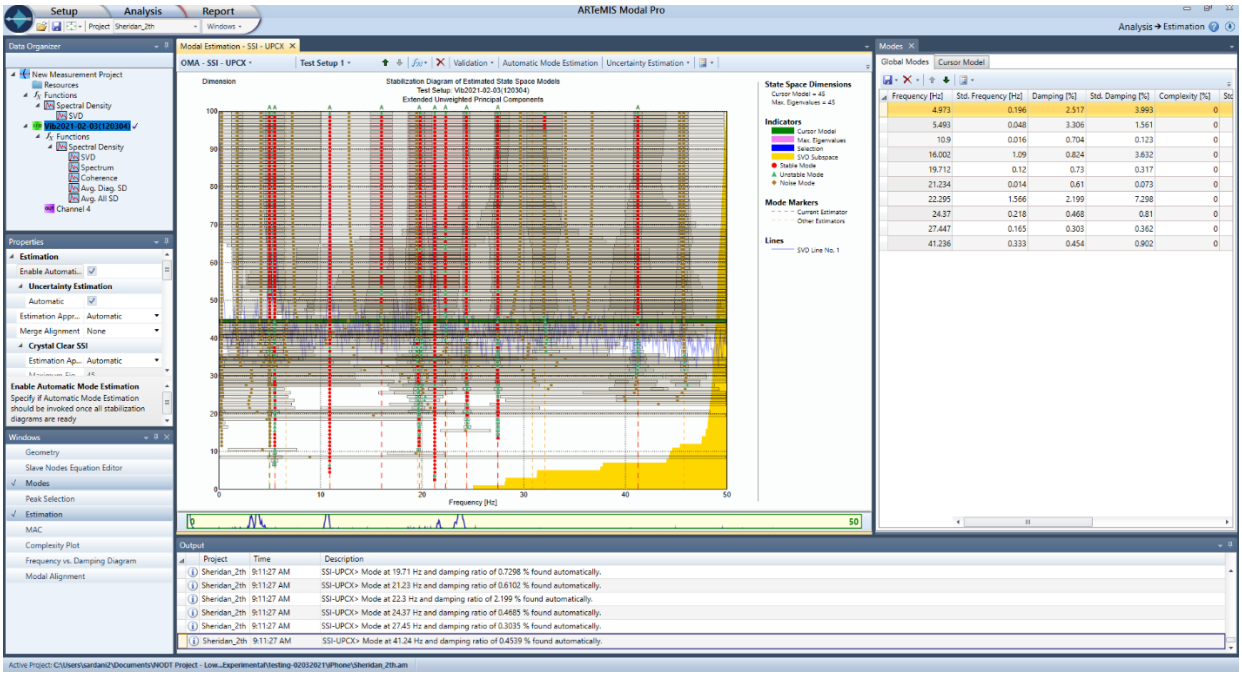

Figure 8: ARTeMIS Modal Pro 6.1 GUI.

3.5 Dynamic Tests and OMA for Nondestructive Load Rating

According to MBE Section 8.4.2.3, dynamic tests are a category of nondestructive tests that can be utilized for calculating the load bearing capacity of a bridge. The principal result of a dynamic test would be bridge dynamic properties. However, MBE Section 8.4.3.2 states that dynamic tests can be used for identifying defects as they alter the dynamic properties.

Load rating examines the live load capacity for the most critical member on a bridge with respect to effects on that member from a specified truck load. For the current study both Load Factor Rating (LFR) and Load and Resistance Factor Rating (LRFR) approaches were used.

For the LFR approach, the resulting rating factor (RF) is determined using Equation 6.3.2.2.1-1 from the MBE:

$$RF = \frac{C - \gamma_{DL} DL}{\gamma_{LL}\, LL\, (1+IM)}, \tag{3.1}$$

where $C = \phi R_n$. In this equation, ϕ and R_n represent the capacity of the critical member and the nominal member resistance. γ_{DL} denotes the dead load factor and γ_{LL} the live load factor. DL is the unfactored dead load and LL the unfactored live load. IM represents the dynamic load allowance.

According to the MBE the LRFR RF is calculated using:

$$RF = \frac{C - \gamma_{DC} DC - \gamma_{DW} DW - \gamma_P P}{\gamma_{LL}\, LL\, (1+IM)}\ . \tag{3.2}$$

Here DC represents dead load effects due from structural components and γ_{DC} their corresponding load factor. DW stands for dead load from the wearing surface and γ_{DW} the corresponding load factor. P denotes permanent loads other than the dead loads and γ_P their load factor.

Development of a nondestructive load rating procedure based on tests performed using the downselected dynamic sensors encompassed: testing bridges under operational traffic loads; estimating dynamic properties of the bridge using OMA techniques; constructing a numerical model of the bridges; performing inverse analyses to calibrate the models; and finally using the calibrated models [22] in conjunction with Equations 1 or 2 to perform the load ratings. A flowchart was developed that summarizes the procedure as shown in Figure 9. In the flowchart, Cells 3.6.1, 3.6.2, 3.6.5, and 3.6.6 are similar to steps presented in in Decision Tree 2 in NDOTs *Protocol to Evaluate and Load Rate Existing Bridges Using Field Testing* report [22].

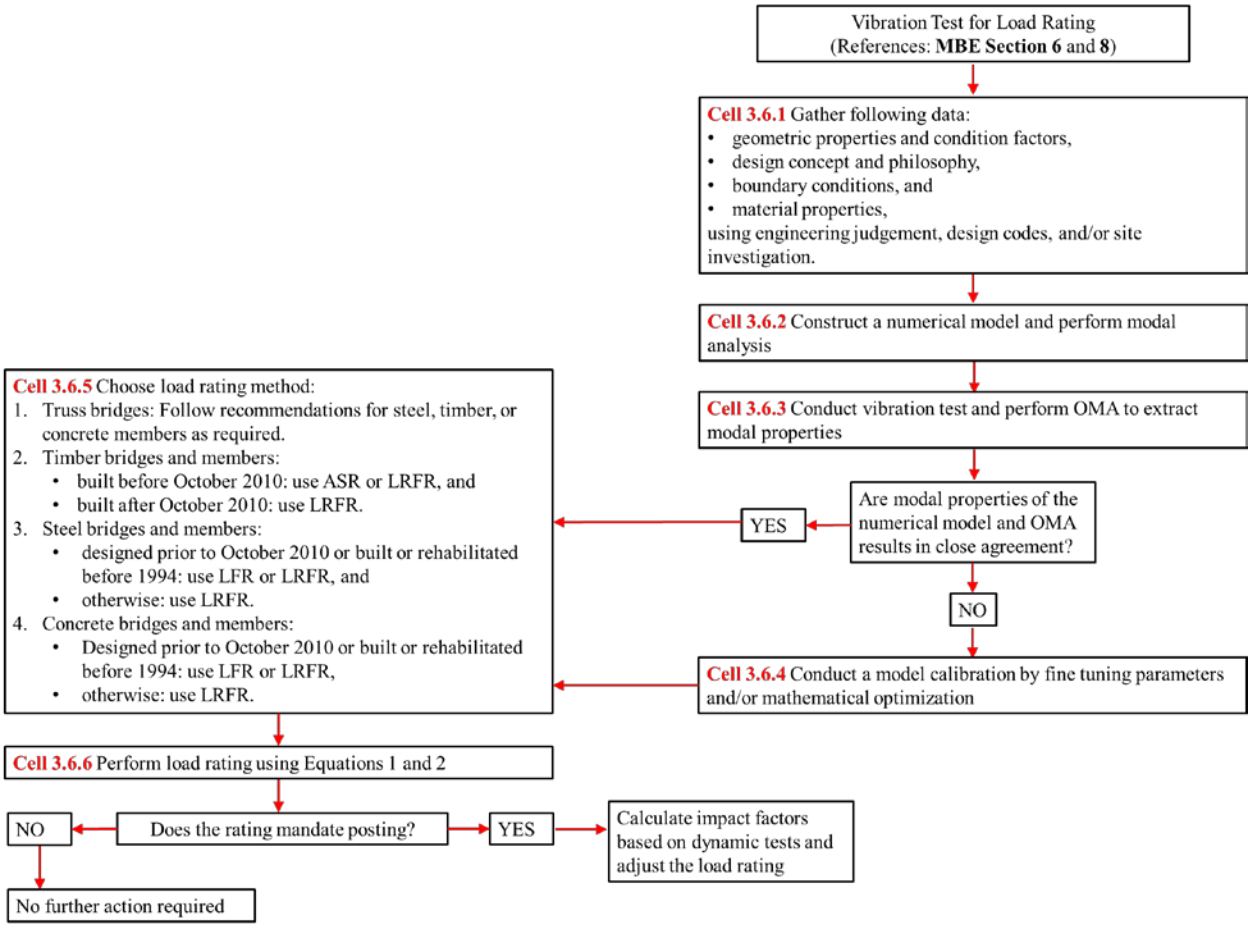

Figure 9: Dynamic testing load rating flowchart.

3.6 Summary

The feasibility of an initial group of five inexpensive dynamic sensors was investigated by investigating the sensor's technical specification, sensor's data acquisition requirements and in initial evaluations. As a result of these investigations, the PCB accelerometer (393B04) with signal conditioner (485B39) and iPhone were downselected for further study via cross-comparison of results obtained from dynamic tests of several bridges under normal traffic and via comparisons of modal parameters. Comparisons also helped identify apporpriate software and the techniques for data reduction using OMA. The following chapter evaluates the low-cost dynamic sensors using OMA to further identify and recommend low costs sensors(s), selected appropriate OMA techniques and validate a proposed dynamic-load rating methodology.

4 SENSOR SELECTION AND METHODOLOGY EVALUATION

This section is divided into two parts. The first reports results for experiments carried out on bridges listed in Table 2 to evaluate OMA performance of downselected sensors via comparisons between the sensors. The second part reports results from a nondestructive, dynamic load rating using the downselected sensors. To ensure validity of the dynamic-based load rating process and rating accuracy, results were compared against load ratings calculated from controlled live load tests where bridge response was measured using conventional strain gages.

4.1 Low-Cost Sensor Validation for OMA

4.1.1 Case Study 1: Multi-Span, Steel, Girder Bridge, Jefferson County (S01502037)

4.1.1.1 Bridge Description

Case Study 1 focused on what is referred to herein as the Fairbury Bridge. It is a two-lane, three-span, steel bridge with 20-degree skew, a 33 ft. width supporting a 7 in. thick concrete slab. The two exterior spans are simply supported and are connected to the middle span through a pin and hanger mechanism. Figure 10 is a simplified schematic plan view of the bridge where the red boxes denote the strain transducer locations.

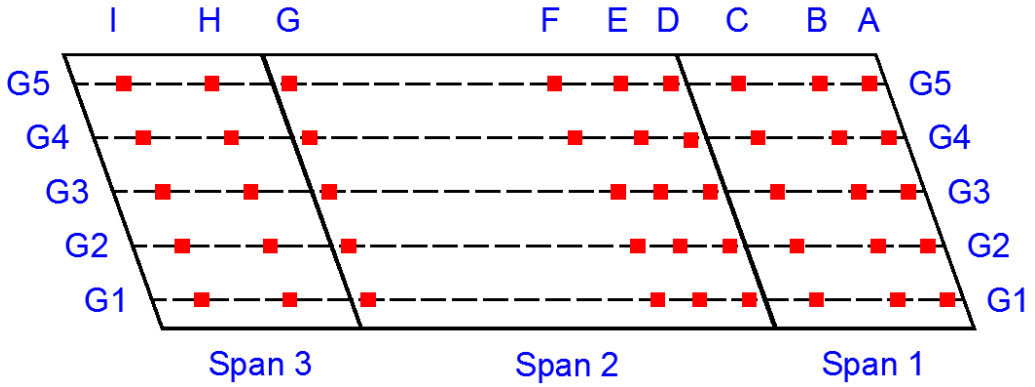

Figure 10: Fairbury bridge plan view squares signify strain transducer locations).

4.1.1.2 Field Testing and Data Collection

As reported in Table 3, the Fairbury Bridge was used for OMA sensor selection and for comparison between a dynamic-based load rating under operational conditions and a load rating obtained from strain gages and known live load. Therefore, field testing and data collection included strain gages and low-cost dynamic sensors. A total of 45 strain transducers were installed on the stringers. Downselected dynamic sensors were placed on the deck near mid-span adjacent to the parapet. Figure 11 and Figure 12 are plan and section views detailing sensor arrangement.

A truck weighing 50.6 kips was used for controlled live load testing. The front axle weighed 15.1 kips and two rear axles 17.7 kips each. Spacing between the axles was 15 ft. between the front and first rear axle and 4.75 ft. between rear axles. As stated earlier, operational traffic loads were used for the dynamic tests. Figure 13a shows an installed strain transducer and Figure 13b illustrates use of the low-cost dynamic sensors. Collected dynamic data from the iPhone 7+ is shown in Figure 14 where Channels 2, 3, and 4 represent acceleration in the x, y, and z directions.

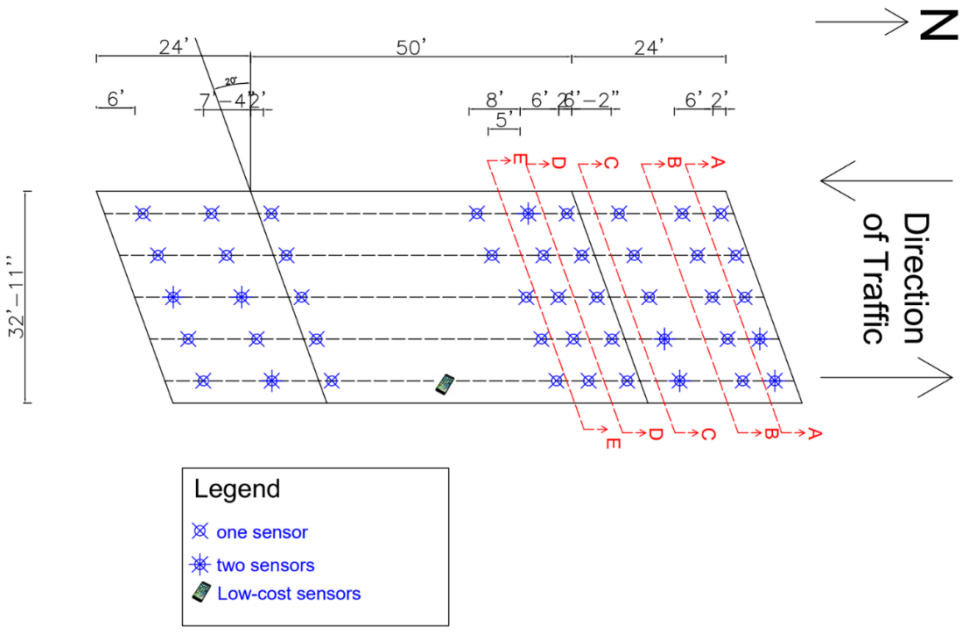

Figure 11: Plan view and sensor locations, Fairbury Bridge.

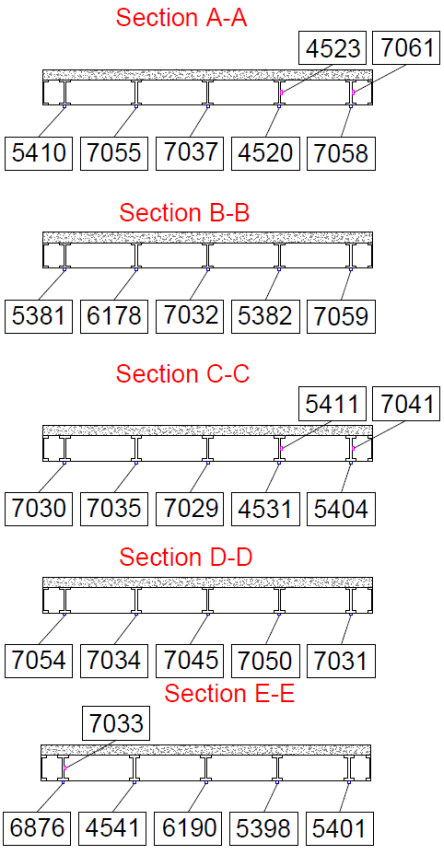

Figure 12: Instrumented sections, Fairbury Bridge.

(a) (b)

Figure 13: Static and dynamic testing details, Fairbury Bridge: (a) strain transducers on stringer bottom flange; (b) dynamic test using an iPhone 7+.

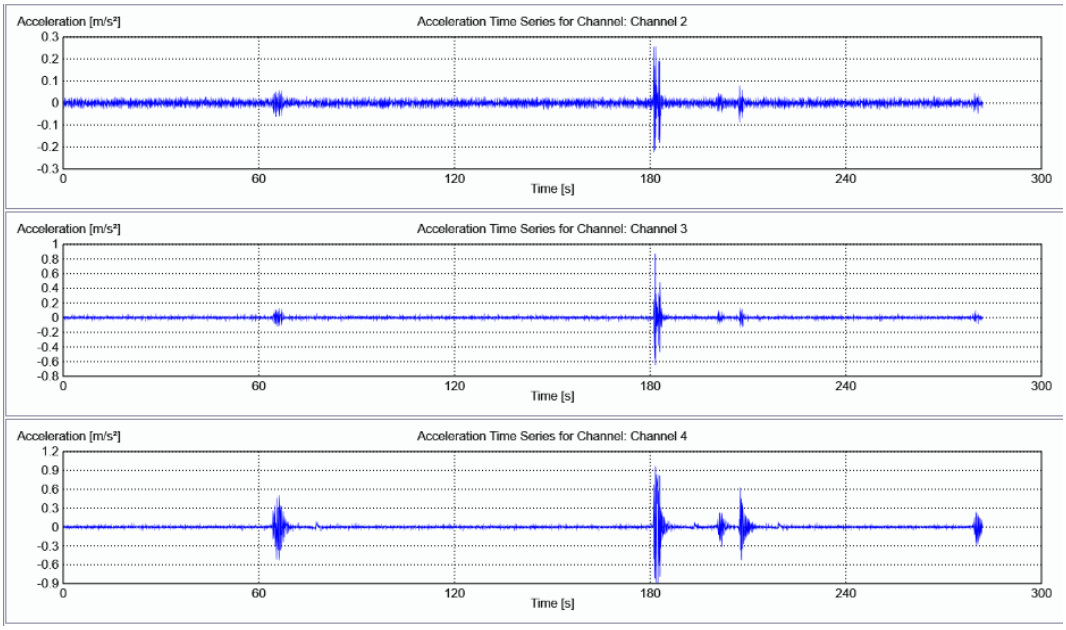

Figure 14: Recorded response using iPhone 7+

4.1.1.3 OMA Results

The measured acceleration data obtained from the low-cost sensors was utilized to estimate bridge modal parameters such as dynamic frequencies and damping ratios. Using OMA, bridge natural frequencies and dynamic response under different traffic loads was determined. Methods presented in Section 3.4 were used to extract bridge modal properties in ARTeMIS.

Figure 15 uses ARTeMIS heatmap spectrograms to compare PSDs of measured accelerations from the iPhone 7+ and PCB sensor. Spectrograms from the iPhone 7+ and PCB show similar amplitude intensity, which supports the premise that the iPhone 7+ sensor has enough precision to capture signals over a wide range of excitations. The SSI-UPC stabilization diagram was utilized to estimate modal parameters. Figure 16 shows the stabilization diagram used to estimate the dynamic frequency and damping ratio for the Fairbury bridge for both devices. Red lines and/or dots in the diagram correspond to stable modes automatically identified using the SSI-UPC method in ARTeMIS. As indicated in Figure 16, the first estimated natural frequencies from the iPhone

7+ and PCB sensor are good in agreement at 7.5 Hz (circled). Other OMA methods provided similar results.

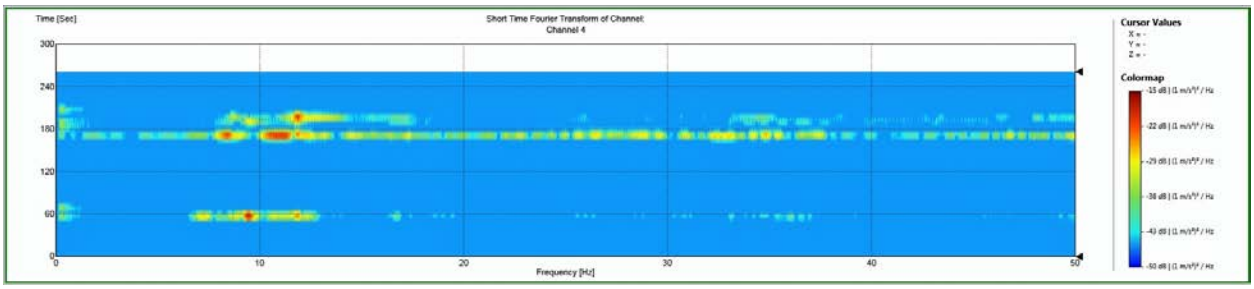

(a)

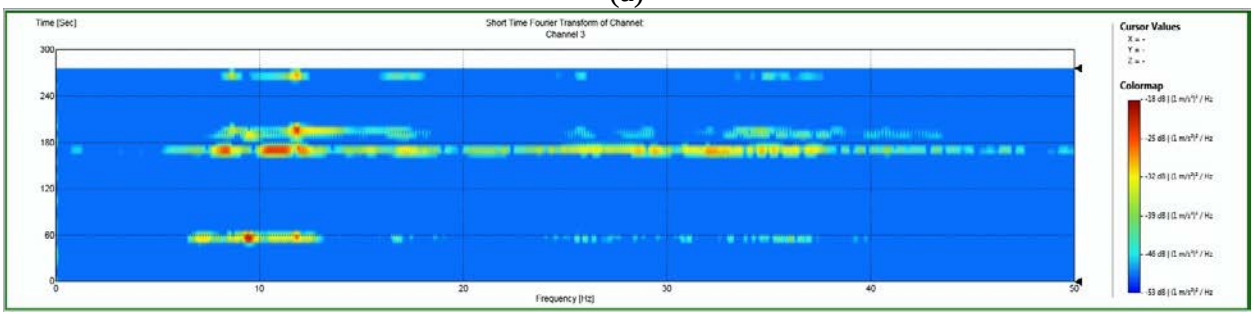

(b)

Figure 15: Bridge acceleration PSDs: (a) iPhone 7+; (b) PCB.

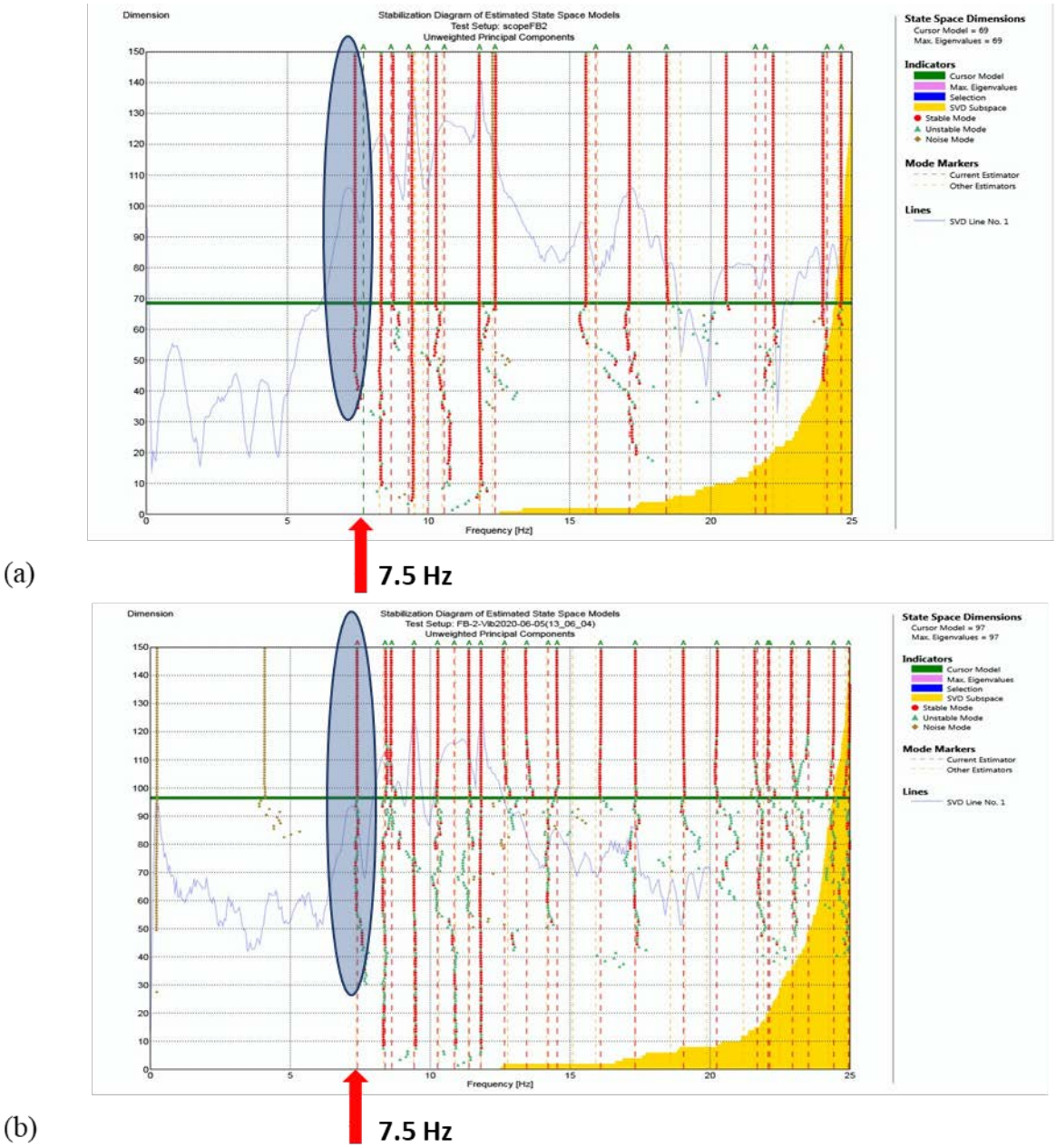

Figure 16: ARTeMIS OMA results using SSI-UPC (red dots represent stable modes): (a) PCB; (b) iPhone 7+.

4.1.2 Case Study 2: Bridge E-171 (ID # C005512015)

4.1.2.1 Bridge Description

Case Study 1 focused on what is referred to herein as the E-171 Bridge. It is a two-lane, single span, simply-supported multi-beam steel bridge that is 24 ft wide, 31 ft long and supports a 6 in. thick concrete slab. Figure 17and Figure 18 are a Google Maps view of the bridge and simplified schematic plan view of the bridge that details sensor locations. Sensors consisted of 48 BDI strain transducers and 4 BDI accelerometers installed at locations shown in Figure 66. The strain transducers were placed at the bottom of the top flange (T) and the bottom of the bottom flange (B) while the BDI accelerometers were installed on the web. Low-cost dynamic sensors were placed on the bridge deck to record accelerations.

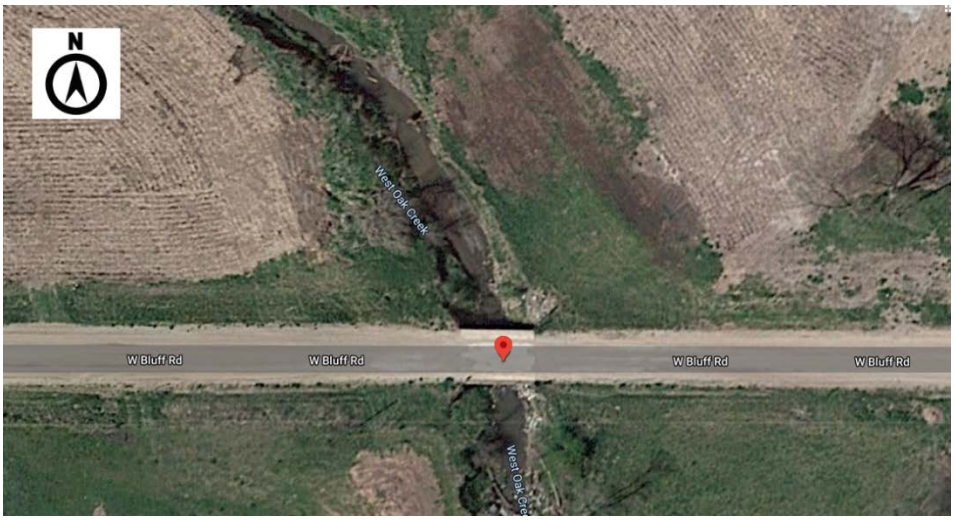

Figure 17: Satellite view of E-171 bridge Google Maps (40°54'56.2"N 96°49'41.8"W)

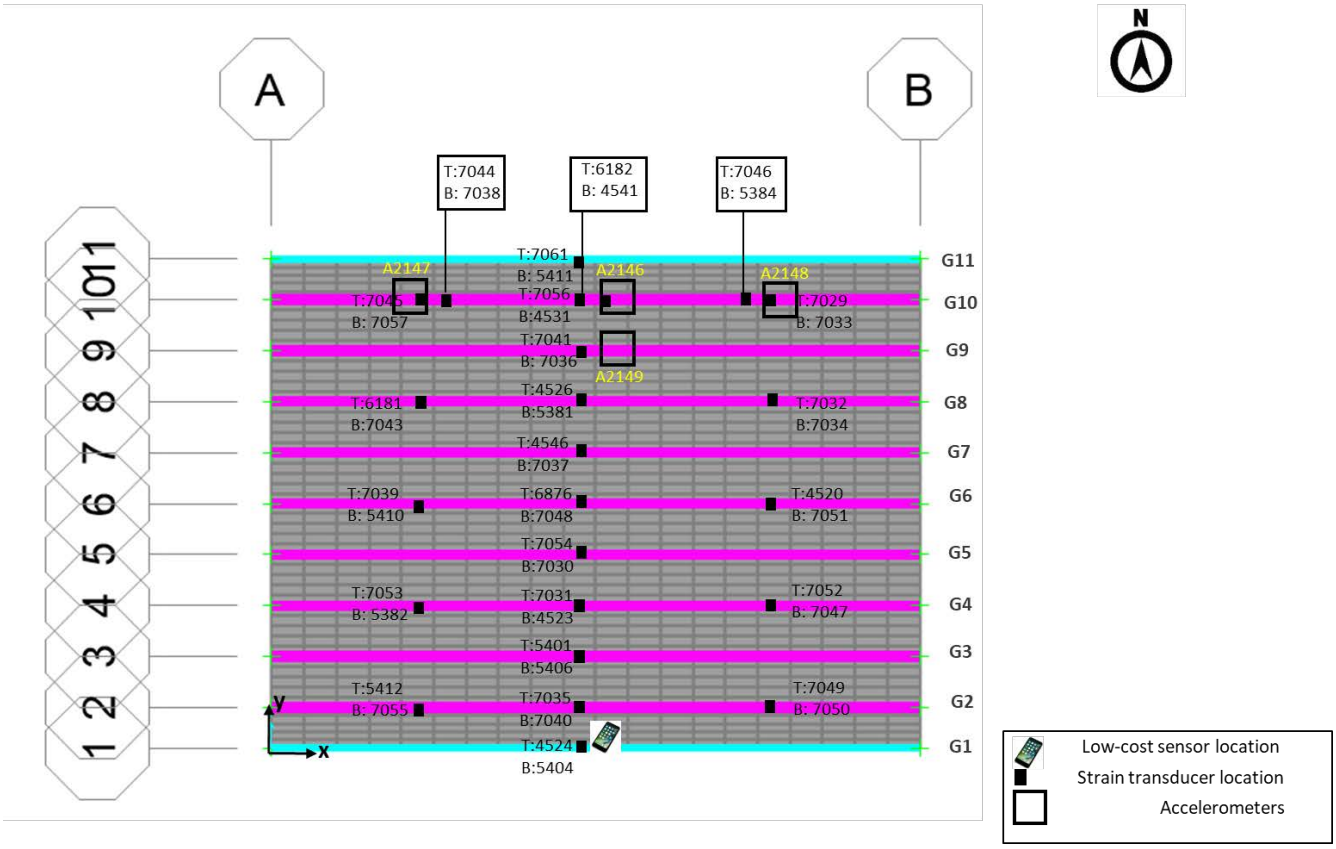

Figure 18: E-171 plan view detailing sensor locations.

4.1.2.2 Field Testing and Data Collection

E-171 was used for experimental OMA based dynamic load rating and for strain-based load rating. Ratings were determined and results compared in similar fashion to the Fairbury Bridge (see Sections 4.1.1). As shown in Figure 19, a U-Haul truck weighing 8.160 kips was used as the testing load. The front and the rear axles weighed 3.56 and 4.6 kips, respectively. Spacing between the axles was 13.25 ft and centerline-to-centerline distance between the front tires was 5.58 ft. Figure 20 and Figure 21 show an iosometric view of the bridge and representative instrumentation. Collected dynamic data from an iPhone 7+ is shown in Figure 22 where Channels 2, 3, and 4 represent acceleration in the x, y, and z directions.

Figure 19: U-Haul truck.

Figure 20: Isometric bridge view.

Figure 21: Bridge instrumentation

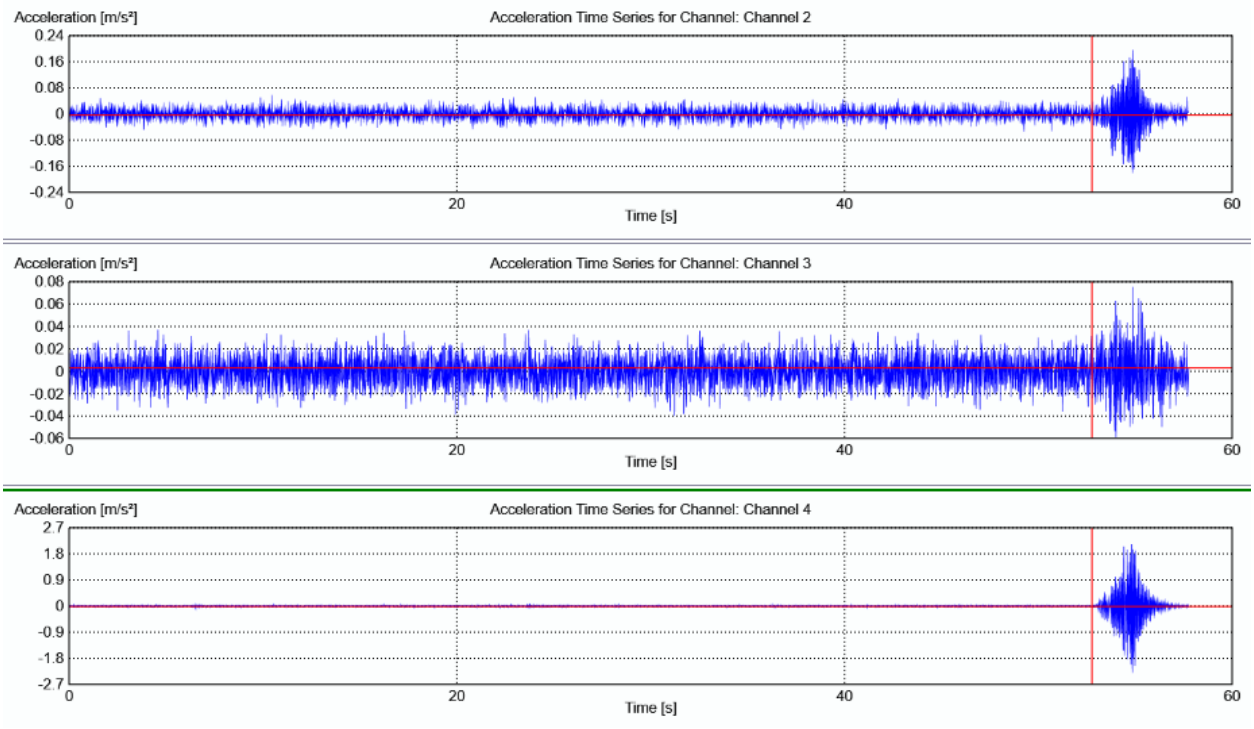

Figure 22: Recorded response using iPhone 7+

4.1.2.3 OMA Results

Measured acceleration data from the low-cost sensors was utilized to estimate bridge dynamic frequencies and damping ratios. Using OMA, bridge natural frequencies and dynamic response under different traffic loads was determined. Methods presented in Section 3.4 were used to extract bridge modal properties in ARTeMIS.

Figure 23 uses ARTeMIS heatmap spectrograms to evaluate PSDs of measured accelerations from the iPhone 7+. The SSI-UPC stabilization diagram was utilized to estimate modal parameters. Figure 24 shows the stabilization diagram used to estimate the dynamic frequency and damping ratio for the E-171 bridge. Red lines and/or dots in the diagram correspond to stable modes automatically identified using the SSI-UPC method in ARTeMIS. As indicated in Figure 24, the first estimated natural frequency and the corresponding damping ratio from the iPhone 7+ are 11.28 Hz and 2.22% respectively.

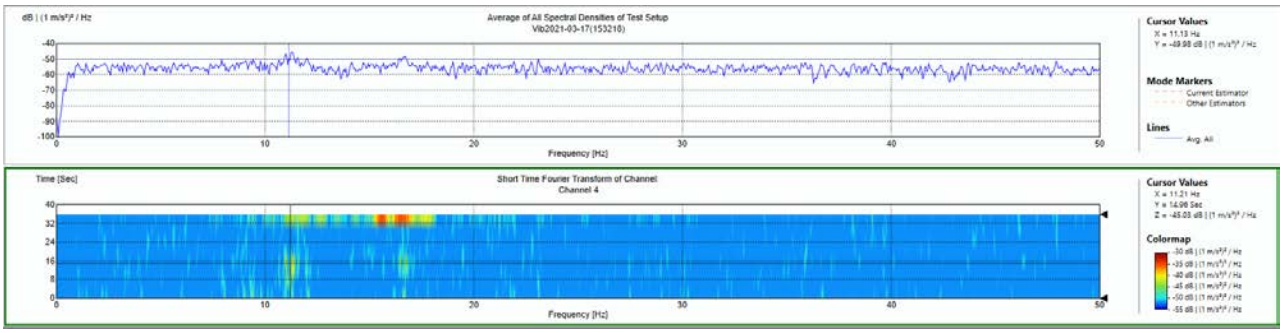

Figure 23: Bridge acceleration spectogram: iPhone 7+

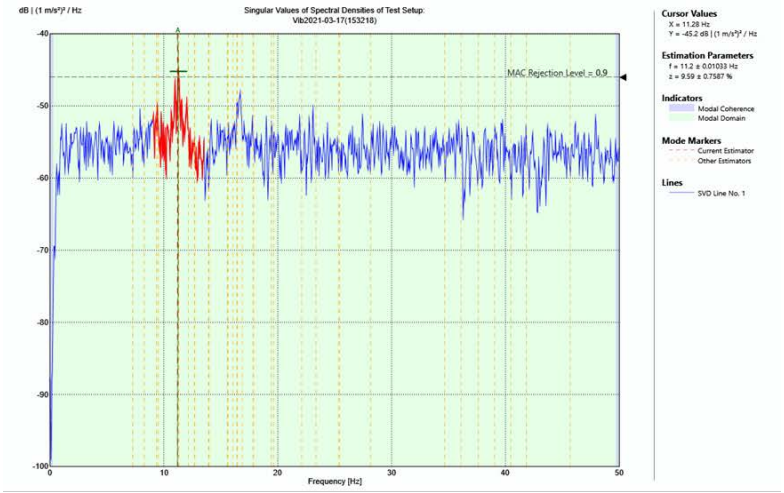

(a)

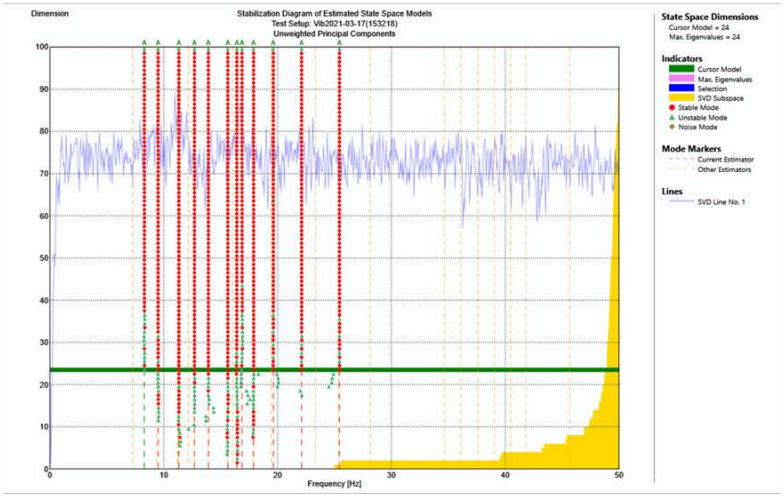

(b)

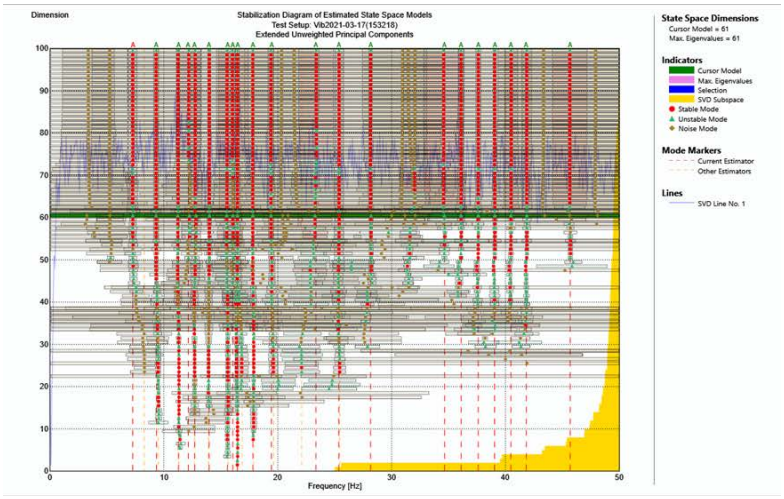

(c)

Figure 24: The estimated modes for iPhone sensor using (a) EFDD, (b) UPC and (c) UPCX methods.

4.1.3 Case Study 3: Bridge M-164 (ID # C005510535)

4.1.3.1 Bridge Description

Case Study 3 focused on what is referred to herein as the M-164 Bridge. It is a two-lane, one-span simply supported, steel bridge with a 33 ft. width, 50 ft span length supporting a 6.5 in. thick concrete slab. Figure 25 and Figure 26 show the satellite view of the bridge from Google Maps and simplified schematic plan view of the bridge and the sensor locations. The total of 42 BDI strain transducers and 4 BDI accelerometers were installed at the locations shown in Figure 26. The strain transducers were placed at the bottom of the top flange (T) and the bottom of the bottom flange (B) while the BDI accelerometers were installed on the web. The low-cost dynamic sensors were located on the bridge deck to record the acceleration.

Figure 25: Satellite view of M-164 bridge from Google Maps (Geographical location: 40°49'20.4"N 96°52'22.7"W)

4.1.3.2 Field Testing and Data Collection

M-164 Bridge is used for OMA and dynamic load rating using dynamic tests. A U-haul truck weighing 8.160 kips was used for experimental dynamic testing. The front and the rear axles weighed 3.56 and 4.6 kips respectively. Spacing between the axles was 13.25 ft and the centerline-to-centerline distance of the front tires was 5.58 ft. As stated earlier, operational traffic loads were used for the dynamic tests. Figure 27 and Figure 28 detail the bridge and representative instrumentation. Collected dynamic data from the iPhone 7+ is shown in Figure 29 where Channels 2, 3, and 4 represent acceleration in the x, y, and z directions.

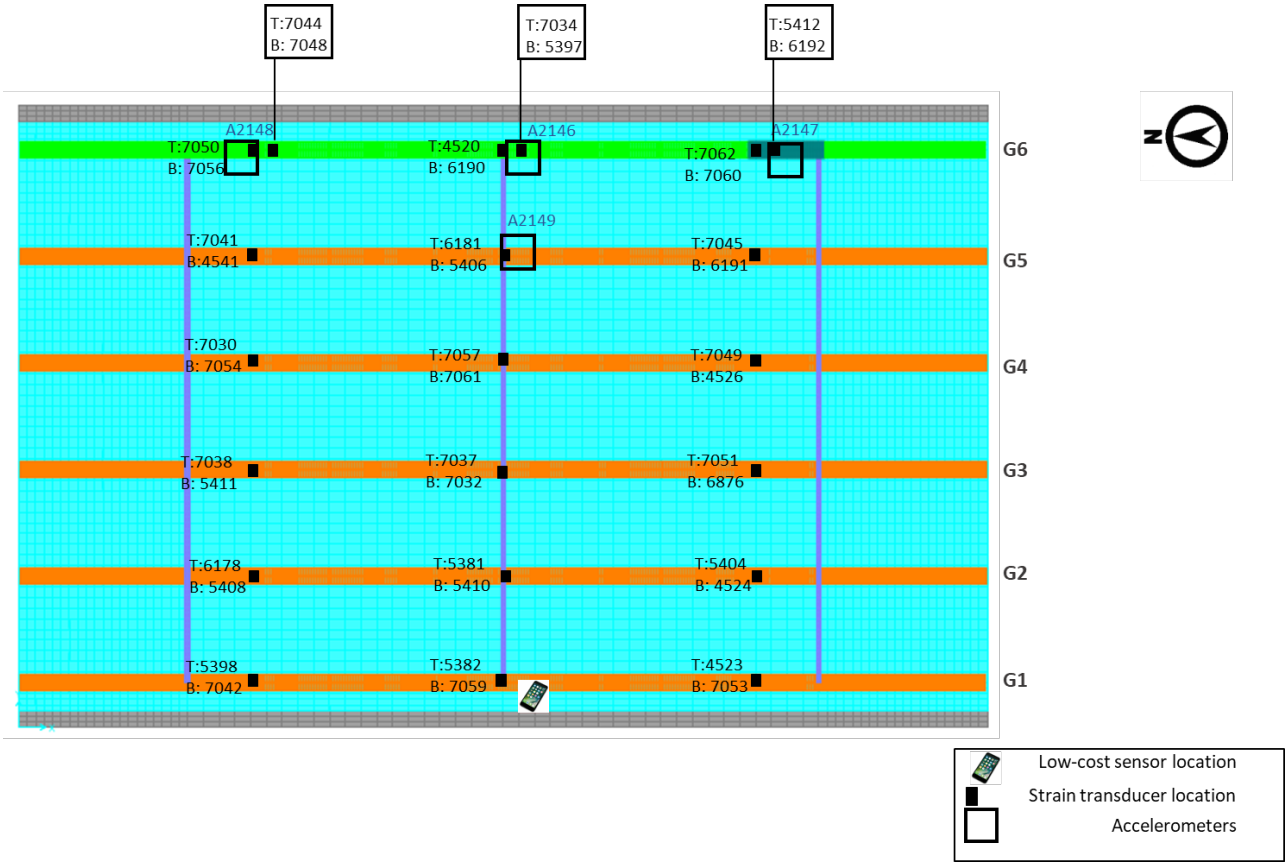

Figure 26: Bridge M-164 plan view detailing sensor locations

Figure 27: Bridge views

Figure 28: Bridge instrumentation

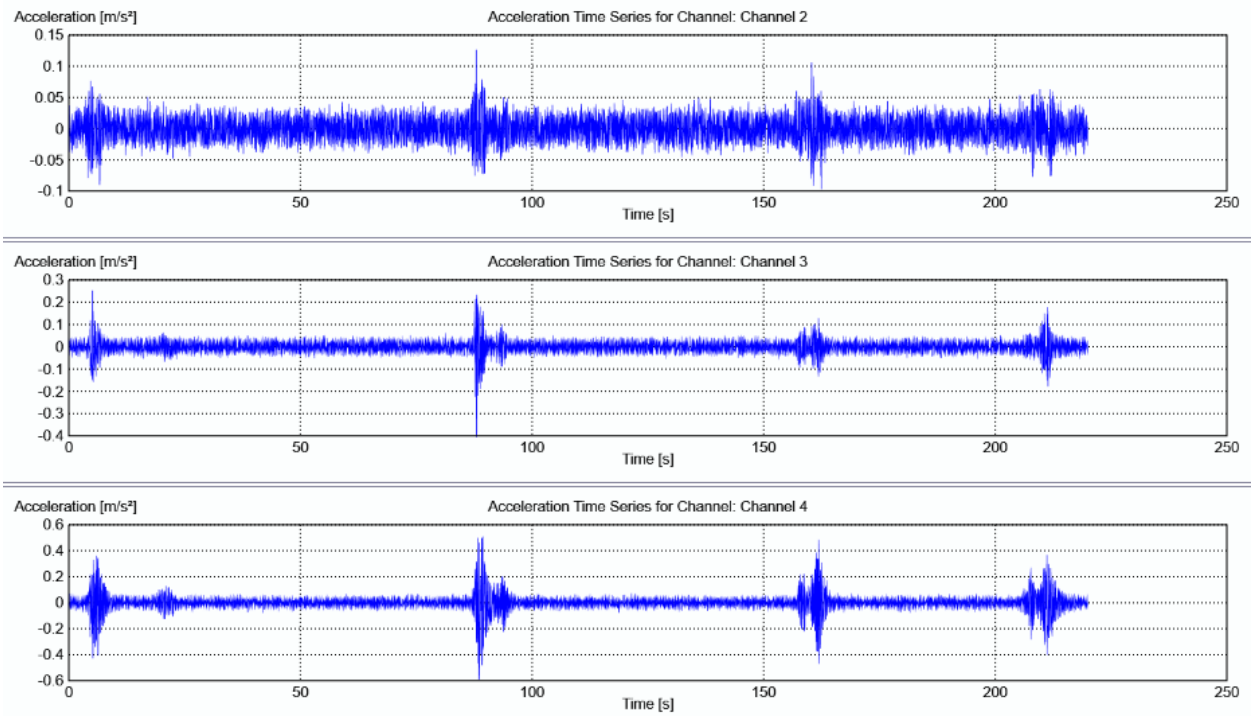

Figure 29: Recorded response using iPhone 7+

4.1.3.3 OMA Results

The measured acceleration data obtained from the low-cost sensors was utilized to estimate bridge modal parameters such as dynamic frequencies and damping ratios. Using OMA, bridge natural frequencies and dynamic response under different traffic loads was determined. Methods presented in Section 3.4 were used to extract bridge modal properties in ARTeMIS.

Figure 30 uses ARTeMIS heatmap spectrograms to compare PSDs of measured accelerations from the iPhone 7+. Figure 31 shows the stabilization diagram used to estimate the dynamic frequency and damping ratio for the M-164 bridge. Red lines and/or dots in the diagram correspond to stable modes automatically identified using the SSI-UPC method in ARTeMIS. As indicated in Figure 31, the first estimated natural frequency and the corresponding damping ratio from the iPhone 7+ are determined 7.5 Hz and 2.11% respectively. Other OMA methods provided similar frequency and damping ratios.

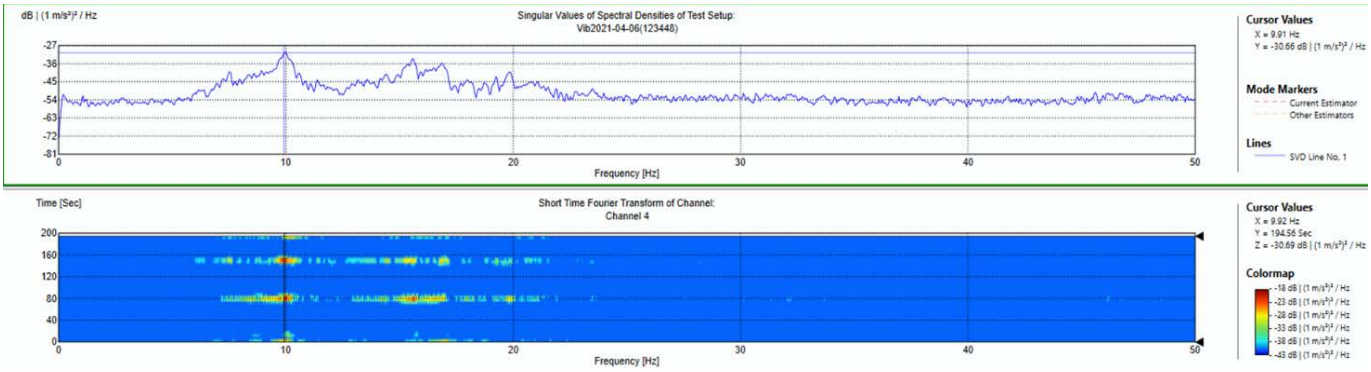

Figure 30: Bridge acceleration PSDs: iPhone 7+

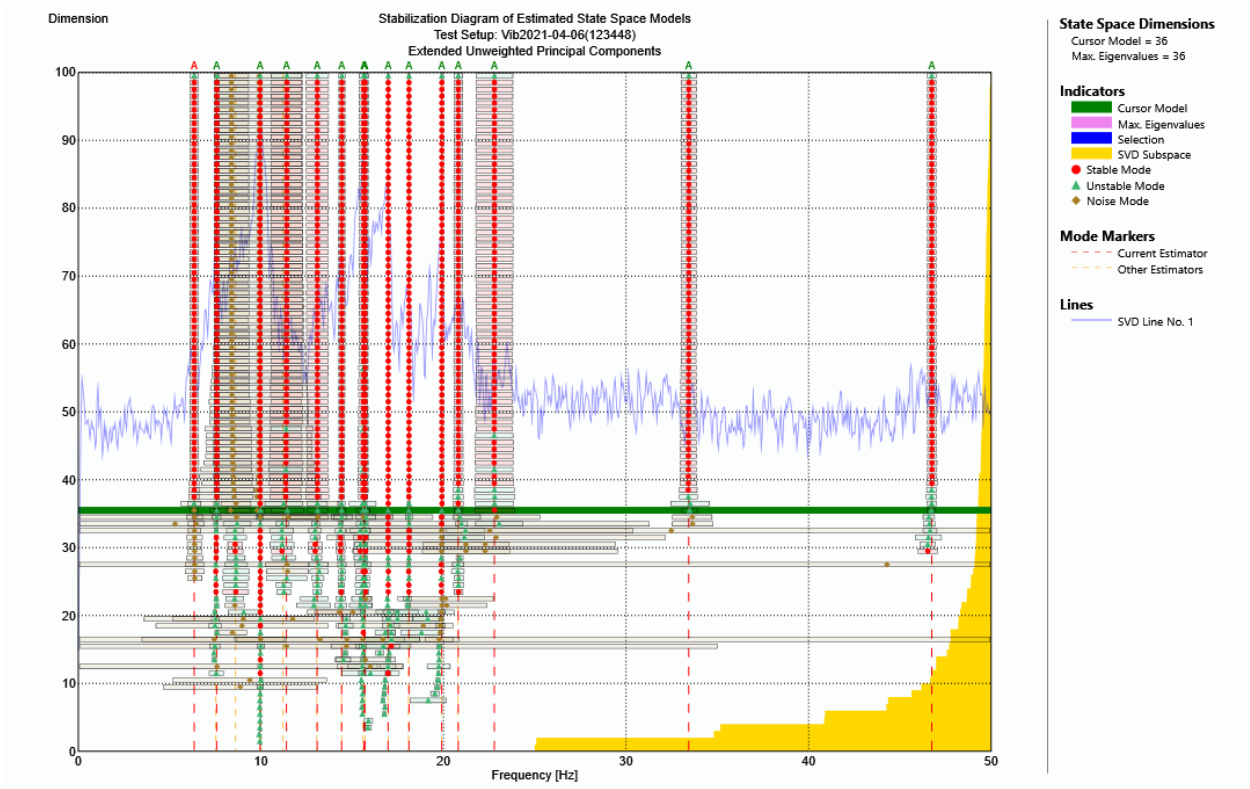

Figure 31: ARTeMIS OMA results using SSI-UPC: iPhone 7+

4.1.4 Case Study 4: Sheridan Blvd. Near 33rd Street (ID # U142503815L)

4.1.4.1 Bridge Description

The Case Study 2 bridge is a single span, simply-supported, prestressed concrete slab having a 100.3 ft. span length, a 20 ft. deck width. Figure 32 contains photos of the bridge from Google maps.

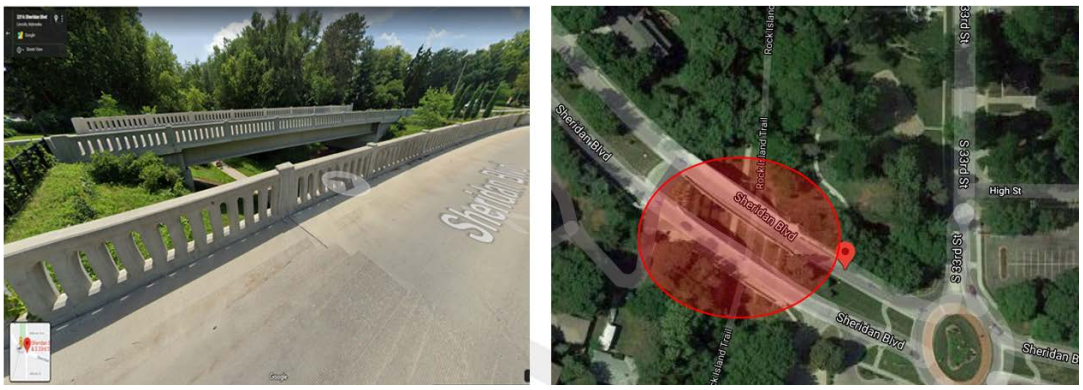

Figure 32: Street and satellite view of Sheridan Blvd. Bridge from Google Maps [23]

4.1.4.2 Field Testing and Data Collection

The bridge was tested twice under operational loads. Dynamic tests were conducted with iPhone and PCB sensors deployed at mid-span and adjacent to the sidewalk. Data from two different iPhones was collected and processed using the VibSensor iOS app at its maximum sampling frequency of 100 Hz. Two iPhones were examined to determine if cellphone version/type affected results. The PCB sensor recorded the data at its minimum sampling frequency of 4000 Hz. Figure 33 details data collection during one of the tests using the PCB sensor and Figure 34a and Figure 34b present recorded acceleration data from the iPhone and PCB.

Figure 33: Data collection, Sheridan Blvd. Bridge

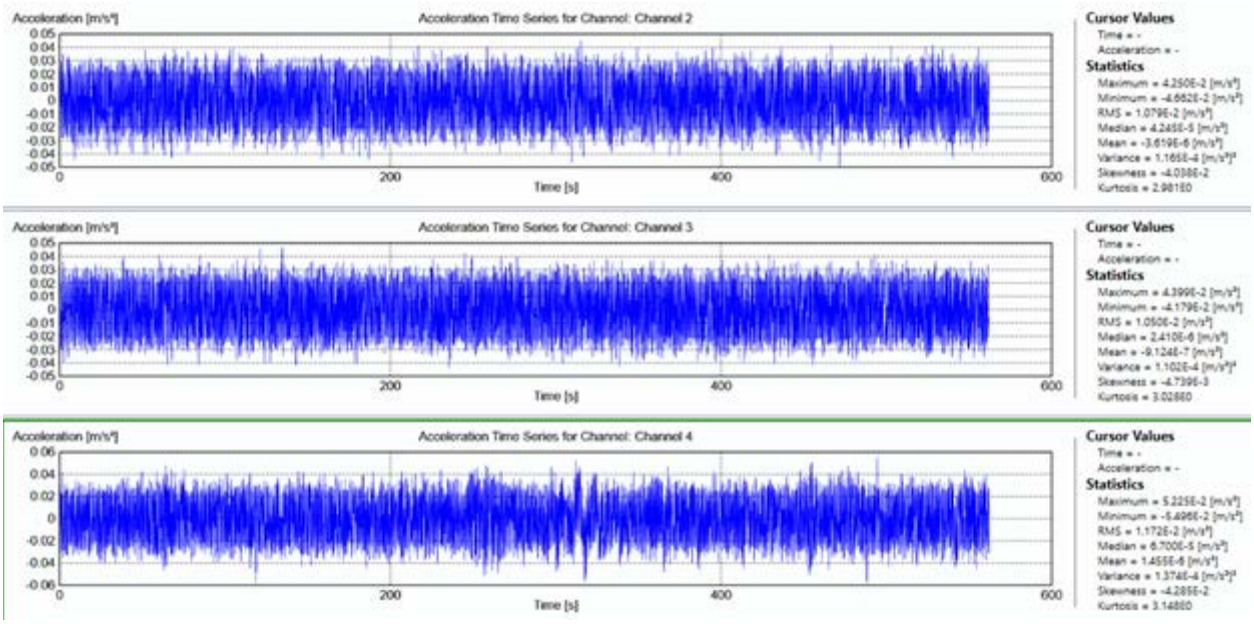

(a)

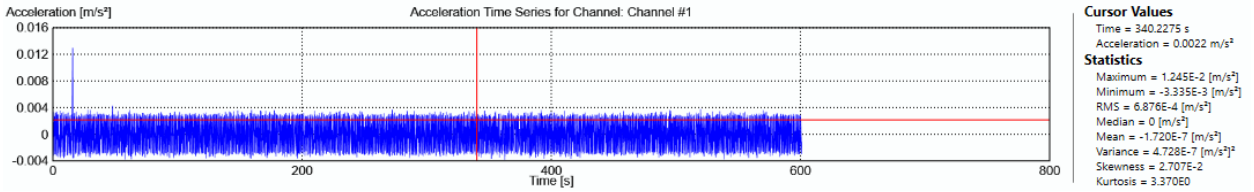

(b)

Figure 34: Recorded acceleration data using: (a) iPhone 7+ and (b) PCB

4.1.4.3 OMA Results

OMA results for each test are discussed below.

First Trial, iPhone 6

Figure 35 shows iPhone 6 OMA results using the UPC, UPCX and EFDD methods. When using SSI-UPC the first dynamic frequency and its corresponding damping ratio were 5.59 Hz and 2.07% (Figure 35a). When using SSI-UPCX the first dynamic frequency and its damping ratio were 5.61 Hz and 2.1% (Figure 35b). Using the EFDD and its peak-picking method the frequency was estimated 5.65 Hz (Figure 35c).

Second Trial, iPhone 6:

Following the same procedure as first trial, the UPC estimated frequency and corresponding damping ratio were 4.93 Hz and 2.57%. The UPCX method estimated the frequency as 4.97 Hz and damping at 2.5%. The EFDD method indicated that the first peak with 5.03 Hz corresponds to a frequency band with a peak at 5.46 Hz. Figure 36 details the results.

Third Trial, iPhone 7+:

As stated earlier, it was of interest to examine if the type of iPhone influenced results. Therefore, a third test was completed using an iPhone 7+. As shown in Figure 37, estimated frequency values for the first mode agree with results from trials one and two. Figure 37 also shows iPhone 7+ OMA results using the UPC and UPCX methods. When using SSI-UPC the first dynamic frequency and its corresponding damping ratio were 5.6 Hz and 2.07%. When using SSI-UPCX the first dynamic frequency and its damping ratio were 5.61 Hz and 2.1%. Similar agreement was obtained using EFDD and results are not included.

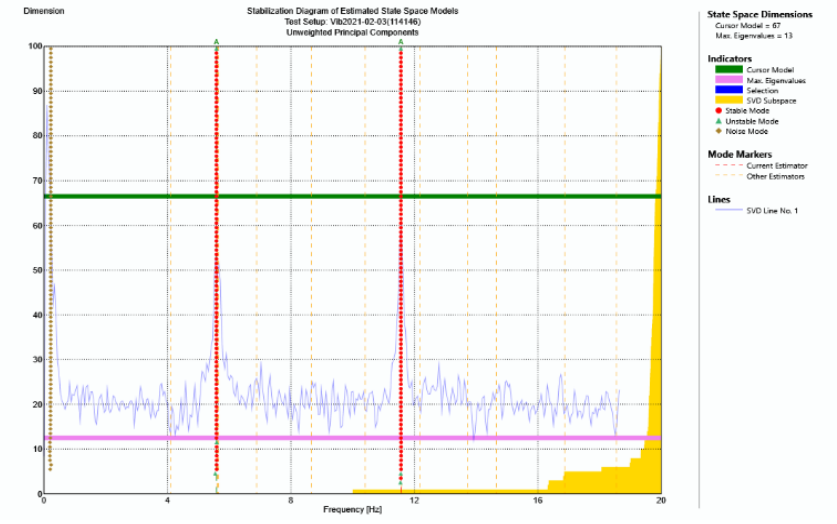

(a)

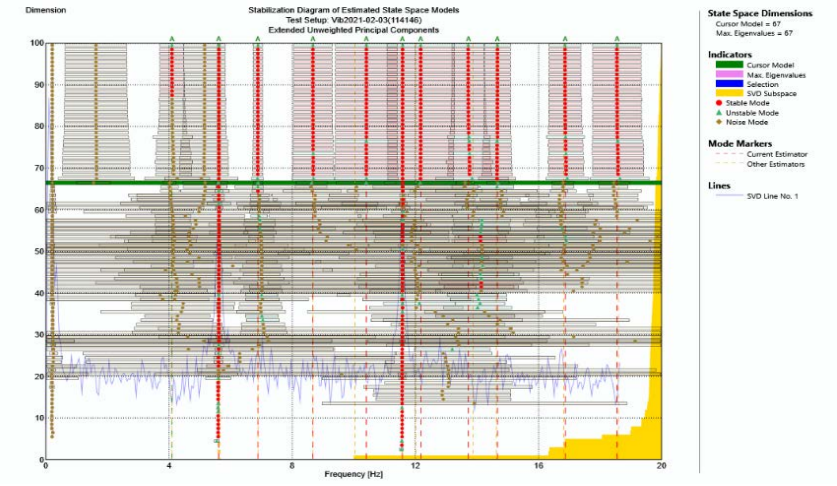

(b)

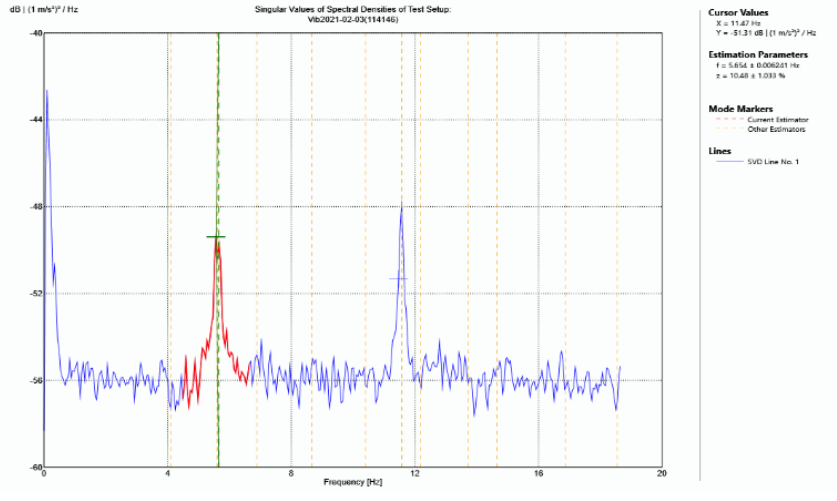

(c)

Figure 35: Trial 1 iPhone 6 ARTeMIS OMA results using: (a) UPC; (b) UPCX; (c) EFDD.

(a)

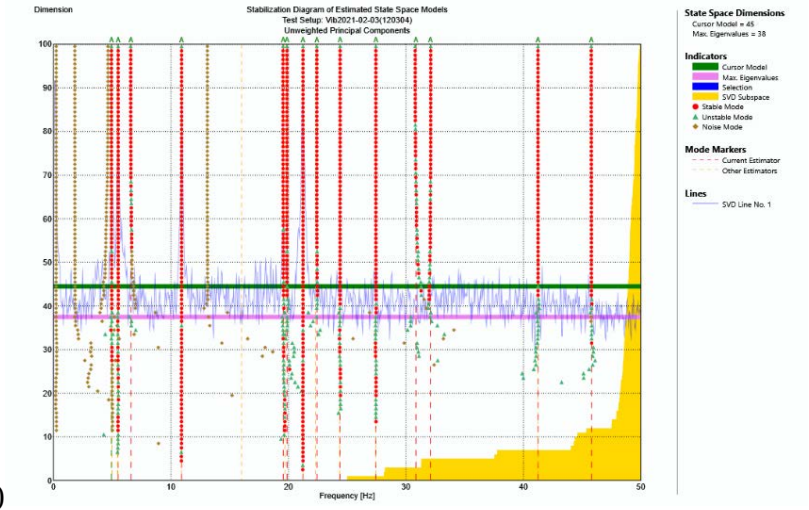

(b)

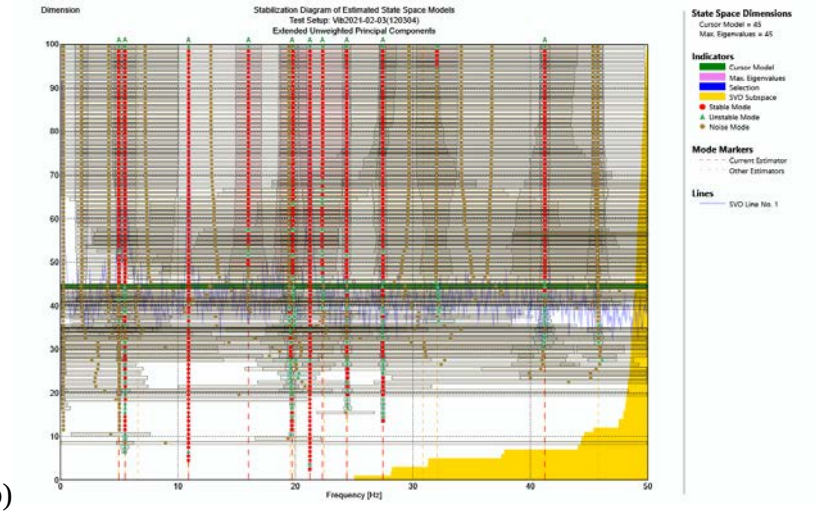

(c)

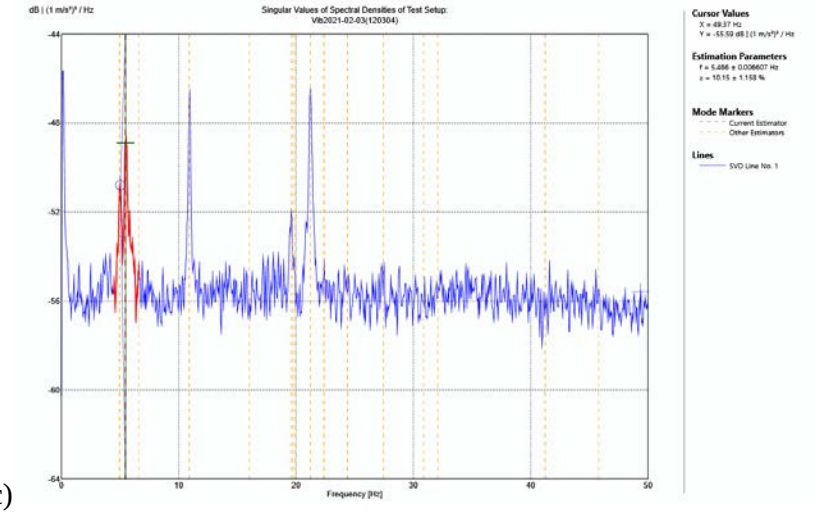

Figure 36: Trial 2 iPhone 6 ARTeMIS OMA results using: (a) UPC; (b) UPCX; (c) EFDD.

(a)

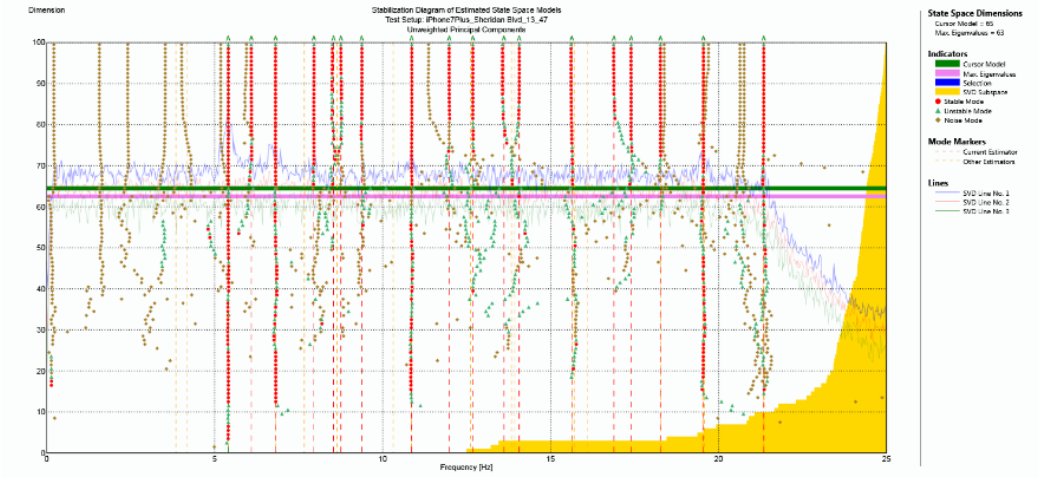

(b)

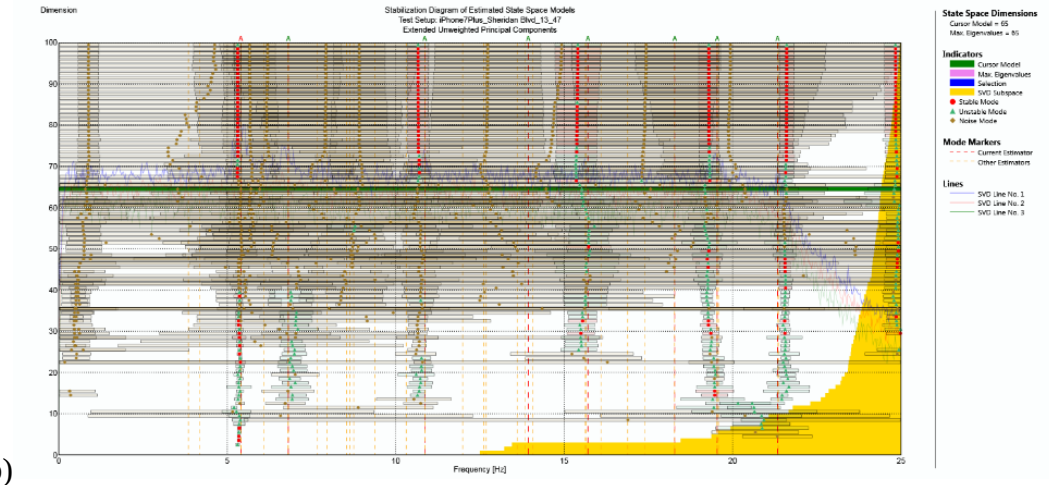

Figure 37: Trial 3 iPhone 7+ ARTeMIS OMA results using: (a) UPC; (b) UPCX.

First Trial, PCB:

Figure 38 shows estimated modes using UPC, UPCX and EFDD. UPC estimated a first mode of 5.3 Hz. UPCX estimated the frequency at 7 Hz but automatically excluded a dynamic frequency of 5.7 Hz because it featured an uncertainty that was slightly over default tolerance settings in ARTeMIS. The EFDD method also showed a distinct peak at 5.8 Hz. Good agreement with the iPhone was demonstrated.

Second Trial, PCB:

As shown in Figure 39, in this trial, UPC estimated the first frequency at 3.85 Hz. However, UPCX shows high uncertainty for this frequency. UPCX estimated a stable first frequency of 5.9 Hz with a damping ratio of 2.5%. These discrepancies were attributed to the high uncertainty for the estimated mode at 3.85 Hz using UPC and, as a result, it could not be detected using UPCX. Similar frequency and damping ratio results were obtained using EFDD.

(a)

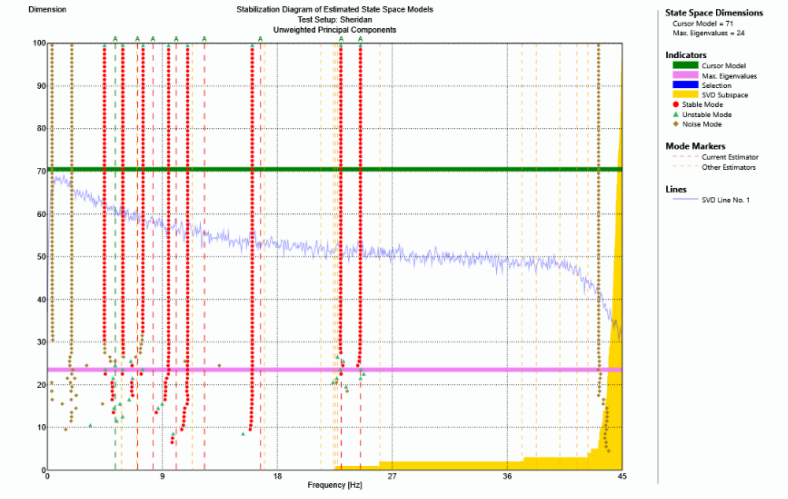

(b)

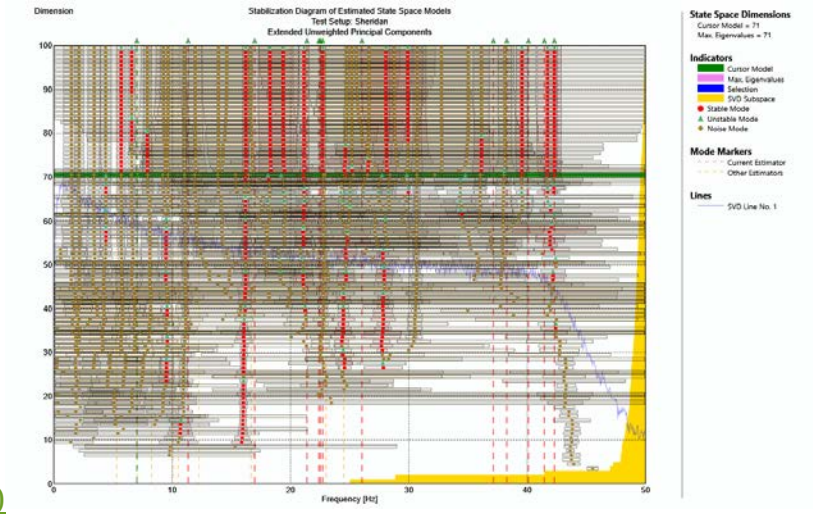

(c)

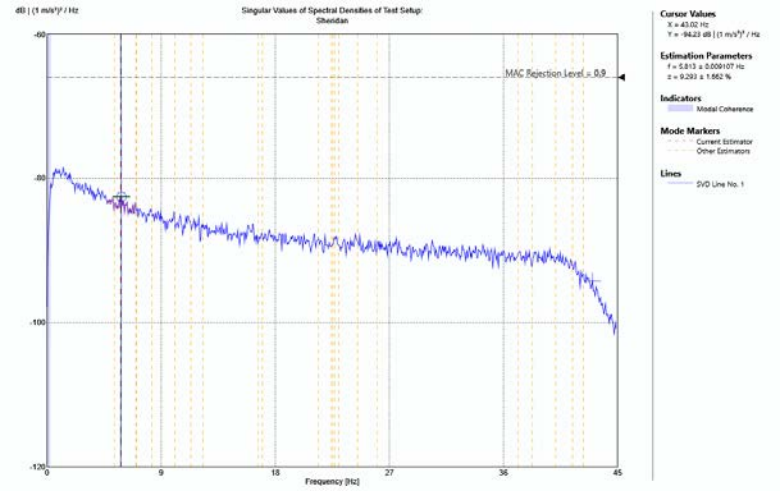

Figure 38: Trial 1 PCB ARTeMIS OMA results using: (a) UPC; (b) UPCX; (c) EFDD.

(a)

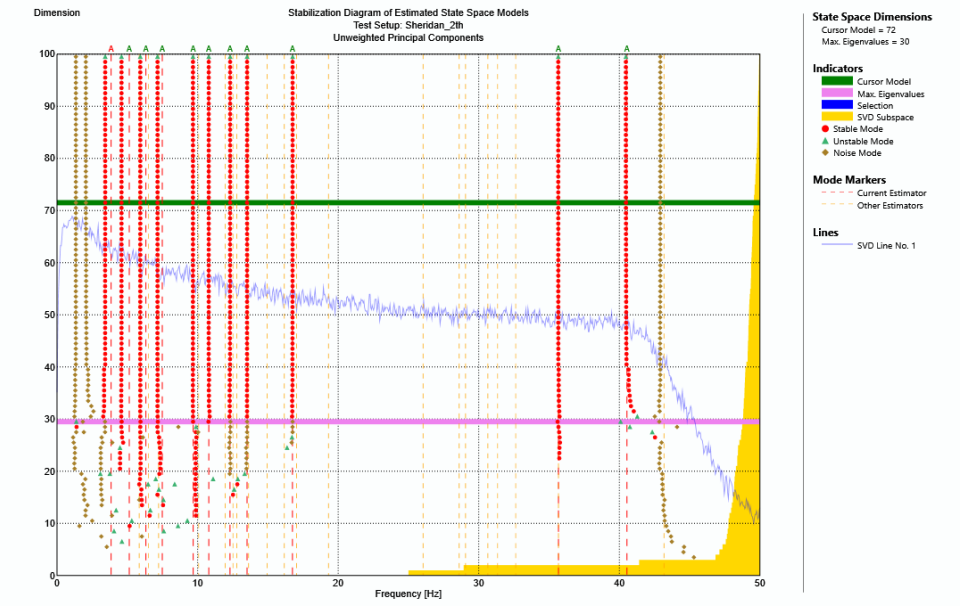

(b)

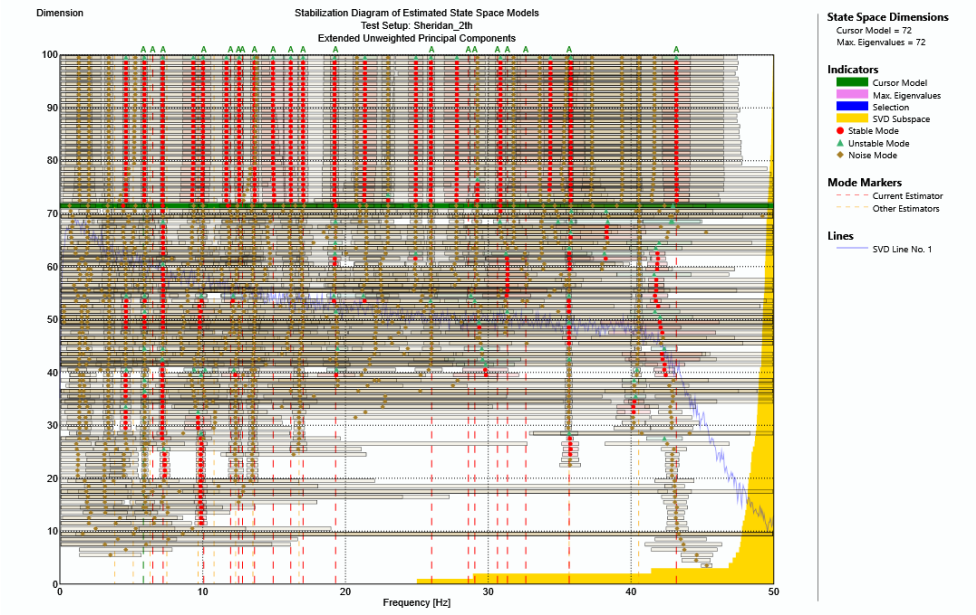

Figure 39: Trial 2 PCB ARTeMIS OMA results using: (a) UPC; (b) UPCX.

4.1.5 Case Study 5: O Street Near 12th Street (ID # U142503455)

4.1.5.1 Bridge Description

The third bridge is a three-span continuous concrete deck slab. The maximum span length is 64 ft., and its width is 94.2 ft. Figure 40 shows relevant views of the bridge from Google Maps.

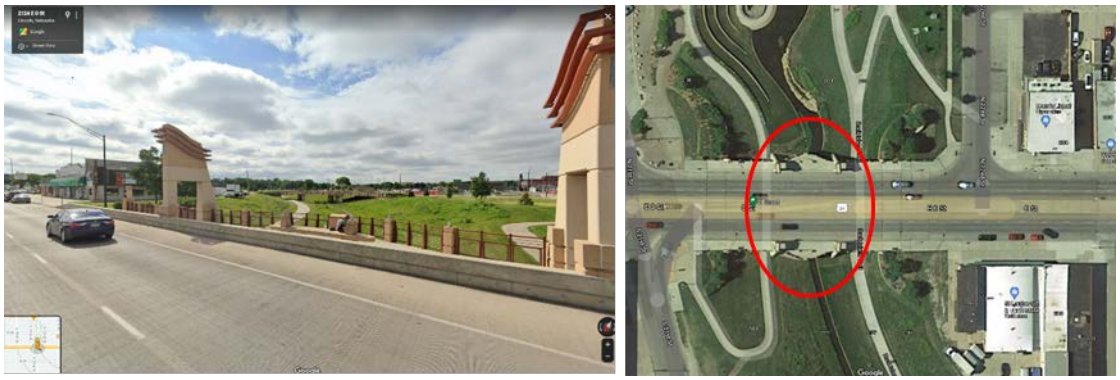

Figure 40: Street and satellite Views of O St. bridge from Google Maps [23].

4.1.5.2 Field Testing and Data Collection

The bridge was tested under operational loads. Dynamic tests were conducted with iPhone and PCB sensors deployed at mid-span and adjacent to the sidewalk. Data from two different iPhones was collected and processed using the VibSensor iOS app at its maximum sampling frequency of 100 Hz. Two iPhones were examined to again examine if cellphone version/type affected results. The PCB sensor recorded data at its minimum sampling frequency of 4000 Hz. Figure 41 shows recorded accelerations for the iPhone and PCB.

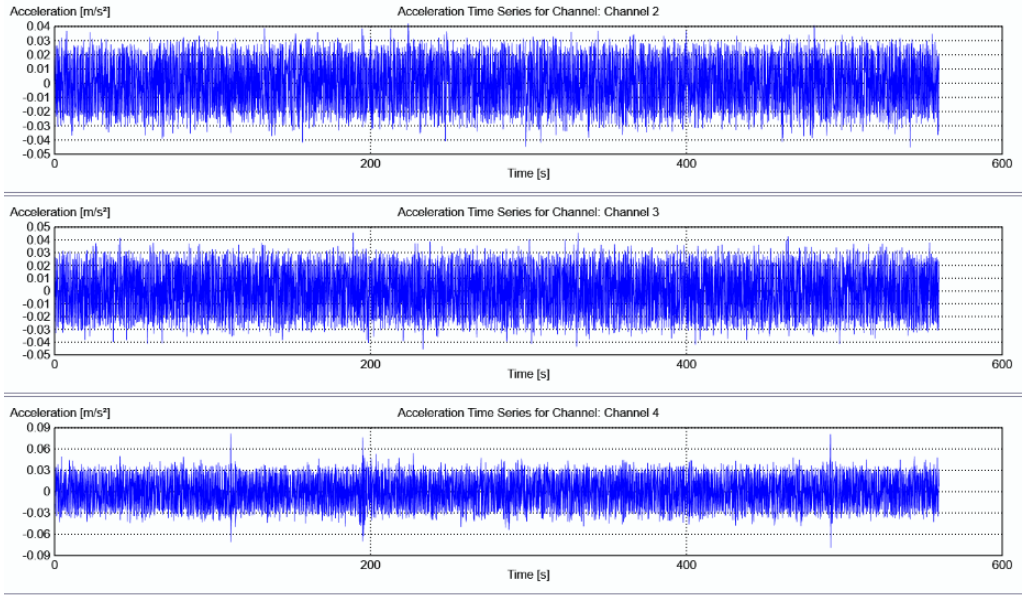

(a)

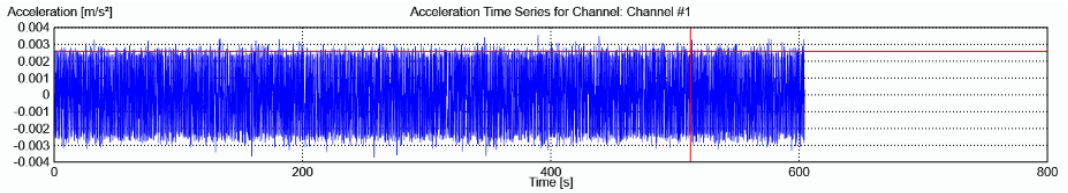

(b)

Figure 41: Recorded acceleration data using: (a) iPhone7+ and (b) PCB.

4.1.5.3 OMA Results

The bridge was tested twice. Two sensors were located at mid-span along one side of the bridge and the test was repeated with the sensors in the same location the other side of the bridge.

First Trial, iPhone 6:

The frequency of the first mode was estimated at 5.9 Hz using the UPC method with the damping ratio estimated at 4.6%. Since the damping ratio was higher than expected, the next estimated frequency was examined. It was estimated at approximately 8.31 Hz using UPC with a corresponding damping ratio of 2.7%. The UPCX method estimated close values to this frequency

and damping ratio. As a result, the first mode frequency and corresponding damping ratio were estimated at 8.3 Hz and 2.2%. Figure 42 shows OMA results for this trial. Similar results for the frequency and damping ratio were obtained using EFDD.

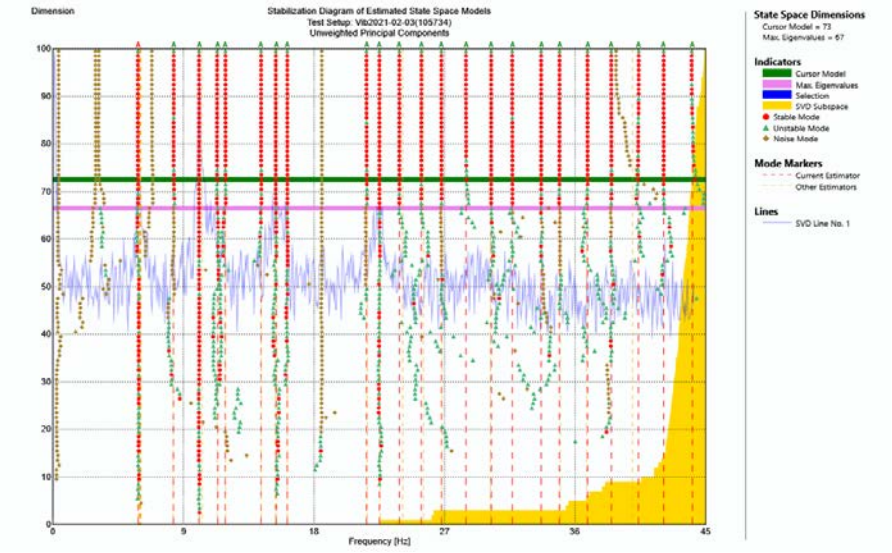

(a)

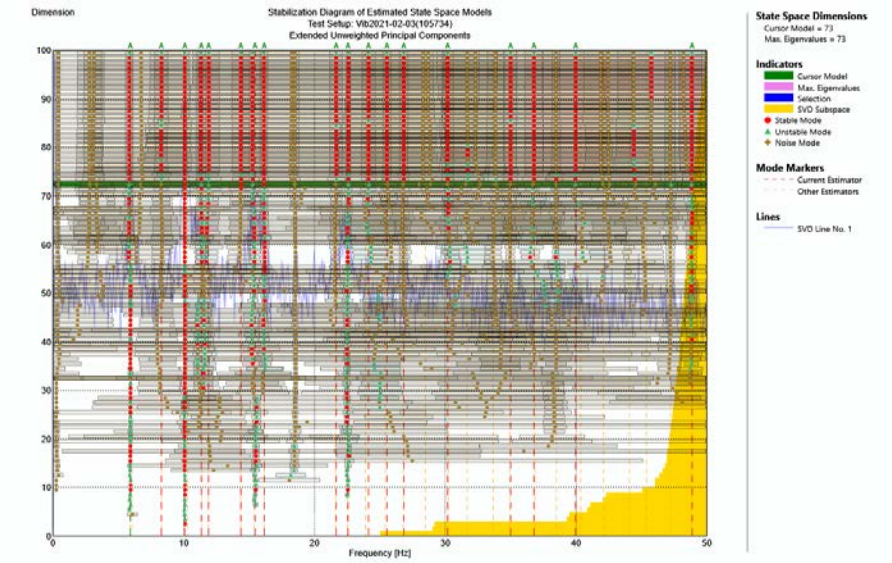

(b)

Figure 42: Trial 1 iPhone 6 ARTeMIS OMA results using: (a) UPC; (b) UPCX.

Second Trial, iPhone 7+:

Data for the second trial was collected using an iPhone 7+. Results using the advanced UPC estimator are shown in Figure 43. The advanced estimator was used as it automatically estimated dynamic modes and provides a similar first frequency of 8.3 Hz, which agreed well with the iPhone 6.

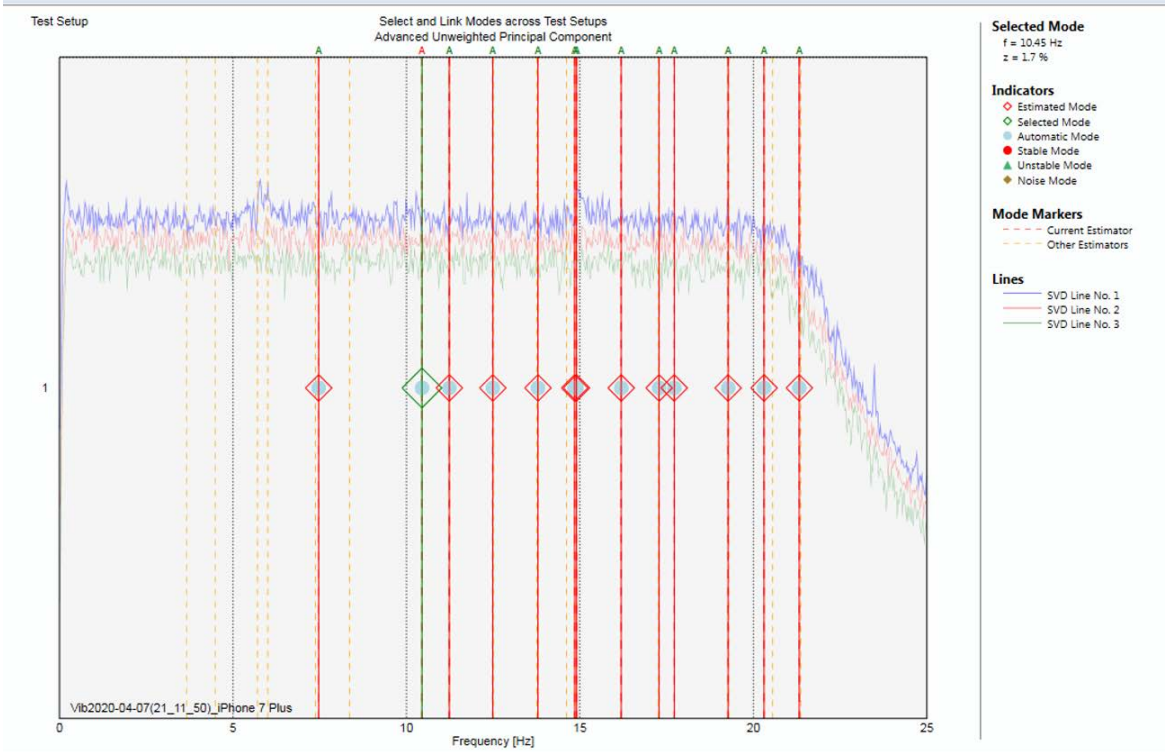

Figure 43: Trial 2 iPhone 7+ ARTeMIS OMA results using advanced UPC.

First Trial, PCB:

For this trial, the UPCX estimator was used to identify modes from the PCB sensor. As shown in Figure 44, the corresponding frequency for the first stable mode was 8.3 Hz. The estimated damping ratio for this mode was 2.5%. Similar estimations were obtained using EFDD and UPC.

Second Trial, PCB:

The UPCX method was again used to estimate the first modal frequency. Figure 45 indicates that first identified mode had a frequency of 6 Hz. This mode was not stable due to high uncertainty and a corresponding negative damping ratio. Therefore, the identified frequency of 8.64 Hz was identified as the first mode. The corresponding damping ratio for this mode was 2.5%. Similar results were obtained using EFDD and UPC.

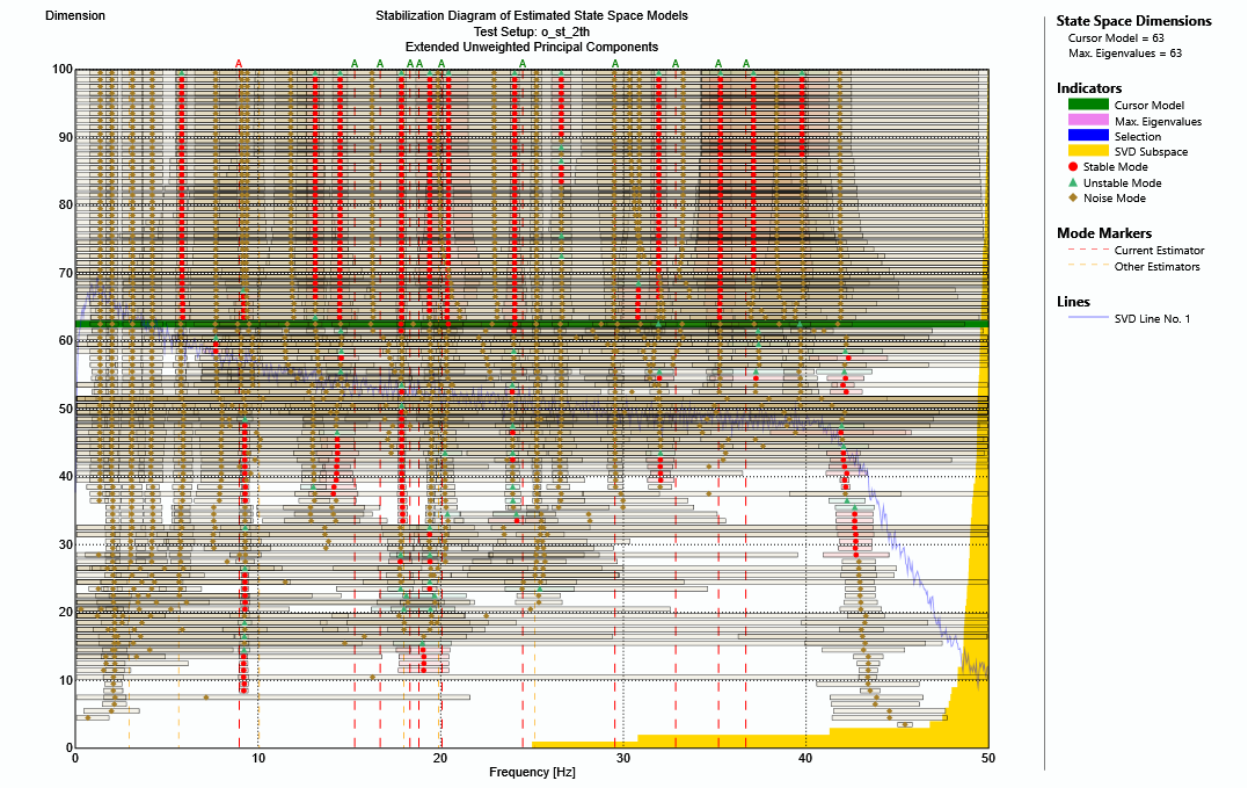

Figure 44: Trial 1 PCB ARTeMIS OMA results using UPCX.

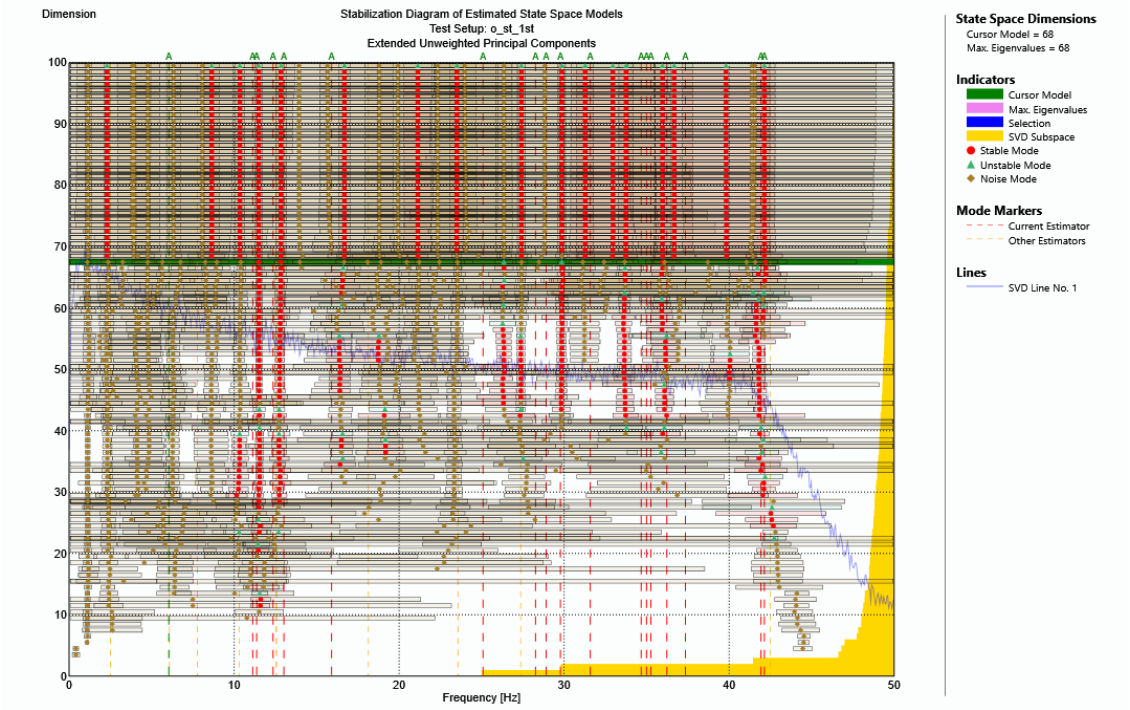

Figure 45: Trial 2 PCB ARTeMIS OMA results using UPCX.

4.1.6 Case Study 6: J Street and 24th Street (ID # U142503410P)

4.1.6.1 Bridge Description

The bridge is a three-span continuous concrete slab. The maximum span length is 42 ft., and the concrete slab is 60.0 ft. wide. Figure 46 shows multiple bridge views, one from Google Maps.

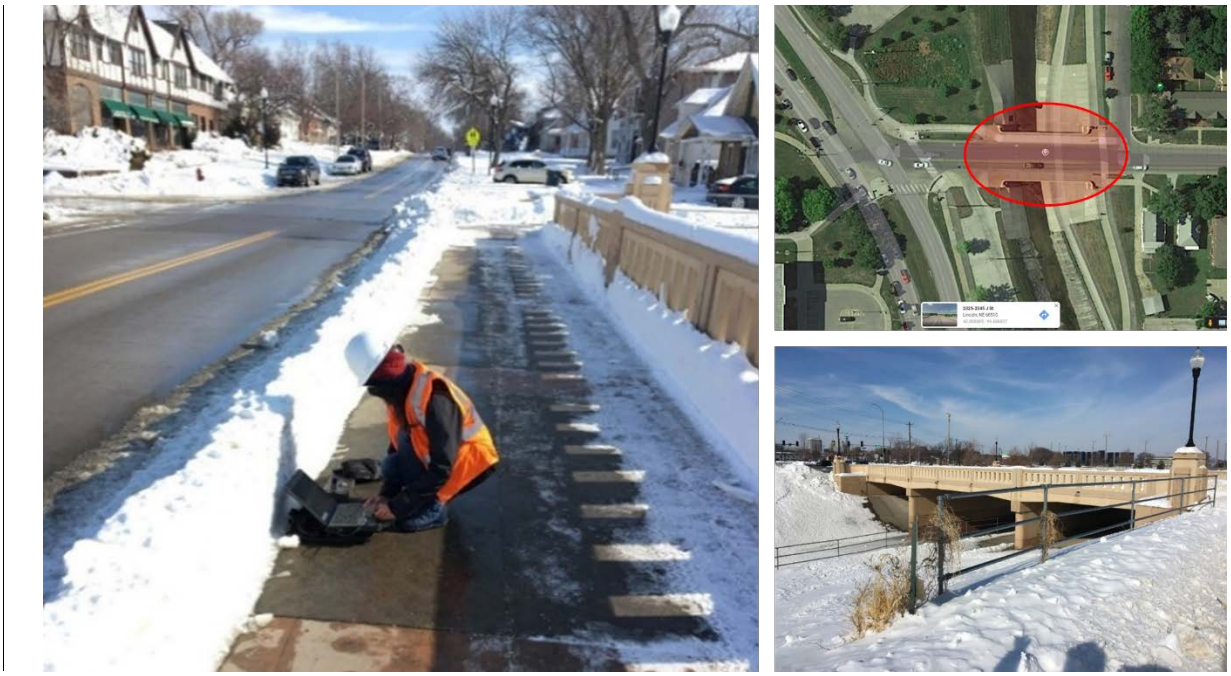

Figure 46: Multiple views of J St. bridge

4.1.6.2 Field Testing and Data Collection

The bridge was tested twice under operational loads. Dynamic tests were conducted with iPhone and PCB sensors deployed at mid-span and adjacent to the sidewalk. Data from the iPhone was collected and processed using the VibSensor iOS app at its maximum sampling frequency of 100 Hz. The PCB sensor recorded data at its minimum sampling frequency of 4000 Hz. Figure 47 shows recorded data.

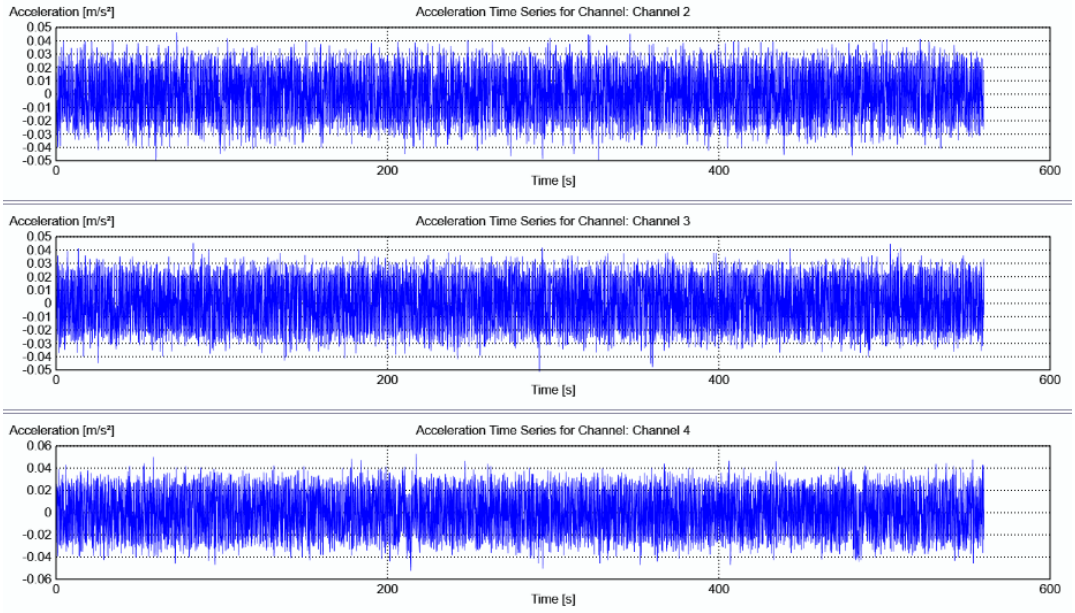

(a)

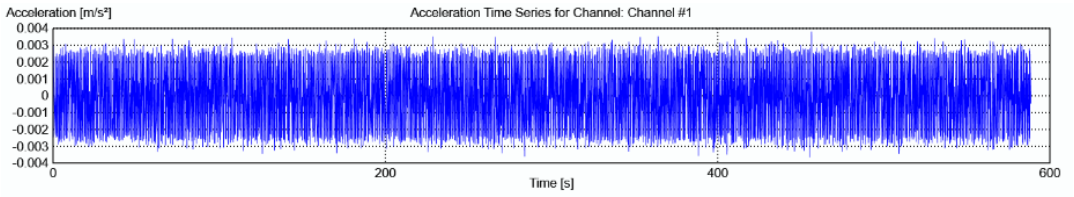

(b)

Figure 47: Recorded acceleration data using: (a) iPhone and (b) PCB.

4.1.6.3 OMA Results

First Trial, iPhone 6:

UPC and UPCX were used to estimate the first modal frequency. As Figure 48 shows, the frequency is estimated 6 Hz and 5.9 Hz using the UPC and UPCX methods.

Second Trial, iPhone 6:

UPCX was used for estimation of the first natural frequency for Trial 2. Figure 49 shows that modal estimation was not successfully performed for this trial indicating that, for this type and size

of bridge, the iPhone sensor may not be a proper dynamic measurement device. Similar estimations were obtained using EFDD and UPC.

First Trial, PCB:

As shown in Figure 50, in this trial UPCX was used to identify the modes. The first modal frequency and corresponding damping ratio was 8.41 Hz and 1.24%, respectively. Comparison between results from the iPhone and PCB sensor shows that the PCB sensor detected more stable modes compare to the iPhone. Similar estimations were obtained using EFDD and UPC.

Second Trial, PCB:

The UPCX method was used to estimate the first natural frequency. As shown in Figure 51, the first frequency was determined to be 3.36 Hz with a corresponding damping ratio of 2.68%. It seems that the deviation in the obtained results is high for this case and modal analysis needed more investigation. Similar estimations were obtained using EFDD and UPC.

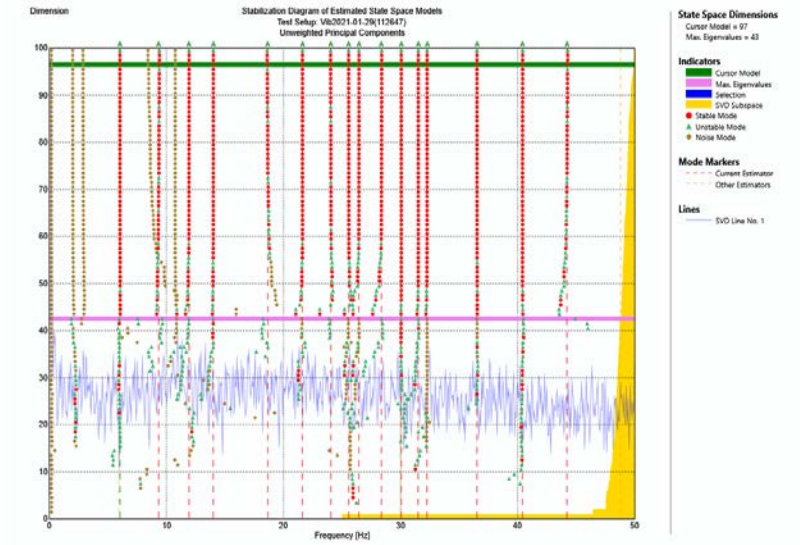

(a)

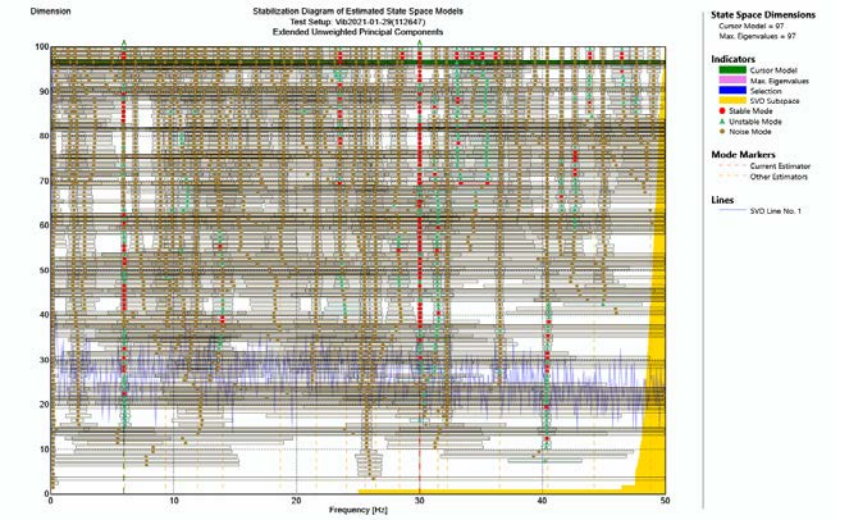

(b)

Figure 48: Trial 1 iPhone 6 ARTeMIS OMA results using: (a) UPC; (b) UPCX.

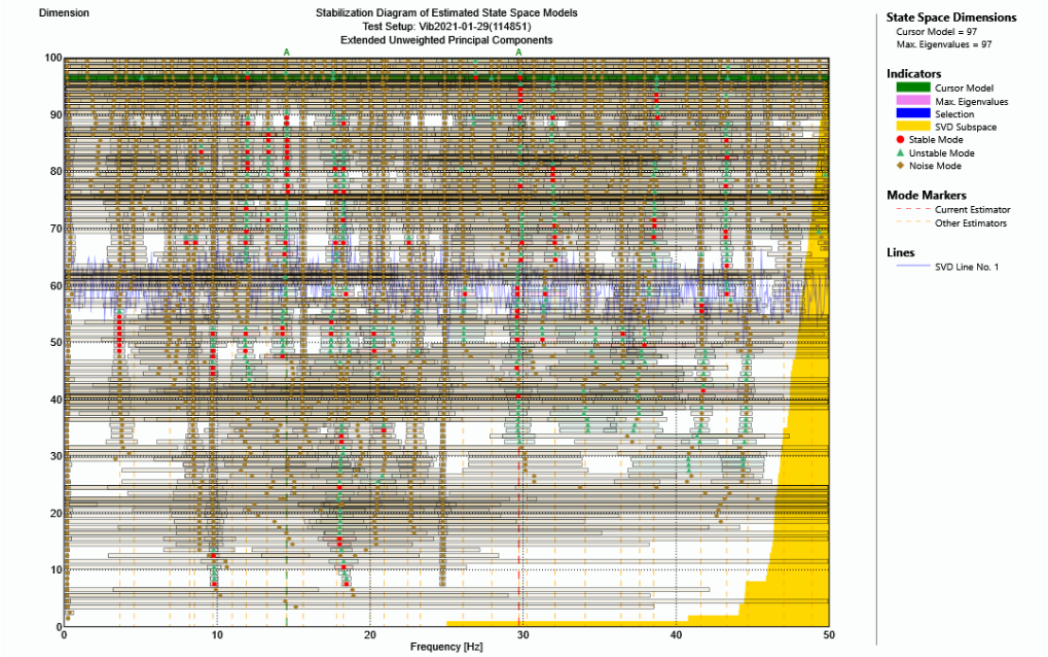

Figure 49: Trial 2 iPhone 6 ARTeMIS OMA results using UPCX.

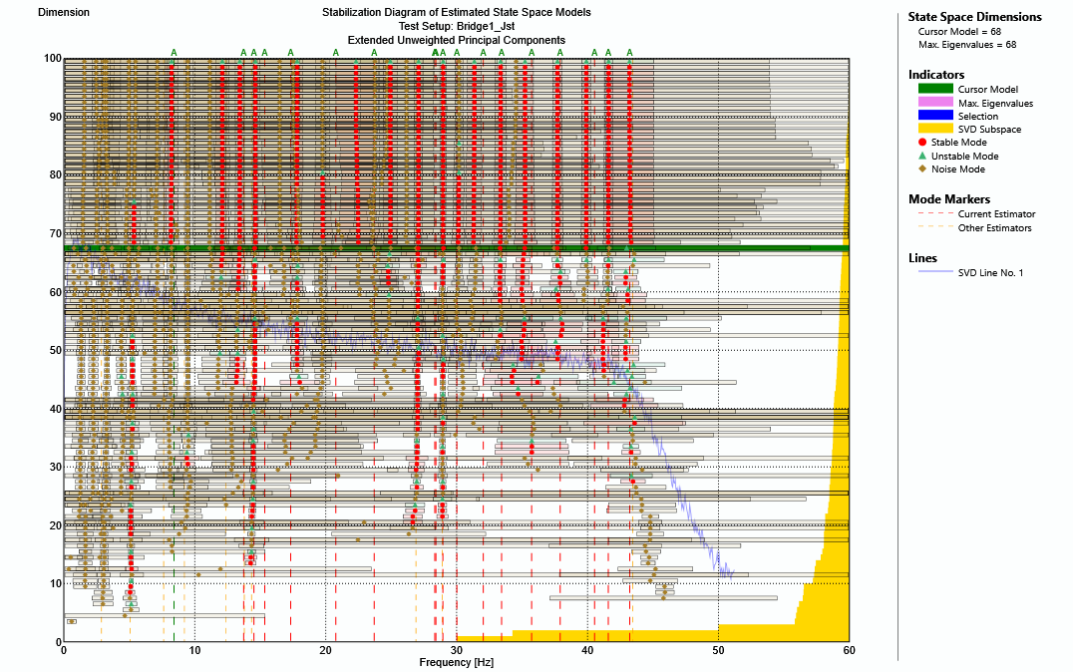

Figure 50: Trial 1 PCB ARTeMIS OMA results using UPCX.

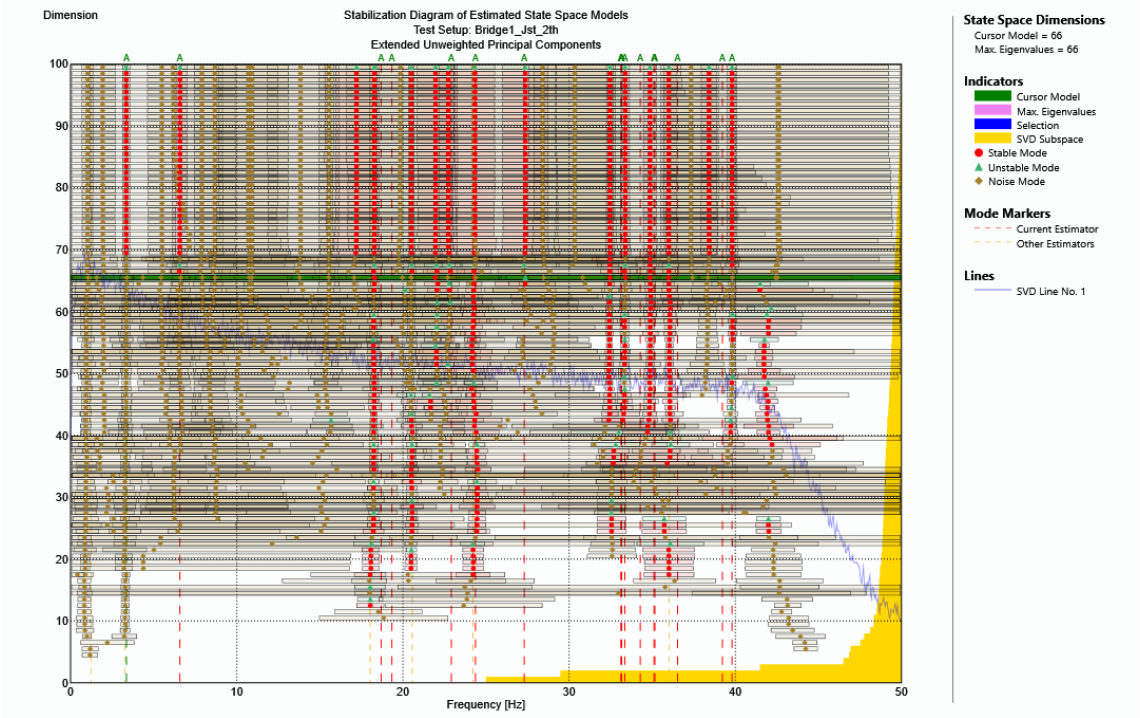

Figure 51: Trial 2 PCB ARTeMIS OMA results using UPCX.

4.1.7 Case study 7: A Street Near Capitol Parkway (ID # U142503610)

4.1.5.1 Bridge Description

The A Street bridge consists of three concrete box culverts. The largest span is 35.1 ft. Figure 52 shows the relevant photos of the bridge, some from Google Maps.

Figure 52: Street and satellite views of the A St. bridge from Google Maps [23]

4.1.7.2 Field Testing and Data Collection

Dynamic tests were conducted with iPhone and PCB sensors deployed at mid-span adjacent to the sidewalk. Data from two different iPhones was collected and processed using the VibSensor iOS app at its maximum sampling frequency of 100 Hz. Two iPhones were examined to determine if cellphone version/type affected results. The PCB sensor recorded data at its minimum sampling frequency of 4000 Hz. Figure 53 shows the recorded data.

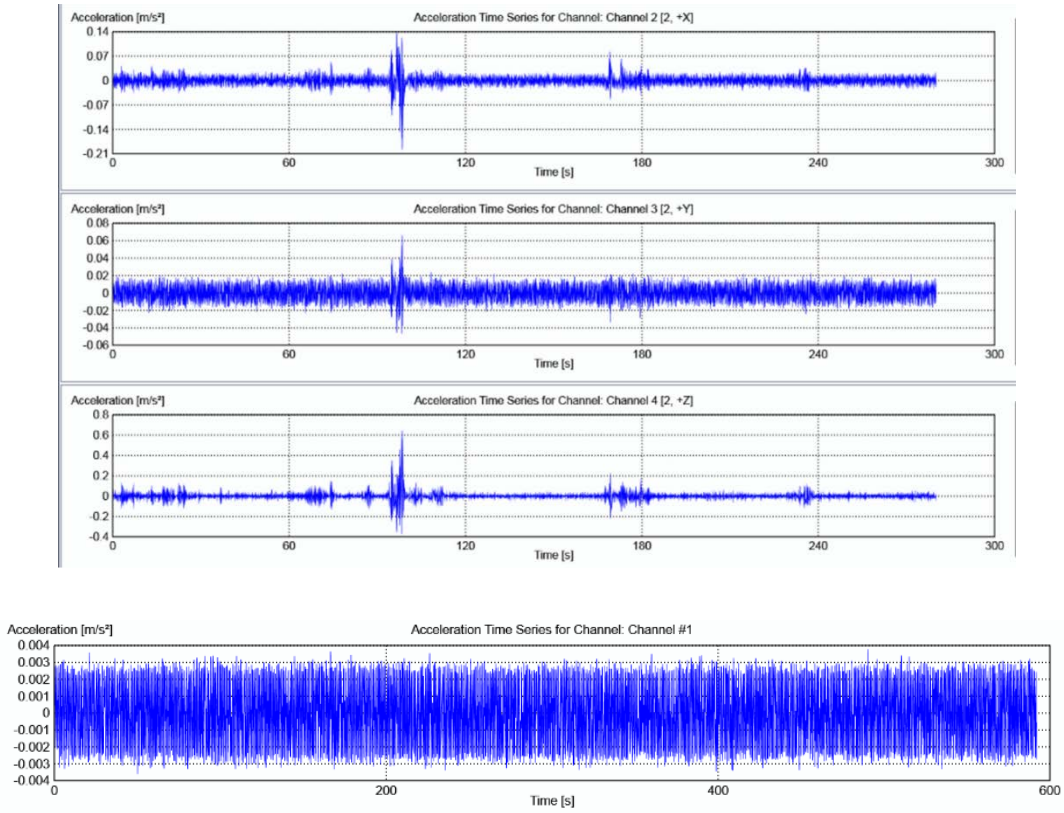

Figure 53: Recorded acceleration data using: (a) iPhone and (b) PCB.

4.1.7.3. OMA Results

First Trial, PCB:

Modal estimation for this trial shows that the first identified mode has the frequency 6.14 Hz using UPCX method. However, the damping ratio for the estimated mode was higher than the accepted range for typical bridge systems. Therefore, the next mode with frequency 7.53 Hz and the damping ratio of 3.35% is obtained for this trial. Figure 54 shows the results of modal estimation for this trial. Similar estimations were obtained using EFDD and UPC.

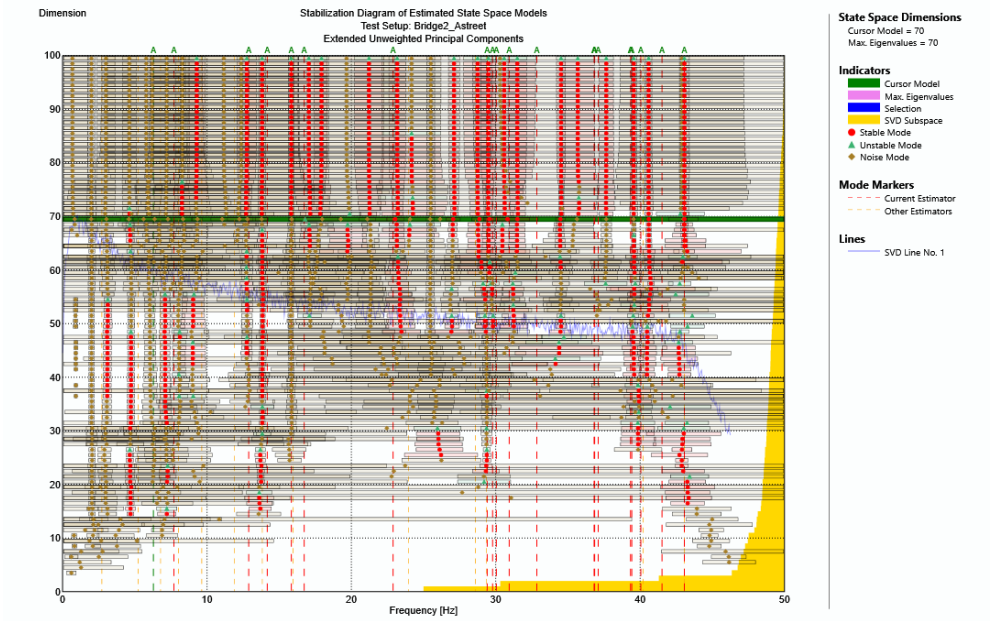

(a)

Figure 54: Trial 1 PCB ARTeMIS OMA results using UPCX.

Second Trial, PCB:

Figure 55 shows PCB OMA results using the UPCX methods. When using SSI-UPC the first dynamic frequency and its corresponding damping ratio were 3.92 Hz and 1.44%. Similar estimations were obtained using EFDD and UPC.

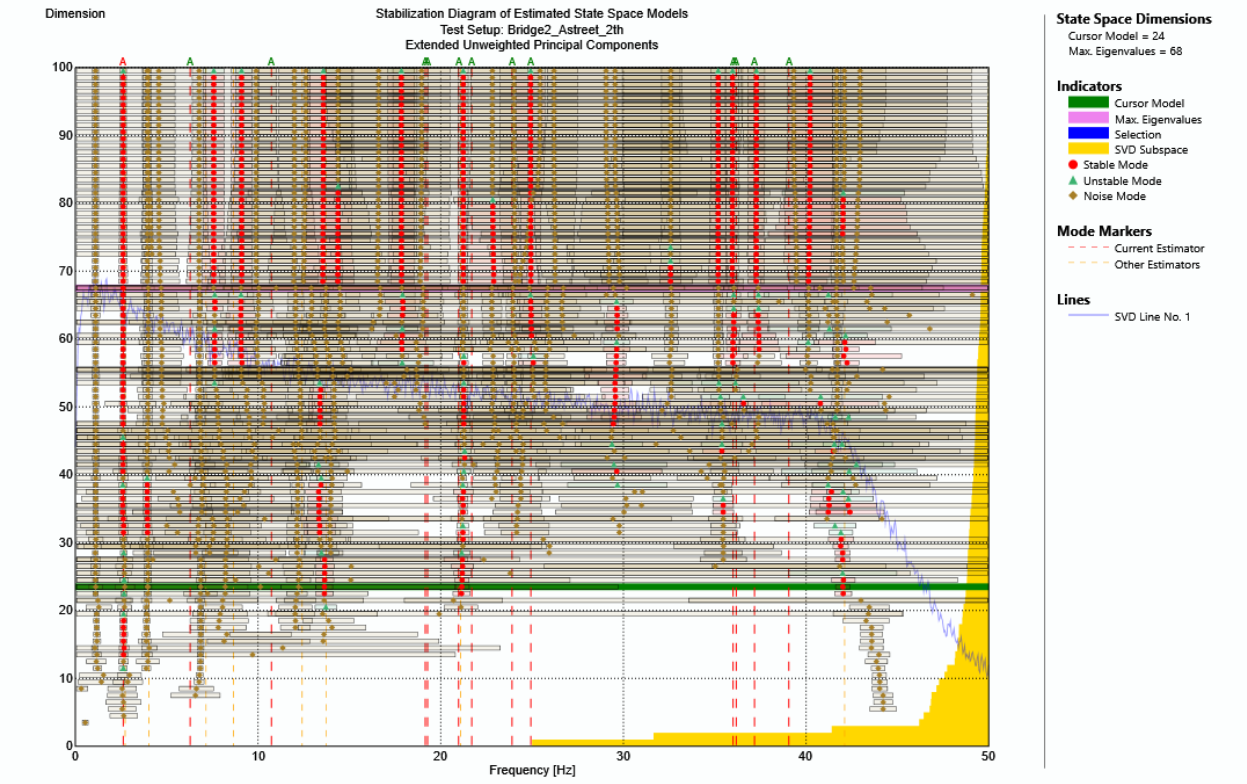

Figure 55: Trial 2 PCB ARTeMIS OMA results using UPCX.

First Trial, iPhone 6:

Figure 56 shows iPhone 6 OMA results using the EFDD, UPC and UPCX methods. When using SSI-UPC the first dynamic frequency and its corresponding damping ratio were 2.33 Hz and 1.06% (Figure 56a). When using SSI-UPCX the first dynamic frequency and its damping ratio were 7.09 Hz and 1.38% (Figure 56b). Discrepancy between results using these two estimators was due to high uncertainty associated with the UPC estimation. Using FDD and its peak-picking method, the spectra peak at that corresponding band is shown (Figure 56c) and, based on these results, the UPCX estimation was selected.

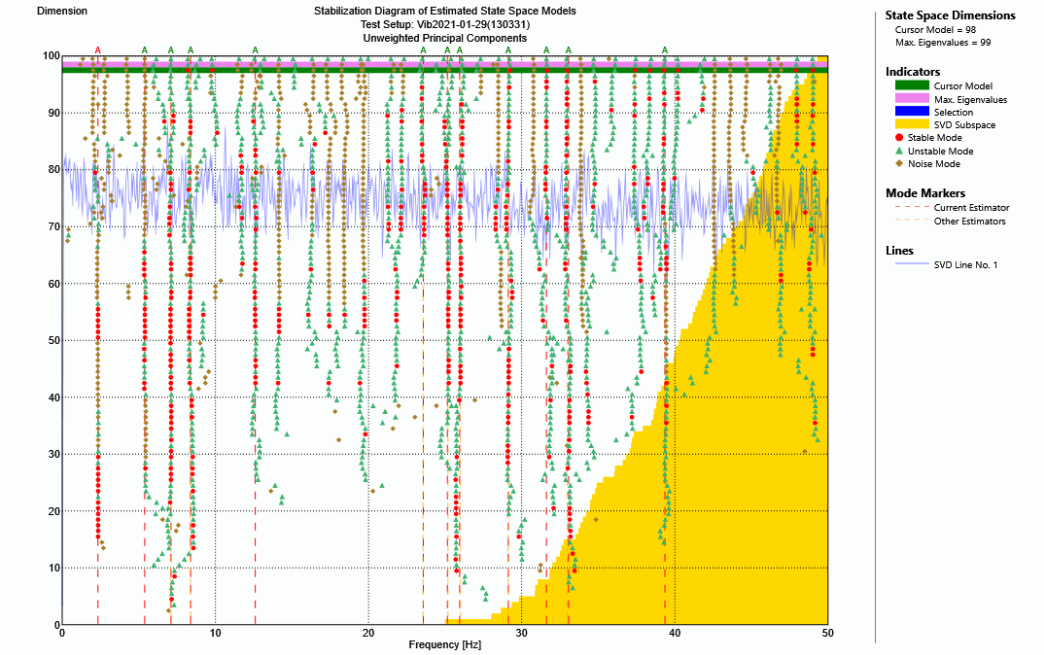

(a)

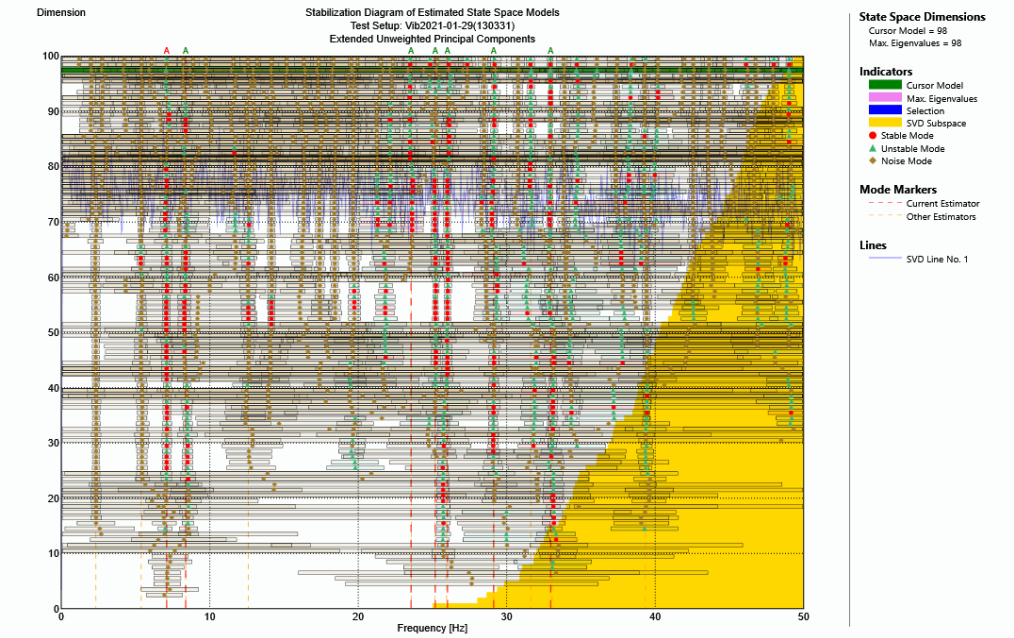

(b)

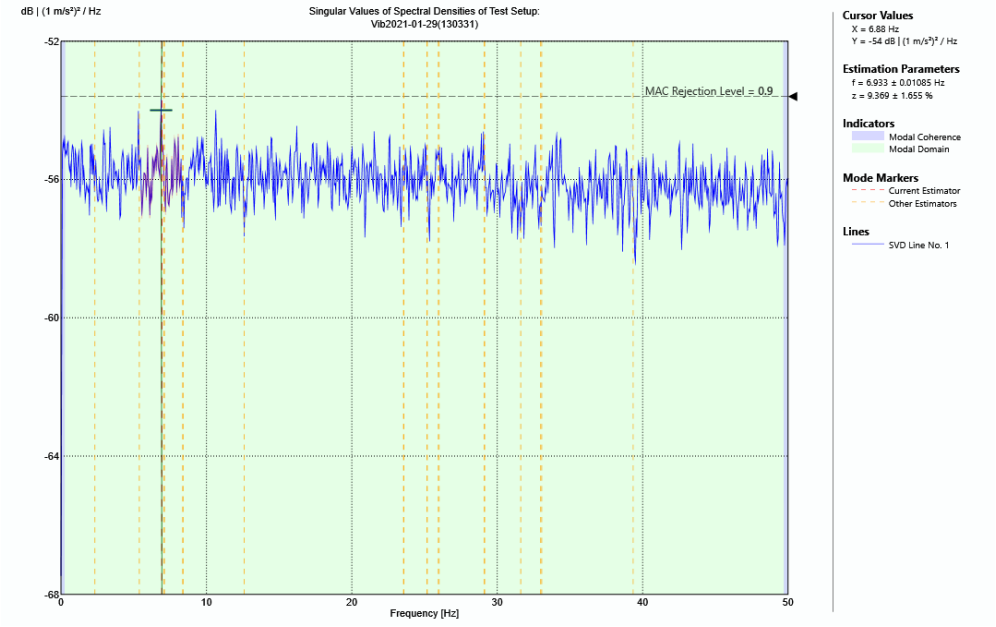

(c)

Figure 56: Trial 1 iPhone 6 ARTeMIS OMA results using: (a) UPC; (b) UPCX; (c) EFDD.

Second Trial, iPhone 7+:

Another test was completed using an iPhone 7+. As shown in Figure 57, estimated values for frequency for the first mode agree with results from trials one and two. Figure 57 also shows iPhone 7+ OMA results using the FDD and UPCX methods. When using FDD the first dynamic frequency had a peak at 7.1 Hz. When using SSI-UPCX the first dynamic frequency and its damping ratio were 7.1 Hz and 2.1%. respectively. Similar results were obtained using EFDD and UPC.

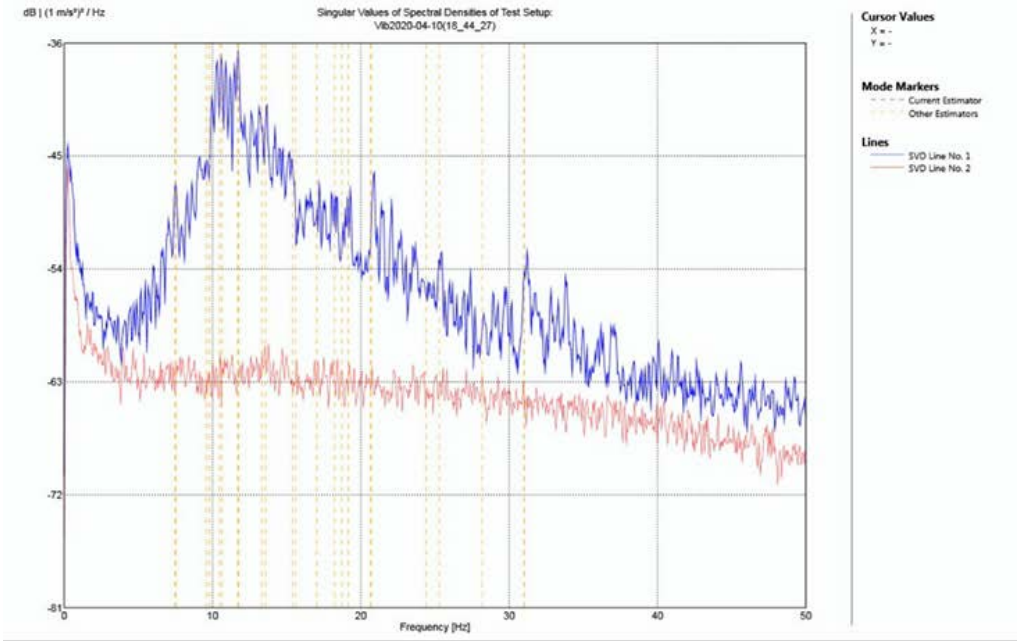

(a)

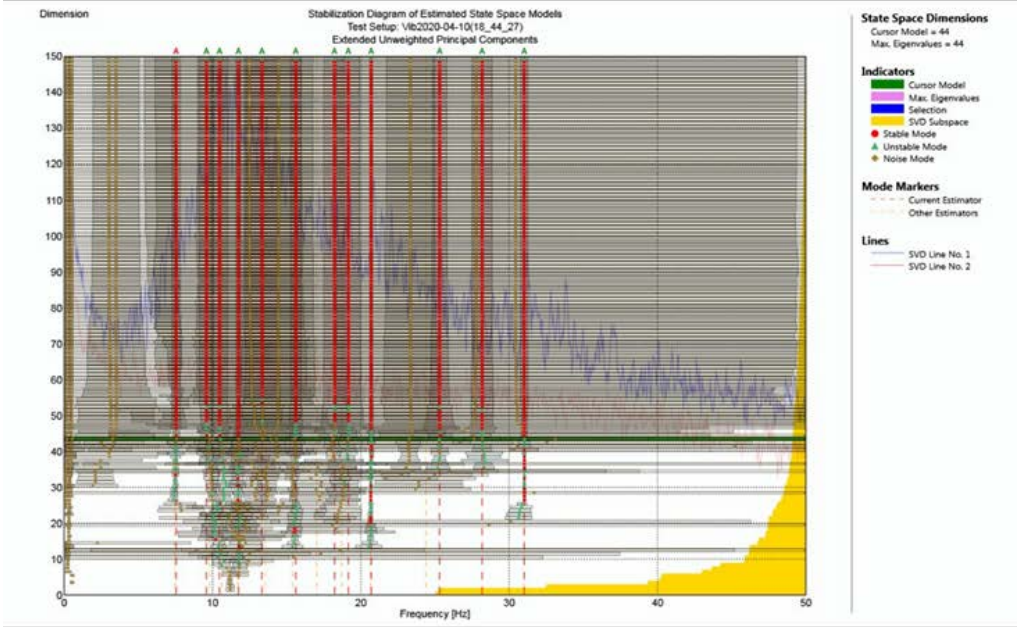

(b)

Figure 57: Trial 2 iPhone 7+ ARTeMIS OMA results using: (a) FDD; (b) UPCX.

4.1.8 Case study 8: 70th Street Near Holmes Lake Park (ID # U142503113)

4.1.8.1 Bridge Description

The Case Study 6 bridge is a three-span continuous concrete slab. Its maximum span length is 27.9 ft. and deck width is 77.4 ft. Figure 58 shows the photos of the bridge from Google Maps.

Figure 58: Satellite and street views of the 70th St. bridge from Google Maps [23]

4.1.8.2 Field Testing and Data Collection

Dynamic tests were conducted with iPhone and PCB sensors deployed at mid-span and adjacent to the sidewalk. Data from two different iPhones was collected and processed using the VibSensor iOS app at its maximum sampling frequency of 100 Hz. The PCB sensor recorded the data at its minimum sampling frequency of 4000 Hz. Figure 59 shows the recorded data.

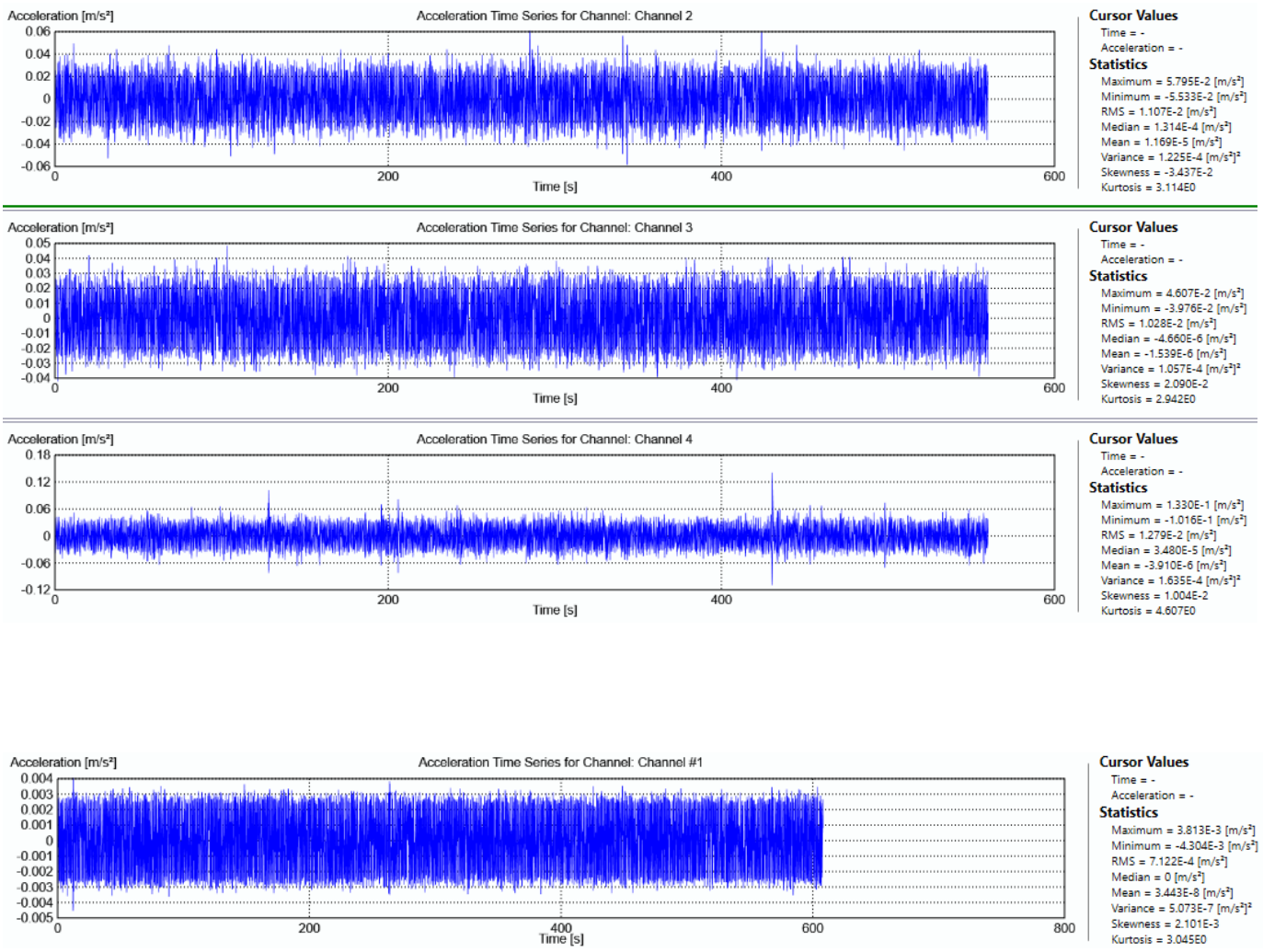

Figure 59: Recorded acceleration data using: (a) iPhone and (b) PCB.

4.1.8.3. OMA Results

First Trial, iPhone 6:

As shown in Figure 60, using the UPC method, the frequency and damping ratio were estimated 7.78 Hz and 2.05%, respectively. The first two identified modes using the UPC method were not acceptable due to high damping ratios and unstable estimation. Using the UPCX method, the first stable frequency and corresponding damping ratio were estimated to be 7.71 Hz and 1.77%.

Second Trial, iPhone 7+:

In similar fashion to bridge tests described previously, to guarantee accuracy of results obtained from a mobile phone, data was collected using a different iPhone. Very good agreement between Trial 2 and Trial 1 results was observed. Figure 61 shows the OMA results using FDD and UPCX methods.

PCB:

As shown in Figure 62, using the UPC method, frequency and damping ratio were estimated 4.33 Hz and 1.49%, respectively. The first identified mode was not acceptable due to the high damping ratio and unstable estimation. The UPCX method provided a first stable frequency and corresponding damping ratio with an acceptable range of uncertainty. These values were estimated at 5.06 Hz and 1.13%, respectively.

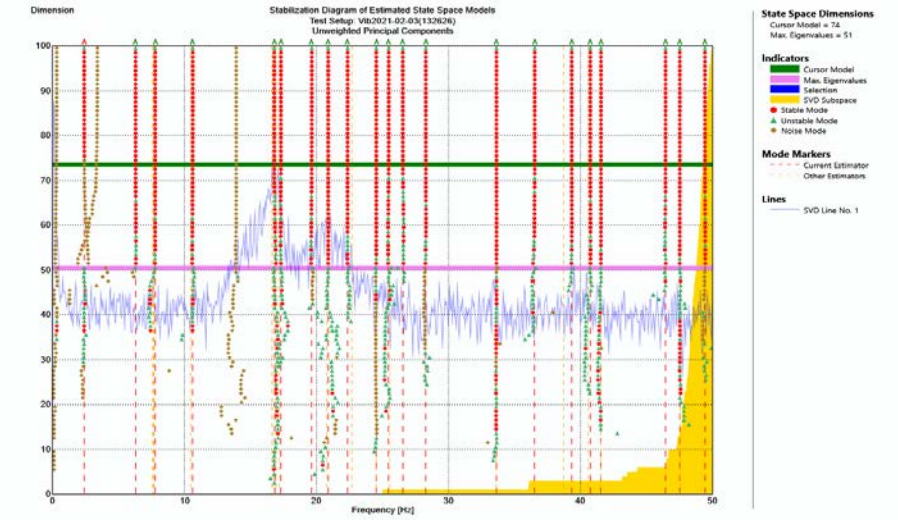

(a)

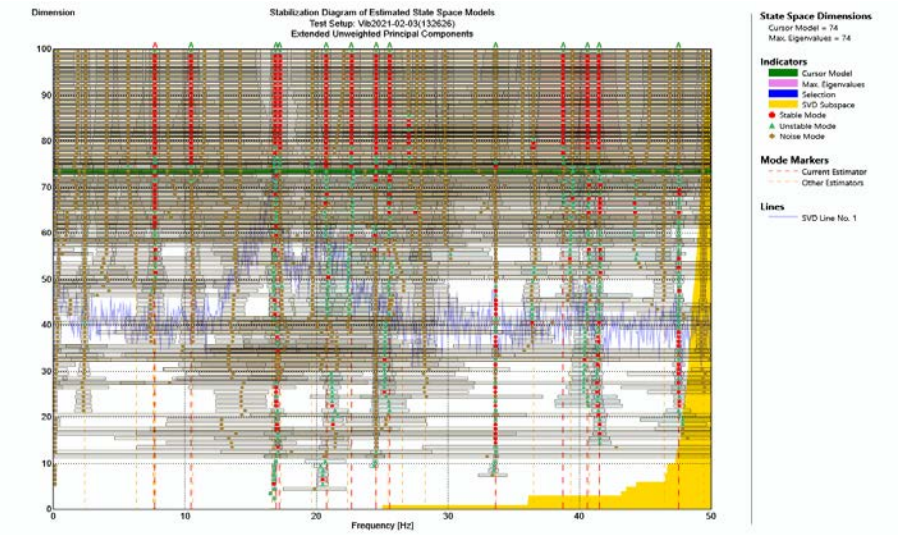

(b)

Figure 60: Trial 1 iPhone 6 ARTeMIS OMA results using: (a) UPC; (b) UPCX.

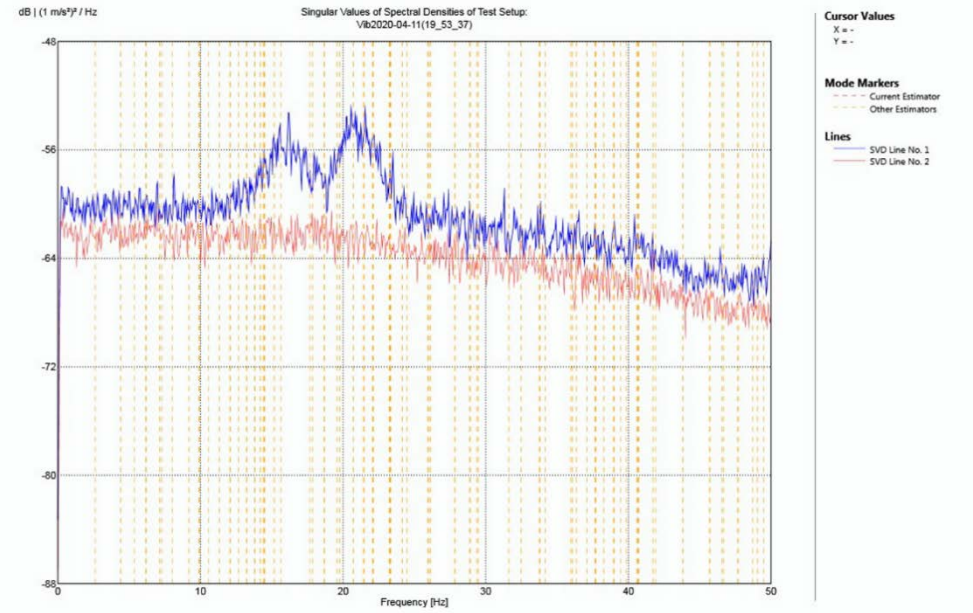

(a)

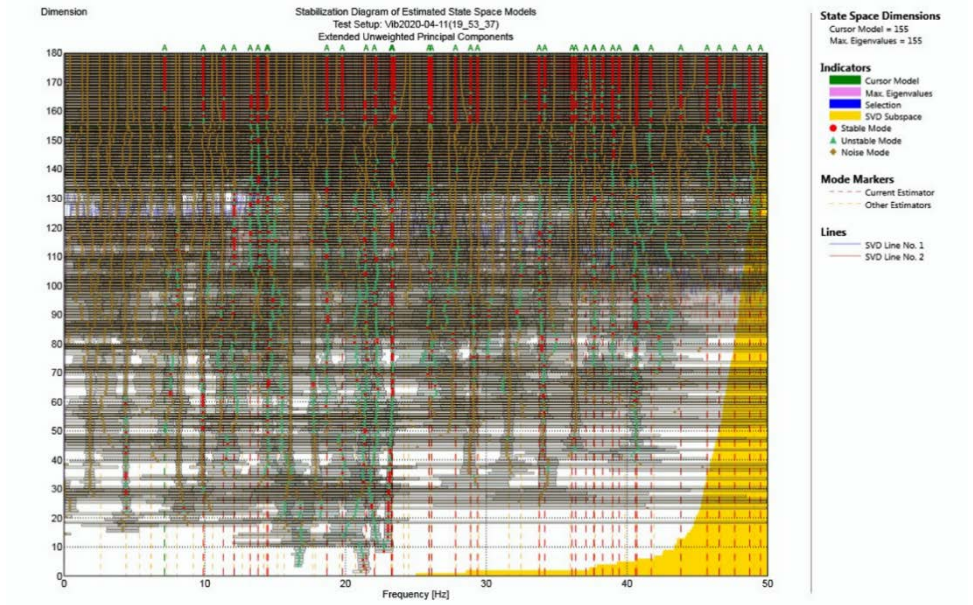

(b)

Figure 61: Trial 2 iPhone 7+ ARTeMIS OMA results using: (a) FDD; (b) UPCX.

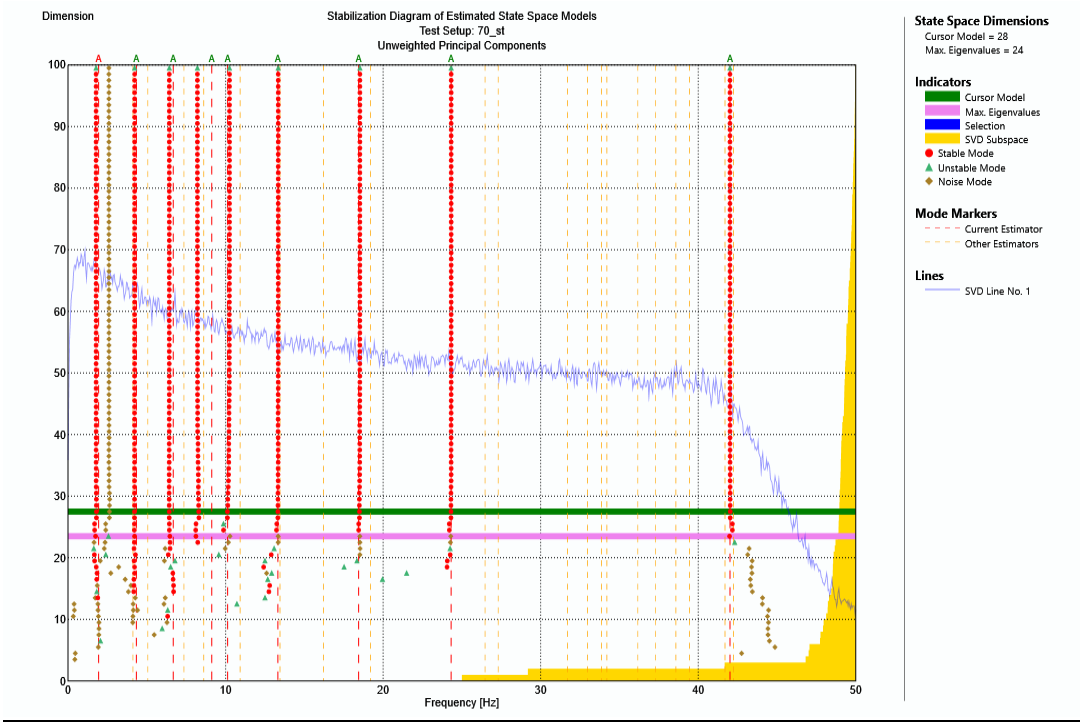

(a)

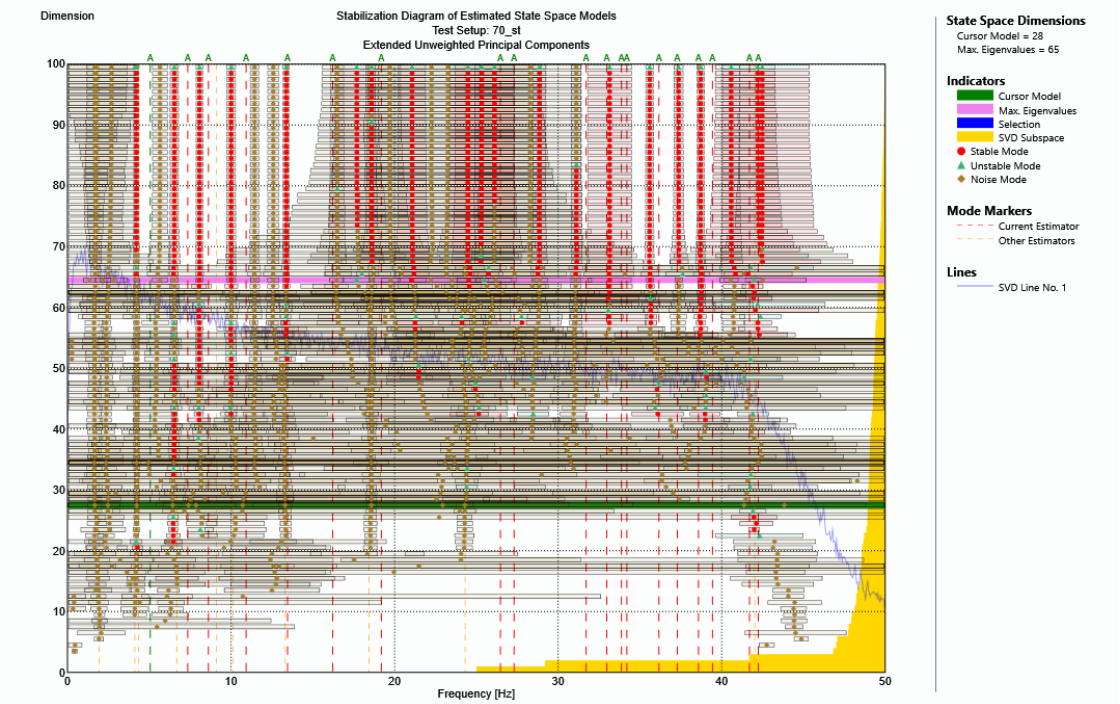

(b)

Figure 62: PCB ARTeMIS OMA results using: (a) UPC; (b) UPCX.

4.1.9 Case study 9: Holmes Lake Footbridge

4.1.9.1 Bridge Description

A flexible struture was included in the study via inclusion of the Holmes Lake Footbridge, located at Lancaster county. As shown in Figure 63, the footbridge includes a truss with a concrete slab.

Figure 63: Holmes Lake footbridge.

4.1.9.2 Field Testing and Data Collection

This footbridge was tested with an iPhone 7+. The iPhone 7+ was deployed along the edge of the bridge at mid-span. Data was recorded for approximately 150 seconds. Data was collected and processed using VibSensor iOS app with its maximum sampling frequency, 100 Hz. Figure 64 shows the recorded iPhone data.

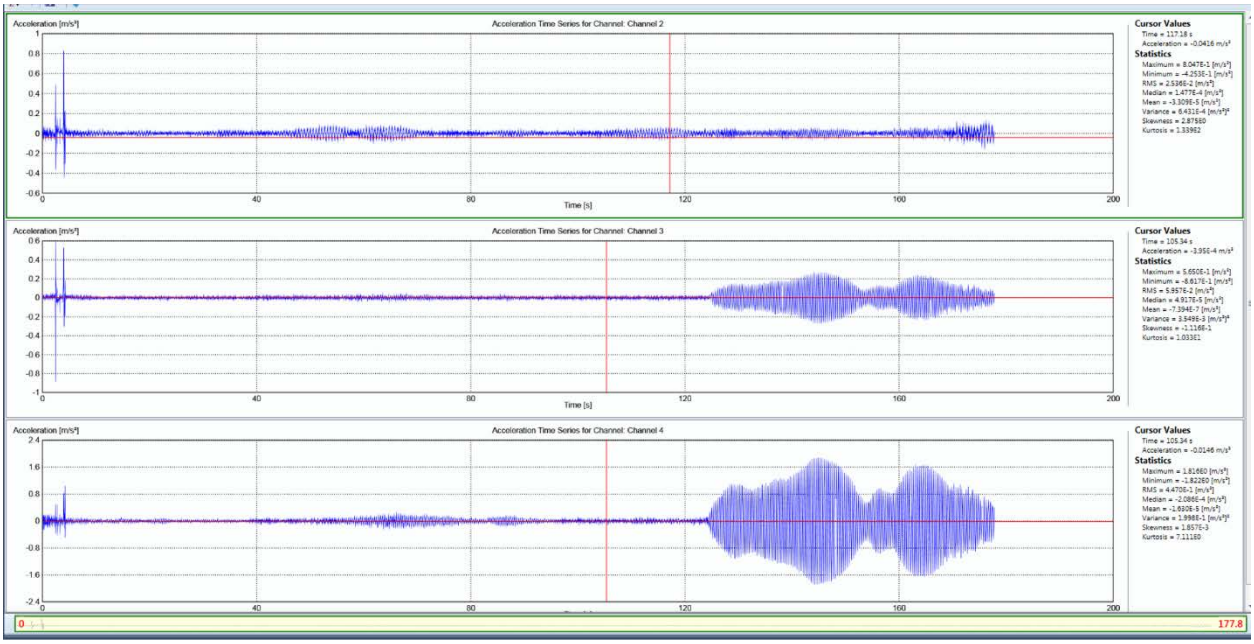

Figure 64: Collected iPhone data.

4.1.9.3. OMA Results

Figure 65 shows iPhone 7+ OMA results using the EFDD, UPC, UPCX methods. Using all three methods, the first dynamic frequency and its corresponding damping ratio were estimated at 2.65 Hz and 0.88%.

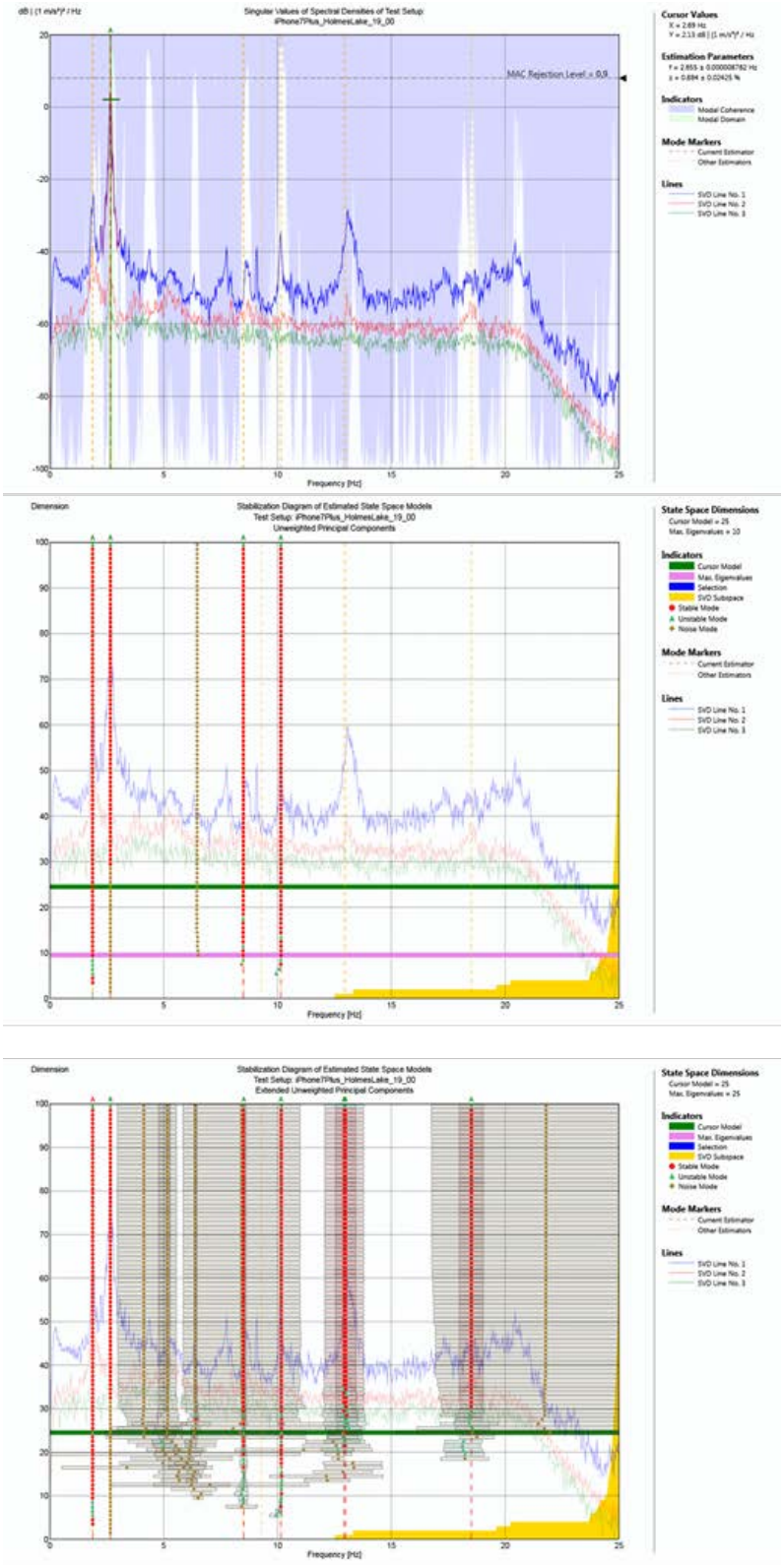

Figure 65: iPhone 7+ ARTeMIS OMA results using: (a) EFDD; (b) UPC; (c) UPCX.

4.2 Nondestructive Load Rating

Three bridges (see Table 2) were used as testbeds for validation of dynamic tests and OMA as tools for bridge load rating. Bridge rating factors were first calculated using OMA results and a FE model. Live load tests and measured strains were then used to determine rating factors and the results from the two approaches were compared.

4.2.1 Case study 1: Fairbury Bridge

4.2.1.1 FE Model Construction

The numerical simulation of the Fairbury Bridge was constructed using SAP2000 v22 [24]. Three-dimensional frame and shell elements were used to complete a dynamic time history analysis under moving truck loads. Views of the model can be found in Figure 66.

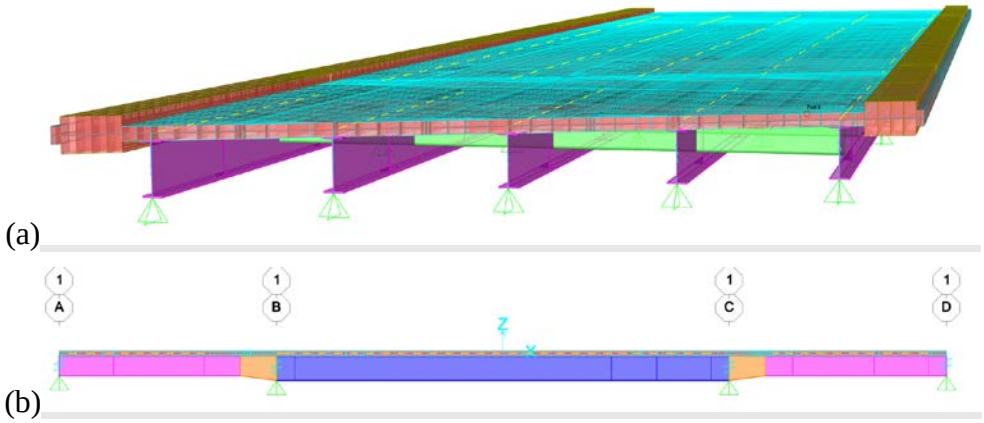

Figure 66: Fairbury Bridge 3D FE model: (a) 3D view and (b) elevation view.

For this analysis, four different live load cases were considered. In Cases 1 and 2, the entire truck load is applied to Path 1 and Path 2 in Figure 67. For Case 3, half of the truck load is applied to Path 3 and the other half to Path 4. For Case 4, a similar load pattern to Case 3 is applied to Path 5 and Path 6. To perform the load rating, the most severe live load scenario was selected.

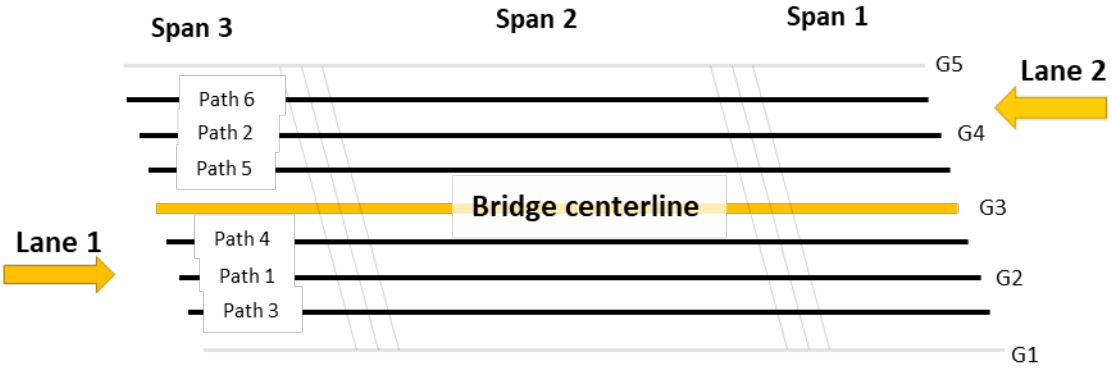

Figure 67: Moving load paths.

4.2.1.2 FE Model Calibration

Ideally, the calibrated model was expected to have the same modal behavior as the actual bridge. For the current study, the objective was to match the first natural frequency of the bridge model to values obtained from OMA. It is known that the level of composite action is one of the main parameters influencing model calibration. Hence, three models with different degrees of composite action were considered:

- Model 1 - Full composite action using direct nodal coupling and an offset deck.
- Model 2 - No composite action.
- Model 3 - Partial composite action via semi-rigid links between the offset deck and floor system.

Figure 68, Figure 69, and Figure 70 depict the first modes from the three models. The three spans of the bridge are linked through a pin and hanger system in the middle span. Therefore, the first dynamic mode does not include deformations of the shorter spans as they have a higher frequency. Using default material properties values from the software, the first natural frequency obtained from OMA was compared against numerical model results as shown in Table 4. OMA results were calculated using the UPC method. It is apparent that Model 1 featured the closest fundamental dynamic frequency to that obtained from OMA. To further investigate influence of model

parameters on the first frequency, sensitivities of each model to varying bridge deck concrete modulus of elasticity was examined. Results are shown in Table 5. Figure 71 depicts model error percentages as a function of varying modulus of elasticity. The results show that minimum error occurs for Model 1 at a modulus of elasticity 6000 ksi. Model 1 was used for further study and the first natural frequency equaled 7.47 Hz, which is in very good agreement with the OMA result.

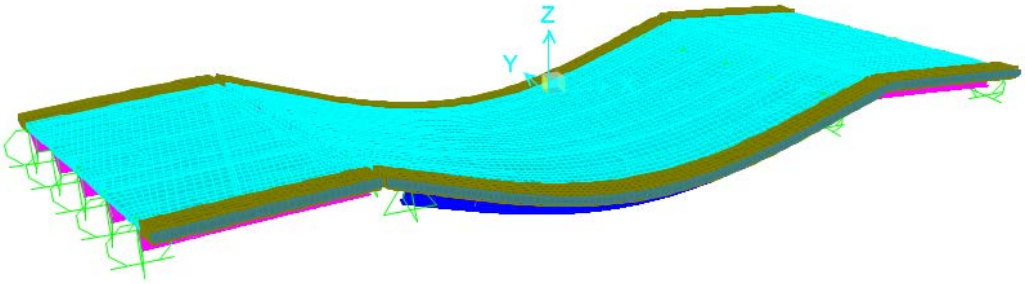

Figure 68: Model 1 modal analysis results before calibration, first natural frequency = 6.96 Hz.

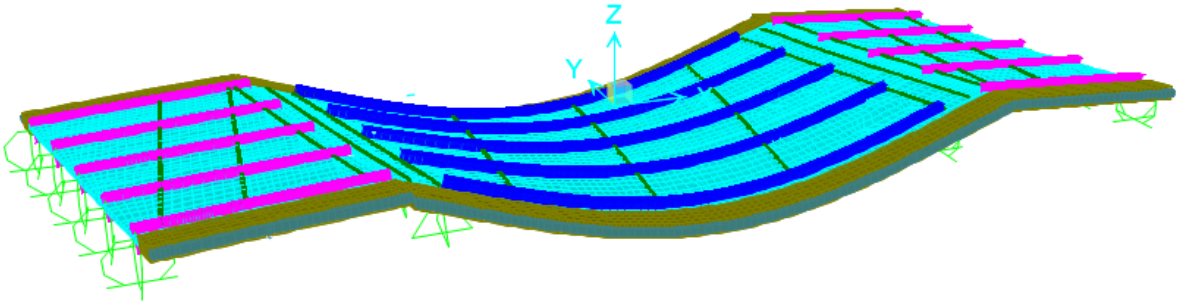

Figure 69: Model 2 modal analysis results before calibration, first natural frequency = 4.68 Hz.

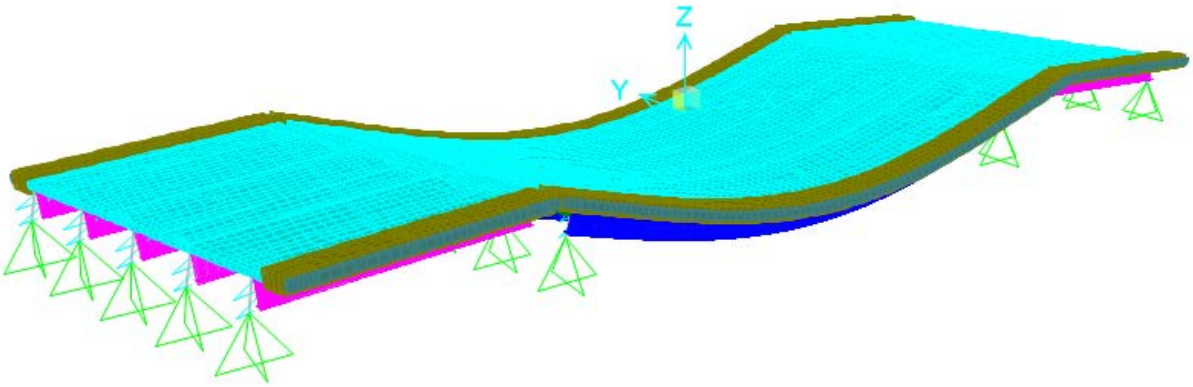

Figure 70: Model 3 modal analysis results before calibration, first natural frequency = 6.67 Hz.

Table 4: Summary of modal analysis results

Type of the analysis	First dynamic frequency (Hz)	$\frac{\text{Model dynamic frequency}}{\text{OMA frequency}}$
OMA	7.5	1
Model 1	6.96	0.93
Model 2	4.68	0.62
Model 3	6.67	0.89

Table 5: Sensitivity of the first dynamic frequency (Hz) to variations in modulus of elasticity (ksi)

	3000	**3500**	**4000**	**4500**	**5000**	**5500**	**6000**
Model 1	6.70	6.93	7.09	7.20	7.30	7.39	*7.47*
Model 2	4.62	4.68	4.72	4.77	4.82	4.86	4.9
Model 3	6.54	6.65	6.75	6.83	6.90	6.97	7.03

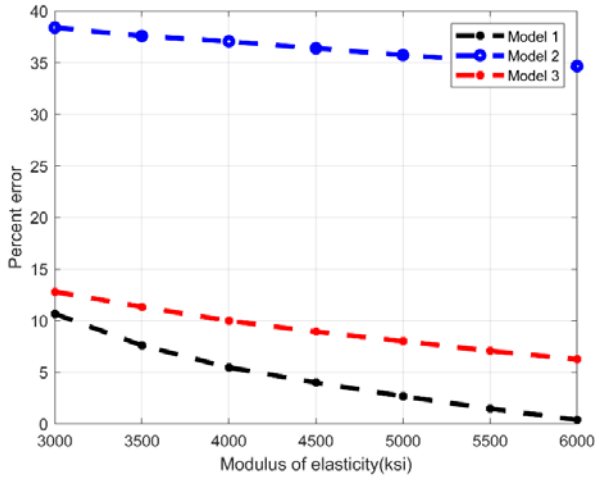

Figure 71: Comparison of the percent error for three models.

4.2.1.3 Calculation of Rating Factors via Dynamic Testing and OMA

As discussed in Chapter 3, capacity of the most critical member is used to load rate a bridge (Eqs. 3.6.1 and 3.6.2). To conduct an experimental load rating, a critical superstructure section was

chosen from the live load tests and strain measurements so that rating factors calculated using dynamic data could be compared to those calculated using string data.

The load rating was performed using both LFR (Eq. 3.6.1) and LRFR (Eq. 3.6.2). Table 6 shows coefficients used for the LFR rating. For comparison, G4 at Section E-E was selected (see Figure 72, Figure 73 and Figure 74). The dynamic load rating was performed using dynamic data recorded from the field. For the analytical load rating, model results without calibration were utilized; however, as recommended by *NCHRP Research Digest 234: Manual for Bridge Rating Through Load Testing* [25], the appropriate model class was identified using OMA results. Experimental load rating results used the calibrated model. Results are presented in Table 7. Table 8 and Table 9 show coefficients and results using LRFR. It is observed that using OMA for calibration of Model 1 prior to using the model for load rating produced a 17% improvement in predicted bridge load capacity. In the next subsection, strain measurements were used for calculating rating factors.

Table 6: LFR factors

Factors	$\emptyset_n$	γ_{DC}	γ_{LL}*(operating)*	γ_{LL}*(inventory)*	*IM*
Value	1	1.3	1.3	2.17	0

Table 7: Fairbury Bridge dynamic LFR summary, G4 Section E-E

Rating Vehicle	**FE analysis**	**Vehicle speed**	**Inventory Rating**			**Operating Rating**		
			Experimental / Analytical	Experimental	Analytical	Experimental / Analytical	Experimental	Analytical
Type 3	Model 1 (Full-composite)	15 mph	1.21	3.17	2.62	1.21	9.52	7.87
Type 3	Model 2 (non-composite)	15 mph	4.0	3.16	0.79	3.88	9.54	2.46

Table 8: LRFR factors.

Factors	$\emptyset_c$	$\emptyset_s$	$\emptyset_n$	γ_{DC}	γ_{DW}	γ_{LL}	IM
Value	1.00	1.00	0.9	1.25	1.5	1.4	0

Table 9: Fairbury Bridge dynamic LRFR summary

Vehicle name	**FE analysis**	**Vehicle speed**	**Inventory Rating**			**Operating Rating**		
			$\frac{\text{Experimental}}{\text{Analytical}}$	Experimental	Analytical	$\frac{\text{Experimental}}{\text{Analytical}}$	Experimental	Analytical
Type 3	Model 1 (Full-composite)	15 mph	1.21	4.40	3.64	1.21	7.95	6.57
Type 3	Model 2 (non-composite)	15 mph	4.0	4.40	1.1	3.88	7.95	2.05

4.2.1.4 Comparison of Dynamic and Strain Based Rating Factors

Load ratings presented in the previous section are compared to those from controlled tests discussed in Section 4.1.1.2. Tests where the truck traversed the bridge at 5 and 15 mph were selected.

Following the MBE and NCHRP *Research Digest 234: Manual for Bridge Rating Through Load Testing* [25], the field testing-based rating equation is:

$$RF_T = RF_c * K \tag{4.1}$$

where: RF_T denotes the rating factor influenced by field test results; RF_c denotes the rating factor based on calculations before accounting for field test results; and K is an adjustment factor found using:

$$K = 1 + K_a * K_b. \tag{4.2}$$

In this equation, K_a incorporates influence of the field tests and according to MBE Section 8.8.2.3 and is calculated using:

$$K_a = \frac{\varepsilon_c}{\varepsilon_T} - 1 \tag{4.3}$$

where ε_T denotes the maximum strain for the critical member from the field test and ε_c is the corresponding strain calculated from the FE model.

K_b depends on factors such as type and frequency of inspection and existence or absence of special damage features and is written as:

$$K_b = K_{b1} * K_{b2} * K_{b3}. \tag{4.4}$$

K_{b1} addresses rating benefits from field testing, K_{b2} addresses the type and frequency of the inspection and K_{b3} the existence or absence of critical failure conditions in the bridge. K_b is determined from MBE Table 8.8.2.3.1-1.

Examination of field results yielded critical elements and their maximum strains. Representative strain plots and corresponding model predictions are shown in Figure 57 and Figure 58. Strains at select locations are presented in Table 10.

The research team used $K_b = 1$ in the adjustment factor calculations. Resulting adjustment factors were then applied to the analytical ratings. Calculations are performed for G4 at Section E-E. Results are summarized in Table 11 and Table 12, with the last rows of Table 11 and Table 12 feature rating factors calculated based on dynamic tests and OMA. Recommended theoretical values for impact factor from the MBE were used for the dynamic ratings. Close agreement is seen between rating factors calculated using both sets of sensors. Differences are attributed to use of calculated dynamic impact factors for the strain-based method.

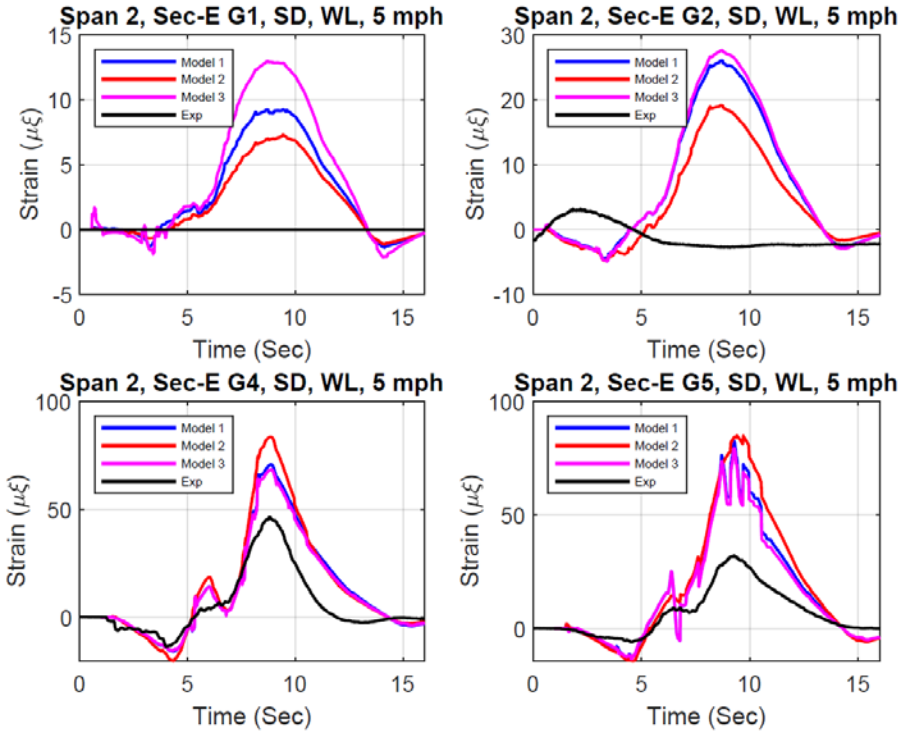

Figure 72: Comparison between measured and modeled strains at Section E-E, vehicle speed = 5 mph.

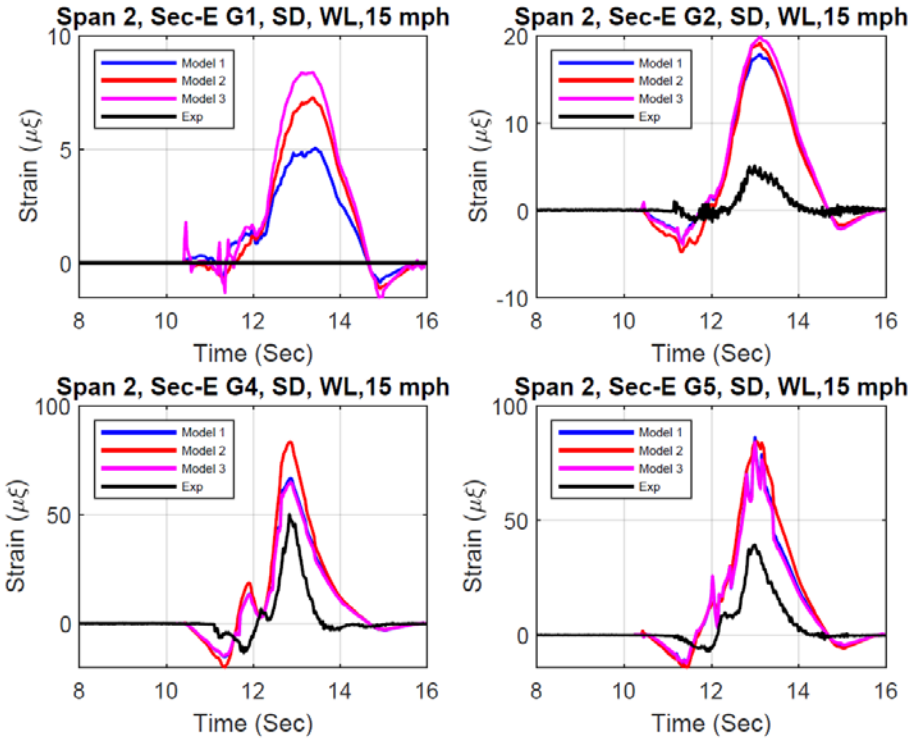

Figure 73: Comparison between measured and modeled strains at Section E-E, vehicle speed = 15 mph.

Table 10: Summary of critical member strain comparisons (vehicle speed: 15 mph).

Location of maximum strain (see Figure 74)	**FE analysis**	**Load case***	**FE model maximum strain (ε_c)**	**Field test maximum strain (ε_T)**	$\frac{\varepsilon_c}{\varepsilon_T}$	K_a	K
Span 2 - Section E-E, G4	Model 1 (Full composite)	WL	66.63	50.06	1.33	0.33	1.33
Span 2 - Section E-E, G4	Model 2 (Non-composite)	WL	83.36	50.06	1.67	0.67	1.67

*WL: West Lane loading, EL: East Lane loading

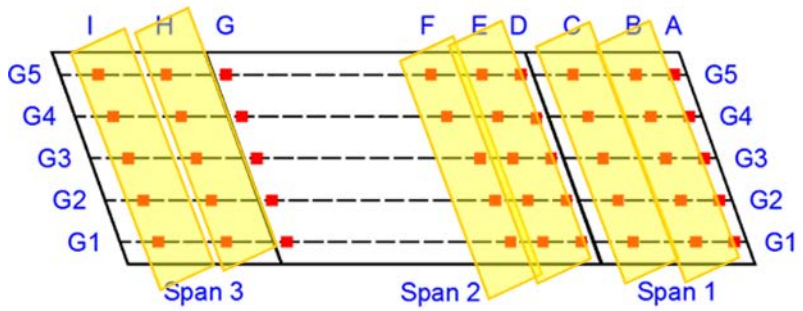

Figure 74: Comparison locations.

Table 11: Fairbury Bridge LFR summary, G4 Section E-E.

Type of measurement	FE analysis	Vehicle speed	Inventory Rating			Operating Rating		
			$\frac{\text{Experimental}}{\text{Analytical}}$	Experimental	Analytical	$\frac{\text{Experimental}}{\text{Analytical}}$	Experimental	Analytical
Strain	Model 1 (Full-composite)	15 mph	1.33	3.48	2.62	1.33	10.46	7.87
Strain	Model 2 (Non-composite)	15 mph	1.67	1.32	0.79	1.67	4.11	2.46
Acceleration	Model 1 (Full-composite)	15 mph	1.21	3.17	2.62	1.21	9.52	7.87
Acceleration	Model 1 (Non-composite)	15 mph	4.0	3.16	0.79	3.88	9.54	2.46

Table 12: Fairbury Bridge LRFR summary, G4 Section E-E.

Type of measurement	FE analysis	Vehicle speed	Inventory Rating			Operating Rating		
			Experimental / Analytical	Experimental	Analytical	Experimental / Analytical	Experimental	Analytical
Strain	Model 1 (Full-composite)	15 mph	1.33	4.84	3.64	1.33	8.74	6.57
Strain	Model 2 (Non-composite)	15 mph	1.67	1.84	1.1	1.67	3.42	2.05
Acceleration	Model 1 (Full-composite)	15 mph	1.21	4.40	3.64	1.21	7.95	6.57
Acceleration	Model 1 (Non-composite)	15 mph	4.0	4.40	1.1	3.88	7.95	2.05

4.2.2 Case study 2: E-171 Bridge

4.2.2.1 FE Model Construction

Bridge rating factors were calculated using results of OMA and a FE model. Numerical simulations were conducted using SAP2000 v22. Three-dimensional frame and shell elements were used to complete a time history analysis under moving truck loads (Figure 75).

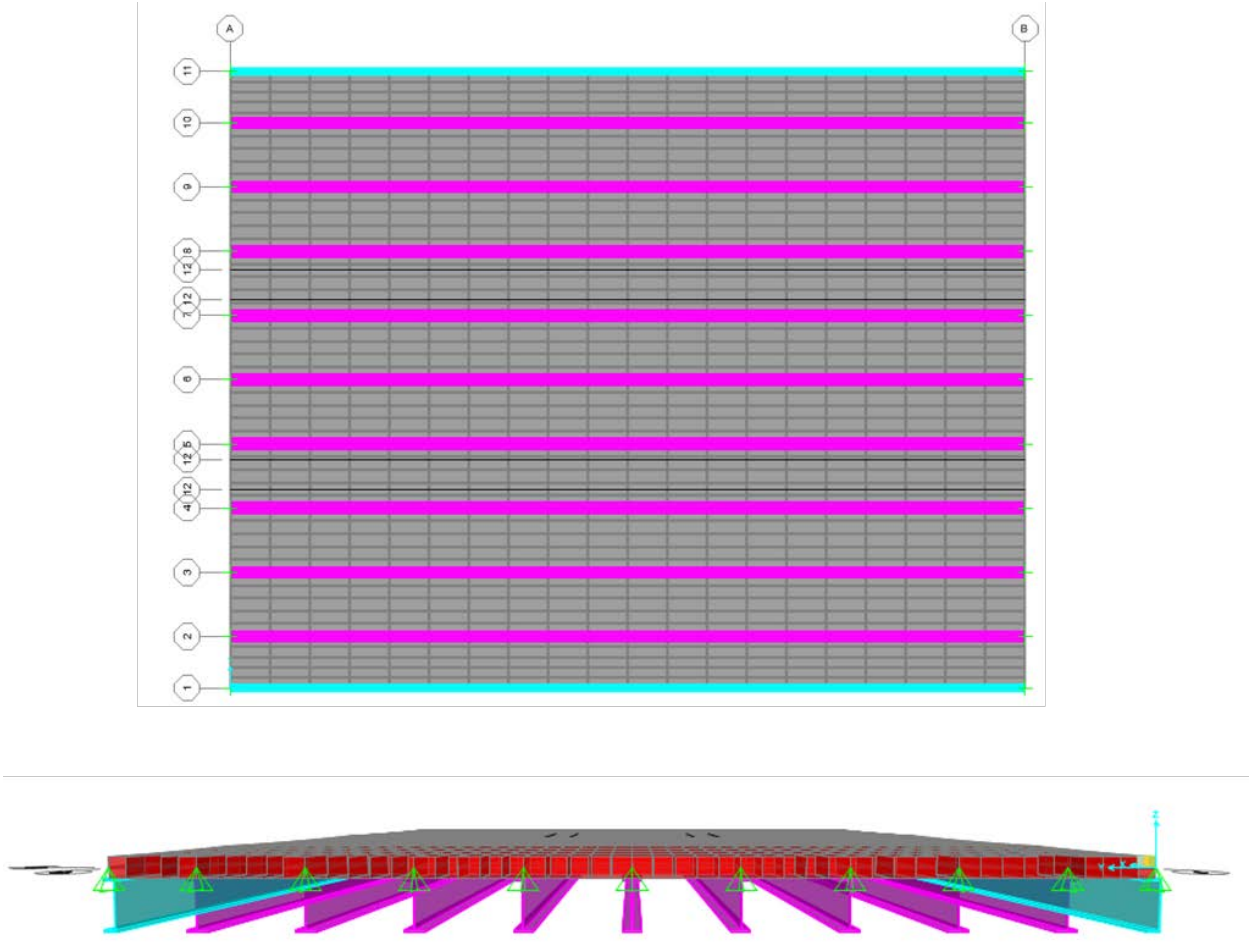

Figure 75: E-171 Bridge 3D FE model mesh: (a) plan view and (b) 3D view

A Type 3 Nebraska legal truck weighing 50.6 kips was used for FE model calibration. The front axle weighed 15.1 kips and the two rear axles 17.7 kips each. Spacing between axles was 15 ft. between the front and first rear axle and 4.75 ft. between rear axles. Three different live load cases were considered. The truck traversed the bridge in each lane 2 ft. from the rail and along the bridge

centerline. In Case 1, the half of the truck load was applied to Path 1 and half to Path 2. For Case 2, half of the truck load is applied to Path 3 and half to Path 4. For Case 3, half of the truck load was applied to Girder 4 and half to Path 3. Figure 76 shows the defined paths for live load configuration. The most severe live load scenario was selected for load rating.

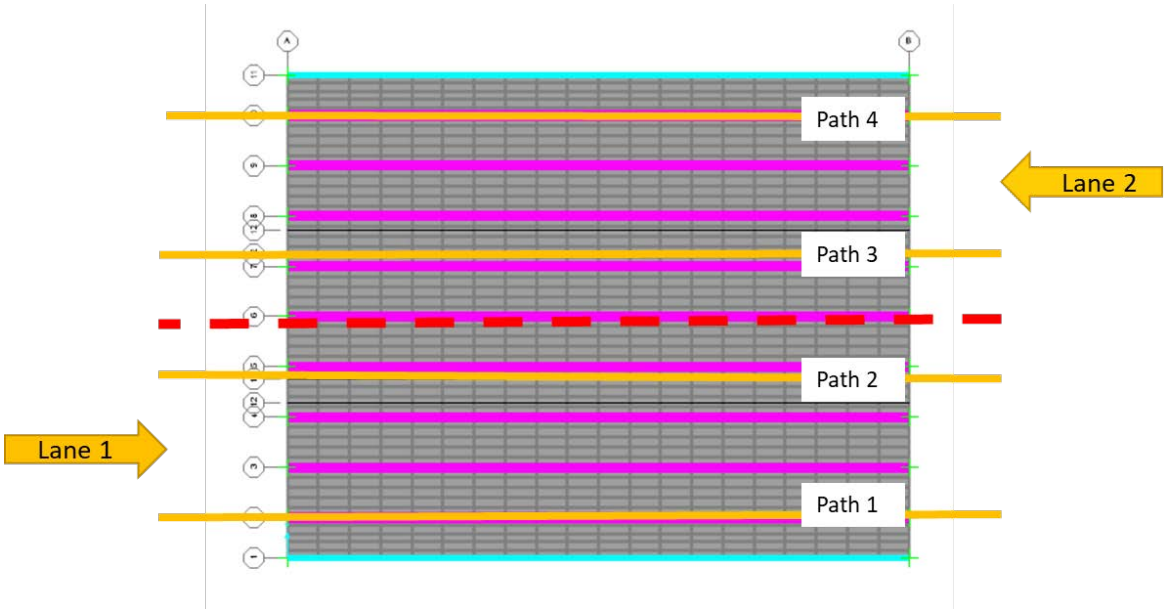

Figure 76: Defining the moving load paths (The red dash-line shows the bridge centerline).

4.2.2.2 FE Model Calibration

Calibration focused on matching the first natural frequency of the model to values obtained from OMA. Two levels of composite action were considered:

- Model 1: Full composite action using direct nodal coupling and an offset deck.
- Model 2: No composite action.

Figure 77 and Figure 78 demonstrate the first dynamic modes for the two models. Nominal material properties were used. The first natural frequency obtained from OMA is compared against numerical model results in Table 13. Model 1 featured the closest fundamental dynamic frequency

to that obtained from OMA. To further investigate influence of model parameters on the first dynamic frequency, sensitivities of each model to varying the bridge deck concrete modulus of elasticity was examined. Results are shown in Table 14. The results show that minimum error occurred for Model 1 with a modulus of elasticity 6000 ksi. Model 1 was used for further study and its first natural frequency equaled 11.07 Hz, which is in good agreement with the OMA result.

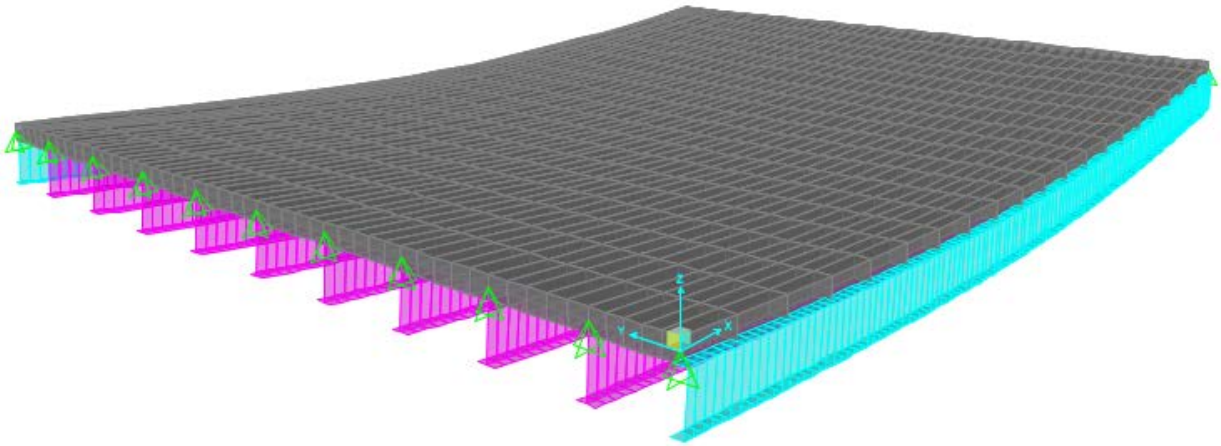

Figure 77: Model 1 modal analysis results before calibration, first natural frequency = 10.32 Hz.

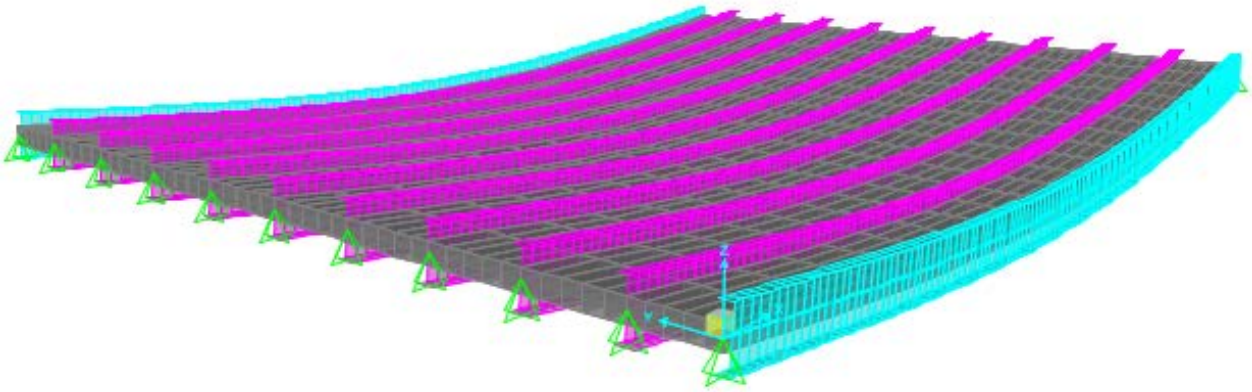

Figure 78: Model 2 modal analysis results before calibration, first natural frequency = 6.38 Hz.

Table 13: Summary of modal analysis results

Type of the analysis	First dynamic frequency (Hz)	$\frac{\text{Model dynamic frequency}}{\text{OMA frequency}}$
OMA	11.28	1
Model 1	10.32	0.91
Model 2	6.38	0.57

Table 14: Sensitivity of the first dynamic frequency (Hz) to variations in modulus of elasticity (ksi)

	3000	**3500**	**4000**	**4500**	**5000**	**5500**	**6000**
Model 1	10.04	10.28	10.48	10.66	10.81	10.95	11.07
Model 2	6.31	6.37	6.43	6.48	6.54	6.59	6.64

4.2.2.3 Calculation of Rating Factors via Dynamic Test and OMA

As discussed in Chapter 3, the capacity of the most critical member of structure is required to load rate the bridge using Eqs. 3.6.1 and 3.6.2. To conduct the experimental load rating, the critical superstructure section was chosen from live load tests.

The dynamic load rating was performed using both LFR (Eq. 3.6.1) and LRFR (Eq. 3.6.2). Table 15 shows coefficients used for the LFR rating. The dynamic load rating was performed using dynamic data recorded from the field. For the analytical load rating, model results without calibration were utilized; however, as recommended by *NCHRP Research Digest 234: Manual for Bridge Rating Through Load Testing* [25], the right model class was chosen using the OMA results. The experimental load rating was completed using results from the calibrated model. Results are presented in Table 16. Table 17 and Table 18 show LRFR coefficients and results. It is observed that using OMA for calibration of Model 1 and subsequent load rating can lead to a

24% improvement in the bridge capacity. For both models, the ratios obtained using LFR and LRFR method were higher than those for the Fairbury Bridge.

Table 15: LFR factors

Factors	$\emptyset_n$	γ_{DC}	γ_{LL}*(operating)*	γ_{LL}*(inventory)*	*IM*
Value	1	1.3	1.3	2.17	0

Table 16: E-171 Bridge dynamic LFR summary

Rating Vehicle	**FE analysis**	**Vehicle speed**	**Inventory Rating**			**Operating Rating**		
			$\frac{\text{Experimental}}{\text{Analytical}}$	Experimental	Analytical	$\frac{\text{Experimental}}{\text{Analytical}}$	Experimental	Analytical
Type 3	Model 1 (Full-composite)	15 mph	1.24	7.95	6.4	1.24	23.98	19.4
Type 3	Model 2 (non-composite)	15 mph	4.29	7.95	1.85	4.01	23.98	5.98

Table 17: LRFR factors

Factors	$\emptyset_c$	$\emptyset_s$	$\emptyset_n$	γ_{DC}	γ_{DW}	γ_{LL}	IM
Value	1.00	1.00	0.9	1.25	1.5	1.4	0

Table 18: E-171 Bridge dynamic LRFR summary

Rating Vehicle	**FE analysis**	**Vehicle speed**	**Inventory Rating**			**Operating Rating**		
			$\frac{\text{Experimental}}{\text{Analytical}}$	Experimental	Analytical	$\frac{\text{Experimental}}{\text{Analytical}}$	Experimental	Analytical
Type 3	Model 1 (Full-composite)	15 mph	1.24	11.06	8.9	1.24	20.0	16.18
Type 3	Model 2 (non-composite)	15 mph	4.33	11.06	2.55	4.03	20.0	4.96

4.2.3 Case study 3: M-164 Bridge

4.2.3.1 FE Model Construction

In this section, bridge rating factors were calculated using the results of OMA and a FE model.

The numerical simulation of the M-164 Bridge was constructed using the SAP2000 v22. Three-dimensional frame and shell elements were used to facilitate a dynamic time history analysis under moving truck loads, see the mesh in Figure 79.

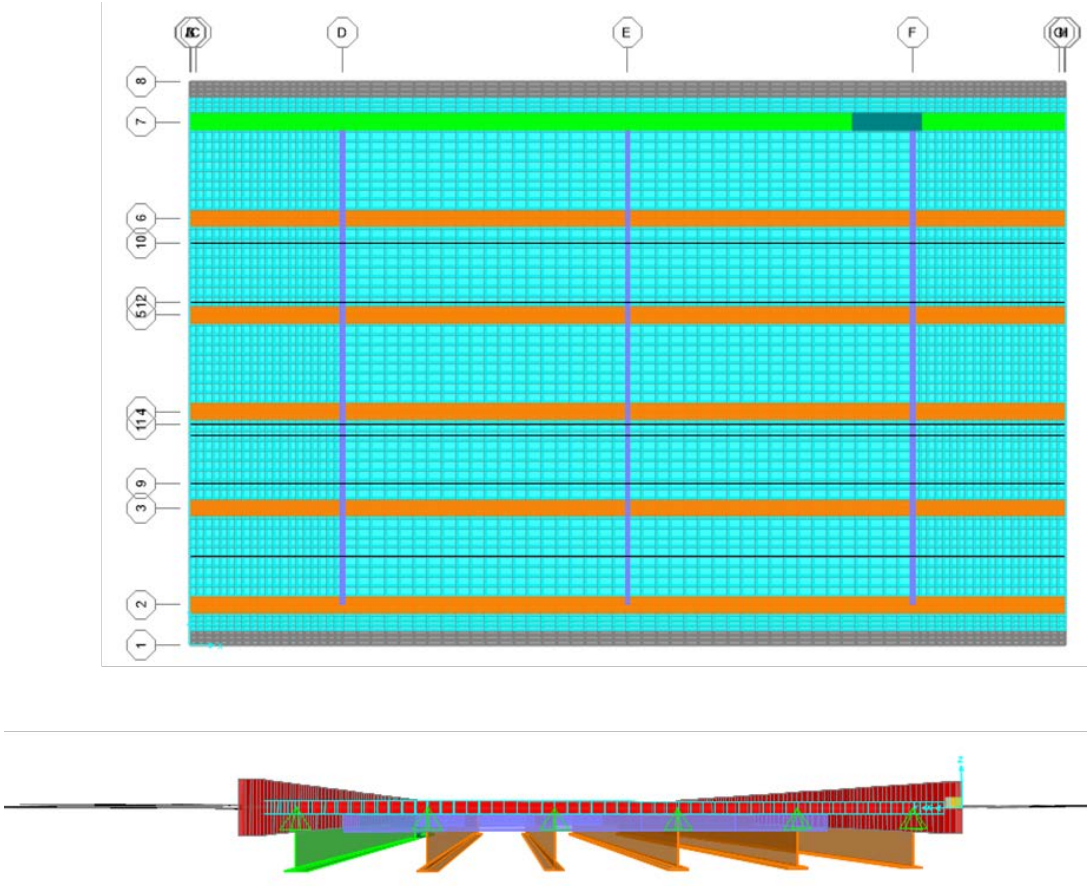

Figure 79: M-164 Bridge 3D FE model mesh: (a) Plan view and (b) 3D view

For this analysis, a Type 3 Nebraska legal truck weighing 50.6 kips was used for dynamic testing. The front axle weighed 15.1 kips and the two rear axles 17.7 kips each. Spacing between the axles was 15 ft. between the front and first rear axle and 4.75 ft. between rear axles.

Five different live load cases were considered. In Cases 1 and 2, the half truck load is applied to Path 1 and Path 2; and Path 3 and 4 respectively. For Case 3, half of the truck load is applied to Path 5 and the other half to Path 6. For Case 4, half of the truck load is applied to Path 7 and the other half to Path 8. Case 5 is a similar load pattern to case 4 on the other lane. Figure 80 shows the defined paths for live load configuration. To perform the load rating, the most severe live load scenario was selected.

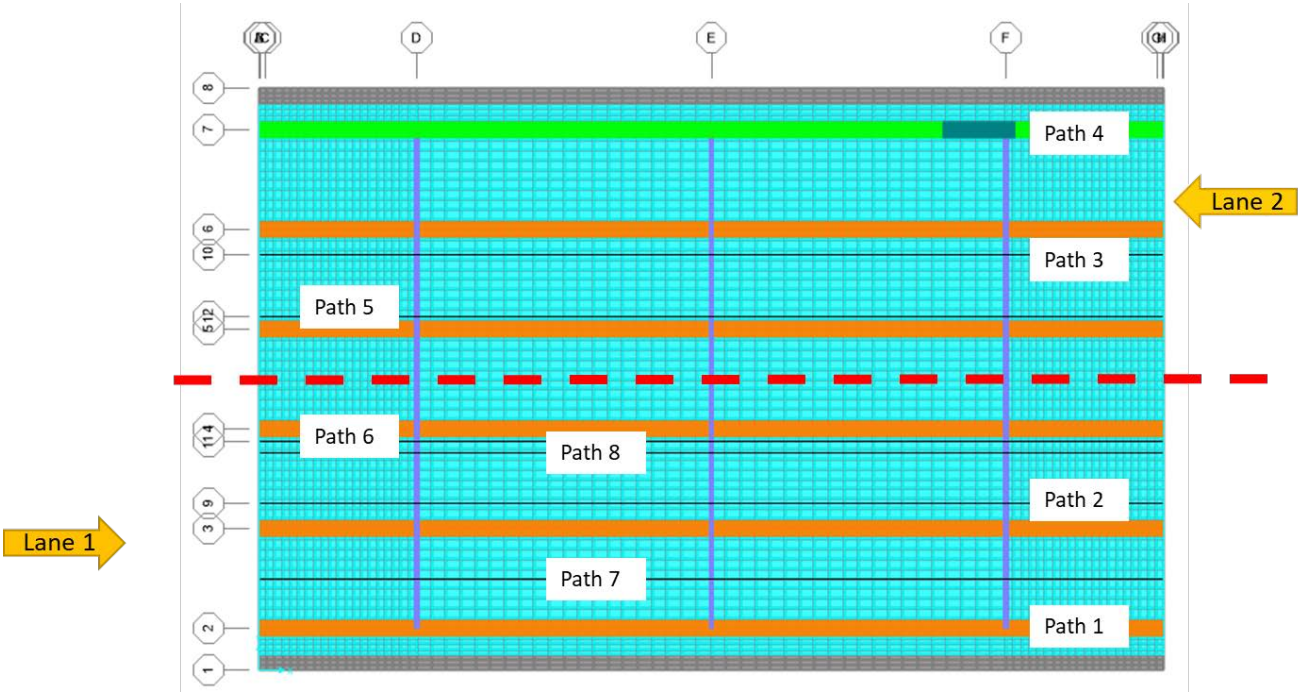

Figure 80: Defining the moving load paths.

4.2.3.2 FE Model Calibration

Ideally, the calibrated model was expected to have the same modal behavior as the real bridge. In this report, the objective was to match first natural frequency of the bridge model to values obtained from OMA. It is known that the level of composite action is one of the main parameters influencing model calibration. Hence, three models with different degrees of composite action were considered:

- Model 1: Full composite action using direct nodal coupling and an offset deck.
- Model 2: No composite action.

Figure 81 and Figure 82 demonstrate first dynamic modes for the two models. Using the default software value for the material properties, first natural frequency obtained from OMA was compared against numerical model results, see Table 19. It is apparent that Model 1 featured the closest fundamental dynamic frequency to those obtained from OMA. To further investigate influence of model parameters on the first dynamic frequency, sensitivities of each model to varying the bridge deck concrete modulus of elasticity was examined. Results are shown in Table 20. The results show that the minimum error occurs for Model 1 at a modulus of elasticity 4100 ksi. Model 1 was used for further study and the first natural frequency equaled 7.58 Hz, which is in excellent agreement with the OMA result.

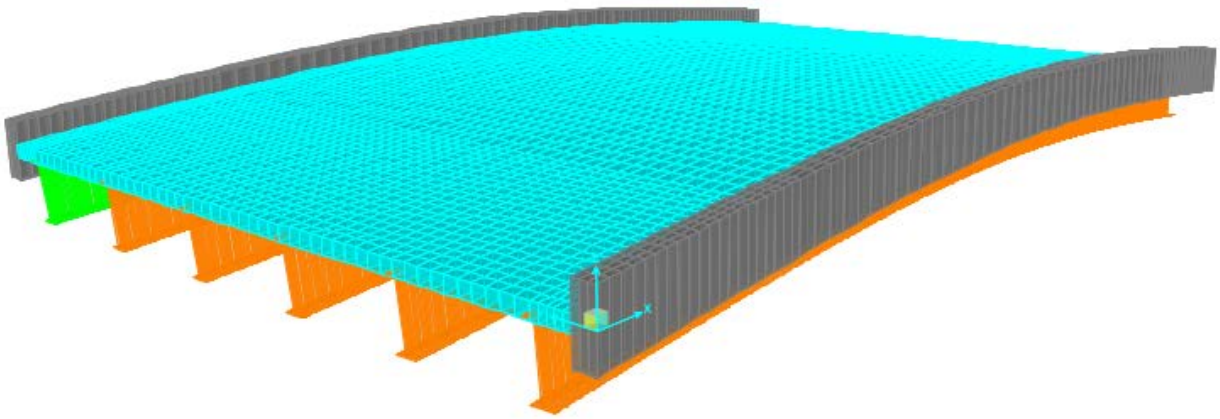

Figure 81: Model 1 modal analysis results before calibration, first natural frequency = 7.37 Hz.

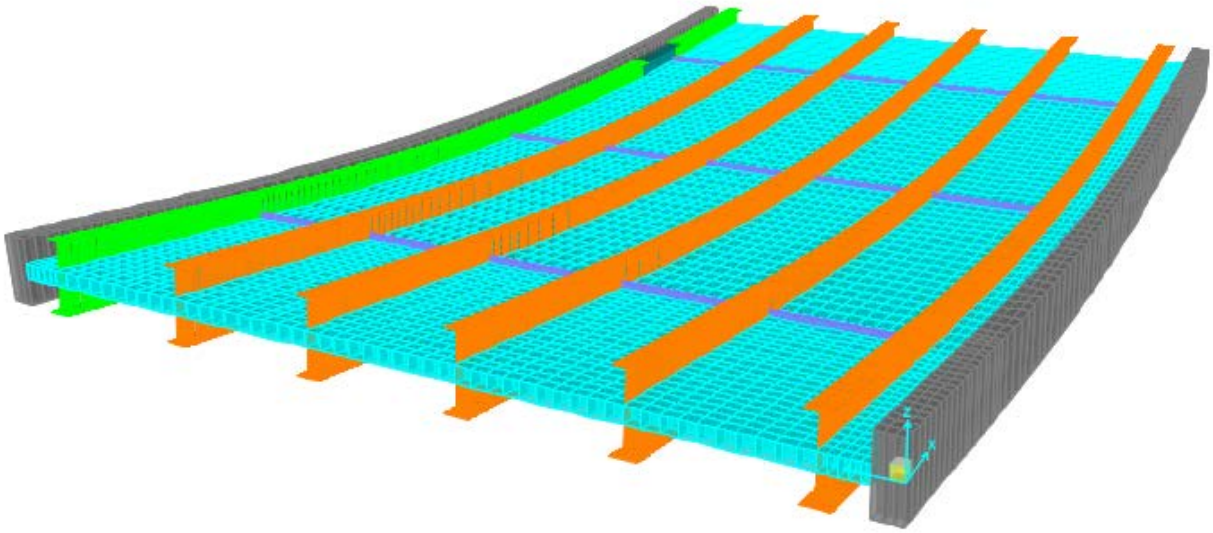

Figure 82: Model 2 modal analysis results before calibration, first natural frequency = 5.02 Hz.

Table 19: Summary of modal analysis results

Type of the analysis	First dynamic frequency (Hz)	$\frac{\text{Model dynamic frequency}}{\text{OMA frequency}}$
OMA	7.58	1
Model 1	7.37	0.97
Model 2	5.02	0.66

Table 20: Sensitivity of the first dynamic frequency (Hz) to variations in modulus of elasticity (ksi)

	3000	**3500**	**4000**	**4100**	**4500**	**6000**
Model 1	7.18	7.34	7.48	7.58	7.6	7.91
Model 2	4.95	5.01	5.06	5.08	5.12	5.3

4.2.3.3 Calculation of Rating Factors via Dynamic Test and OMA

As discussed in Chapter 3, the capacity of the most critical member of structure is required to load rate the bridge (Eqs. 3.6.1 and 3.6.2). To conduct the experimental load rating, the critical superstructure point was chosen from the live load tests.

The load rating was performed using both LFR (Eq. 3.6.1) and LRFR (Eq. 3.6.2). Table 21 shows coefficients used for the LFR rating. The dynamic load rating was performed using dynamic data recorded from the field. For the analytical load rating, model results without calibration were utilized; however, as recommended by *NCHRP Research Digest 234: Manual for Bridge Rating Through Load Testing* [25], the right model class was chosen using the OMA results. whereas for the experimental load rating results of calibrated model were used for calculating the load rating. Results are presented in Table 22. Table 23 and Table 24 show LRFR coefficients and results. It is observed that using the OMA for calibration of Model 1 and load rating can lead to 4% improvement in the bridge load bearing capacity, which were lower than those for the other two bridges.

Table 21: LFR factors

Factors	$\emptyset_n$	γ_{DC}	γ_{LL}*(operating)*	γ_{LL}*(inventory)*	*IM*
Value	1	1.3	1.3	2.17	0

Table 22: M-164 Bridge dynamic LFR summary

Rating Vehicle	**FE analysis**	**Vehicle speed**	**Inventory Rating**			**Operating Rating**		
			$\frac{\text{Experimental}}{\text{Analytical}}$	Experimental	Analytical	$\frac{\text{Experimental}}{\text{Analytical}}$	Experimental	Analytical
Type 3	Model 1 (Full-composite)	15 mph	1.04	13.9	13.38	1.04	43.03	41.49
Type 3	Model 2 (non-composite)	15 mph	4.15	13.9	3.35	3.63	43.03	11.84

Table 23: LRFR factors

Factors	$\emptyset_c$	$\emptyset_s$	$\emptyset_n$	γ_{DC}	γ_{DW}	γ_{LL}	*IM*
Value	1.00	1.00	0.9	1.25	1.5	1.4	0

Table 24: M-164 Bridge dynamic LRFR summary

Rating Vehicle	**FE analysis**	**Vehicle speed**	**Inventory Rating**			**Operating Rating**		
			$\frac{\text{Experimental}}{\text{Analytical}}$	Experimental	Analytical	$\frac{\text{Experimental}}{\text{Analytical}}$	Experimental	Analytical
Type 3	Model 1 (Full-composite)	15 mph	1.04	19.25	18.53	1.04	35.82	34.53
Type 3	Model 2 (non-composite)	15 mph	4.25	19.25	4.53	3.67	35.82	9.75

5 CONCLUSIONS

This report outlined a procedure for load rating existing bridges using low-cost dynamic sensors and OMA that, according to the *AASHTO Manual for Bridge Evaluation* (MBE), can be used to calibrate numerical models perform load ratings. In this regard, several dynamic sensors that could be used for bridge testing independent of a computer were selected as candidates. The original group was reduced to two sensors based on cost, resolution and operational information provided by the manufacturer or via tests completed at UNL. A set of bridges featuring various span lengths, ages, structural systems, and construction materials were used for studying the effectiveness of the two downselected sensors via recording acceleration time histories under operational conditions. Based on these tests, it was determined that a PCB 393B04 and 485B39 signal conditioner would yield the most consistent measurements. Embedded iPhone sensors, which were also downselected, were shown to yield accurate results for longer span bridges, as the signal to noise ratio was higher for those bridges. It was determined that different types of phones (e.g. iPhone 7+ verses iPhone 6) did not always feature consistent outcomes. Given this variability, when using iPhone or other smartphone sensors it is recommended that those sensors be calibrated against industry grade dynamic sensors, such as the PCB sensor selected in this study, prior to using them in the field.

Selected low-cost sensors were utilized for dynamic testing and rating of three bridges in Nebraska. A flowchart developed in Section 3.5 outlines the process that was utilized to determine rating factors for the bridges. Results from a conventional live load test were also used to calculate rating factors using known truck loads and strain measurements. Close agreement was observed between rating factors calculated using the two different data sets using calibrated models that considered full composite action, despite substantial differences in the number of sensors and, subsequently, cost associated with completing the tests. While the amount of benefit varied, in all cases using

field data to complete rating calculations improved resulting rating factors. It is believed that the level of benefit provided from dynamic field test load ratings is directly tied to bridge stiffness, with more flexible bridges realizing more benefit. However, additional research is needed to confirm these beliefs over a range of bridge types and sizes.

6 REFERENCES

[1] NBI, "https://www.fhwa.dot.gov/bridge/nbi.cfm," 2012. [Online].

[2] T. O. S. o. B. AASHTO., The manual for bridge evaluation, Washington, D.C. : American Association of State Highway and Transportation Officials, 2018.

[3] G. Morgenthal and H. Höpfner, "The application of smartphones to measuring transient structural displacements," *Journal of Civil Structural Health Monitoring,* vol. 2 , no. 3-4, pp. 149-161, 2012.

[4] M. Feng, Y. Fukuda, M. Mizuta and E. Ozer, "Citizen sensors for SHM: Use of accelerometer data from smartphones," *Sensors,* pp. 2980-2998, 2015.

[5] Q. Kong, R. M. Allen, M. D. Kohler, T. H. Heaton and J. Bunn, "Structural health monitoring of buildings using smartphone sensors," *Seismological Research Letters,* pp. 594-602, 2018.

[6] T. Oraczewski, W. J. Staszewski and T. Uhl, "Nonlinear acoustics for structural health monitoring using mobile, wireless and smartphone-based transducer platform," *ournal of Intelligent Material Systems and Structures,* pp. 786-796, 2016.

[7] Y. Yu, R. Han, X. Zhao, X. Mao, W. Hu, D. Jiao and J. Ou, "Initial validation of mobile-structural health monitoring method using smartphones," *International Journal of Distributed Sensor Networks,* pp. 274-391, 2015.

[8] P. Dey, V. Akhil and A. I. Laskar, "Application of smartphone and model updating technique in structural health monitoring," *Journal for Science and Engineering,* pp. 4819-4828, 2019.

[9] "https://www.keuwl.com/apps.html," [Online].

[10] A. K. Ndong, O. E. Ozbulut and D. K. Harris, "Identifying Modal Characteristics of Reinforced Concrete Bridges Using Smartphones," in *Dynamics of Civil Structures*, Springer, 2019, pp. 345-354.

[11] E. OZER, "Monitoring Bridge Vibrations via Pedestrians and Mobile Sensing," in *Proceeding of NDT Canada*, 2018.

[12] E. Ozer and M. Q. Feng, "Direction-sensitive smart monitoring of structures using heterogeneous smartphone sensor data and coordinate system transformation," *Smart Materials and Structures*, pp. 26-45, 2017.

[13] S. E. Chen, P. Siswobusono, N. Delatte and S. B. J., "Feasibility Study on Dynamic Bridge Load Rating," University Transportation Center for Alabama, (UTCA), 2002.

[14] A. K. M. Islam, F. Li, H. Hamid and A. Jaroo, "Bridge condition assessment and load rating using dynamic response (No. FHWA/OH-2014/7).," Ohio. Dept. of Transportation. Office of Statewide Planning and Research, 2014.

[15] D. K. Harris, O. Ozbulut, A. Bagheri, M. S. Dizaji, A. K. Ndong and M. Alipour, "Load Rating Strategies for Bridges With Limited or Missing As-Built Information (No. FHWA/VTRC 20-R27).," University of Virginia, 2020.

[16] R. Brincker and P. Andersen, " Understanding stochastic subspace identification," in *IMAC-XXIV: A Conference & Exposition on Structural Dynamics. Society for Experimental Mechanics*, 2006.

[17] H. Shokravi, H. Shokravi, N. Bakhary, S. S. R. Koloor and M. Petrů, "A Comparative Study of the Data-driven Stochastic Subspace Methods for Health Monitoring of Structures: A Bridge Case Study," *Applied Sciences (2020),* vol. 10, no. 9, p. 3132, 2020.

[18] M. Döhler, P. Andersen and L. Mevel, "Variance computation of modal parameter estimates from UPC subspace identification," in *IOMAC-7th International Operational Modal Analysis Conference.*, 2017.

[19] R. Brincker, L. Zhang and P. Andersen, "Modal identification of output-only systems using frequency domain decomposition," *Smart materials and structures,* vol. 10, no. 3, p. 441, 2001.

[20] R. Brincker, C. E. Ventura and P. Andersen, "Damping estimation by frequency domain decomposition," in *Proceedings of IMAC 19: A Conference on Structural Dynamics* , Hyatt Orlando, Kissimmee, Florida, 2001.

[21] N. J. Jacobsen, P. Andersen and R. Brincker, "Applications of frequency domain curve-fitting in the EFDD technique," in *IMAC-XXVI: A Conference & Exposition on Structural Dynamics. Society for Experimental Mechanics.*, 2008.

[22] M. Szerszen, D. Linzell and S. Eftekhar Azam, "Protocol to Evaluate and Load Rate Existing Bridges Using Field Testing," 2019.

[23] "Bridge images," Google Maps, January 2021. [Online]. Available: https://www.google.com/maps/.

[24] C. a. S. Inc., "Sap 2000 Integrated software for structural analysis and design," Berkeley, California.

[25] T. R. Board, "MANUAL FOR BRIDGE RATING THROUGH LOAD TESTING," Transportation Research Board, 1998.

[26] R. Brincker and C. Ventura, Introduction to operational modal analysis, John Wiley & Sons, 2015.

APPENDIX I: Setting Up PCB Sensor, Its Signal Conditioner, and Data Acquisition Software

A I.I PCB Sensor and ICP Signal Conditioner

- *Field setup:*

Before the recording is started, the PCB sensor must be deployed at a secure position on a smooth metal surface which is heavy enough to have no movement when it is placed on the bridge surface. To ensure that the PCB sensor has no relative movement respect to the metal surface, the UNL researcher team used a heavy magnet block which is attached to the bottom of the sensor at its interface with metal surface.

- *Sensor and signal conditioner setup:*

Once the signal conditioner is plugged into a USB port, there will be a new “Microphone array" labeled with the device model name which needs to be set as a default microphone.

A I.II Data Acquisition Software

In this analysis, the SpectraPLUS-SC software was used for collecting the dynamic data and it is recommended for future data collection. SpectraPLUS-SC includes a base analyzer and a set of options. Using the base analyzer, one can perform single channel operations in real time mode. The spectrum plot, time series of the recorded data, and phase displays are available in narrowband FFT sizes through 32,768 points, 1/1, and 1/3 Octave Analysis. Before initializing the data collection, it is required to calibrate the analyzer and specify the processing settings and sensitivity parameters in the SpectraPLUS software. Figure 83 shows the SpectraPLUS-SC interface. The highlighted tab shows where the processing setting are specified.

By clicking the “Processing Settings” tab, the user can specify the FFT setting, Scaling, Calibration and the I/O Device parameters. In “Calibration” tab, the sensitivity number corresponding to the type of the device which in this study is an accelerometer, must be entered. The sensitivity is provided by the sensor manufacturer. Figure 84 shows the calibration interface.

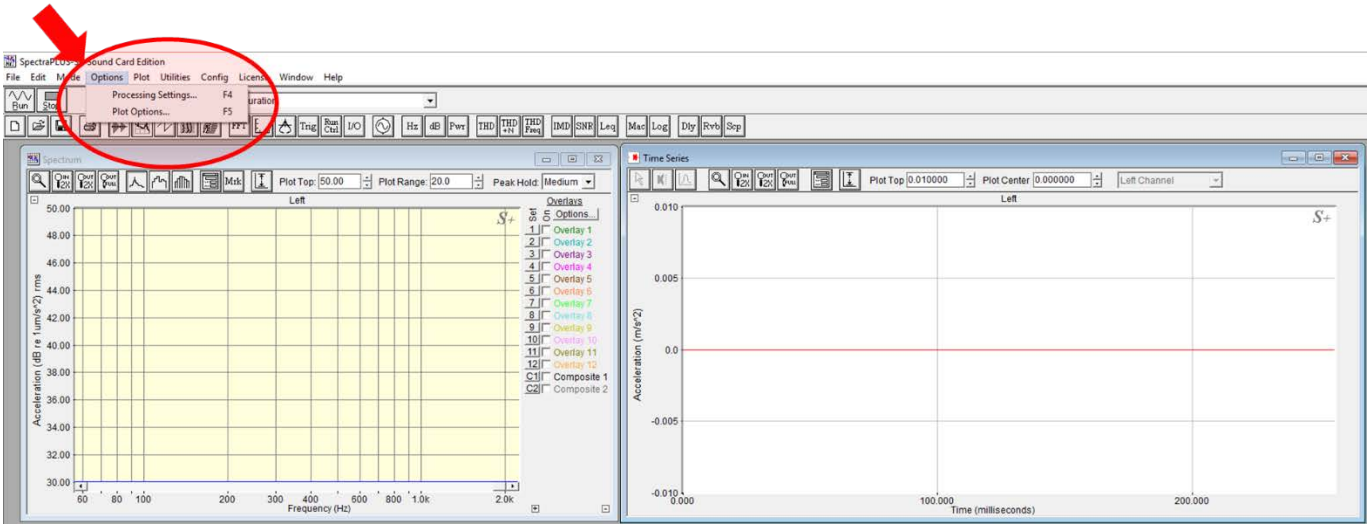

Figure 83: SpectraPLUS-SC interface. The " Processing Settings” menu is highlighted.

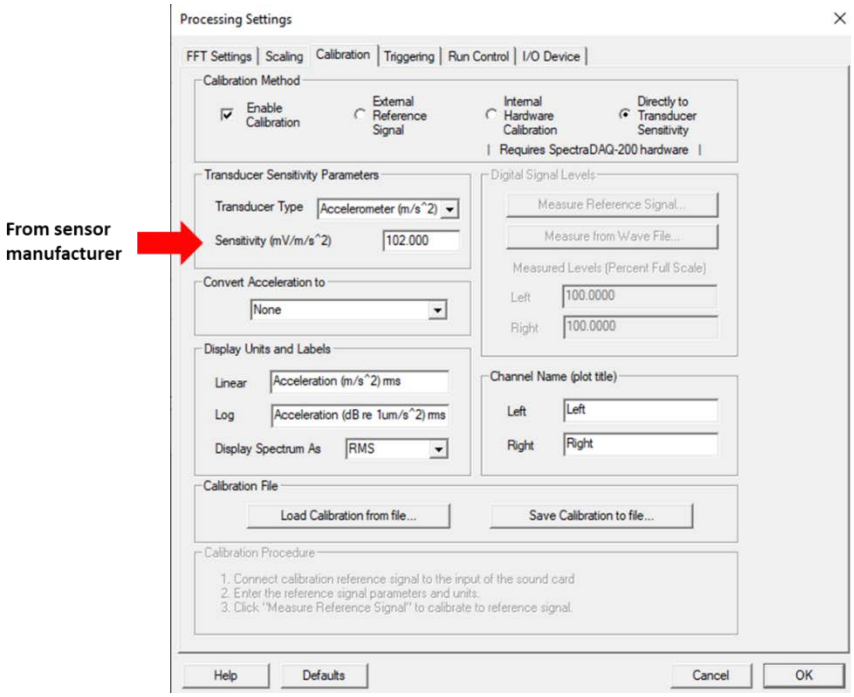

Figure 84: Calibration interface in SpectraPLUS-SC analyzer

The FFT size directly affects the resolution of the calculated spectra. The sampling rate of 4000 Hz with FFT size of 1024 samples would be suitable for this analysis. Depending on which analyzer options used, the other parameters such as sampling format is chosen, Figure 85 shows the FFT settings interface.

I/O device tab allows user to specify the sound card. Since the signal conditioner is used as an input device, it is required to assign it as a default sound card. The user needs to assure that the other sound card devices are inactive at the time of collecting the data. By checking the advance properties of the input device, the required sampling rate and the bit used when running in the share mode is selected. It is recommended to use 24 bit with the 48000 Hz. Figure 86 shows the I/O device interface.

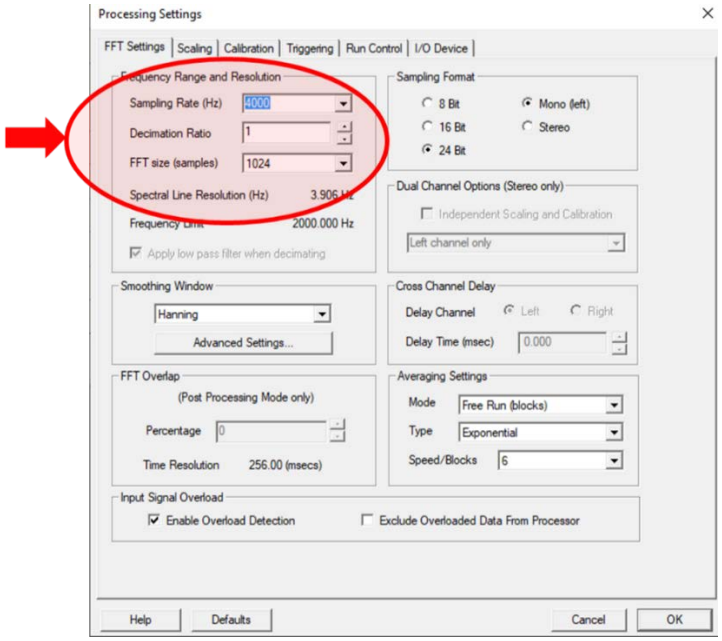

Figure 85: FFT settings interface in SpectraPLUS-SC analyzer

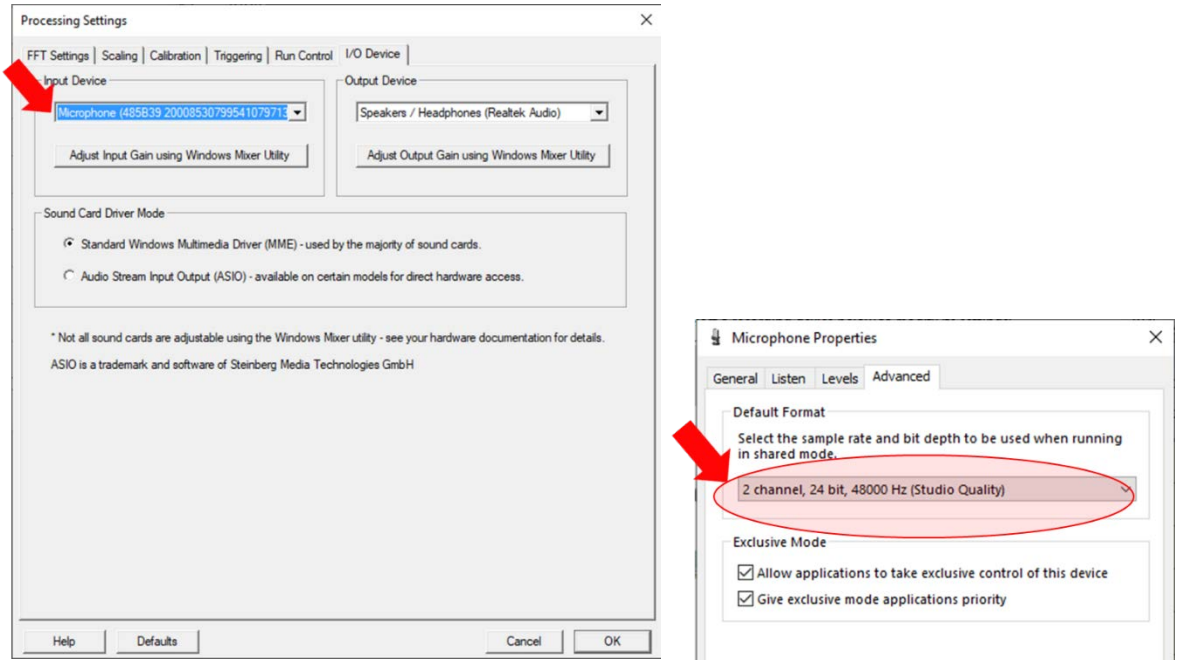

Figure 86: the I/O device interface in SpectraPLUS-SC analyzer. (a) the signal conditioner is selected as an input device. (b) the advanced settings of input device

APPENDIX II: Guidelines for Using iPhone Embedded Accelerometer

- *Field setup:*

Before the recording is started, the iPhone sensor must be placed at a secure position on a smooth surface on the bridge. To guarantee the quality of the collected data, the iPhone sensor must have no relative movement respect to the bridge surface. To do so, the user may remove the cell phone cover if it has any or use covers that have enough friction against the bridge surface.

- *Sensor setup:*

Not applicable since the sensor is manufactured during the iPhone assembly process.

- *Data acquisition software:*

In preparation of this report the VibSensor application was used for collecting the dynamic data. Figure 87 shows the VibSensor interface. After specifying the duration of data collection (Figure 87a) and tapping the “Start”, the app starts recording the data. It is recommended to choose the sampling rate of 100 Hz marked as “High” sampling range in “Settings” (Figure 87b). Once the recording is terminated, the user will be able to view a power spectrum and time series of the recorded data for initial evaluation of the data.

Figure 87: VibSensor interface. (a) recording the data (b) the record settings and (c) a sample collected dynamic data